ICMR Summer School on Materials in 3D:
Modeling and Imaging at Multiple Length Scales
University of California, Santa Barbara, CA, USA
Monday, August 19, 2013
ESB 1001
2:00pm – 3:30pm

Electron tomography observation of microstructure in crystalline materials

Satoshi Hata

Department of Electrical and Materials Science

Kyushu University, Japan

hata.satoshi.207@m.kyushu-u.ac.jp

Location of Kyushu University

1. Hakozaki Campus
2. Hospital Campus
3. Chikushi Campus
4. Ohashi Campus
5. University Farm
6. Advanced Medical Center at Beppu
7. Institute of Seismology and Volcanology
8. Amakusa Marine Biological Laboratory
9. Kuju Agricultural Research Center
10. Shiiba Research Forest
11. Ibusuki Experimental Station
12. Ashoro Research Forest
13. Kyushu University Nishijin Plaza
14. Ito Campus (New Campus)
15. Kyushu University International House
16. Tokyo Office, Kyushu University Faculty of Design Tokyo Lounge
17. Osaka Office

Campuses of Kyushu University

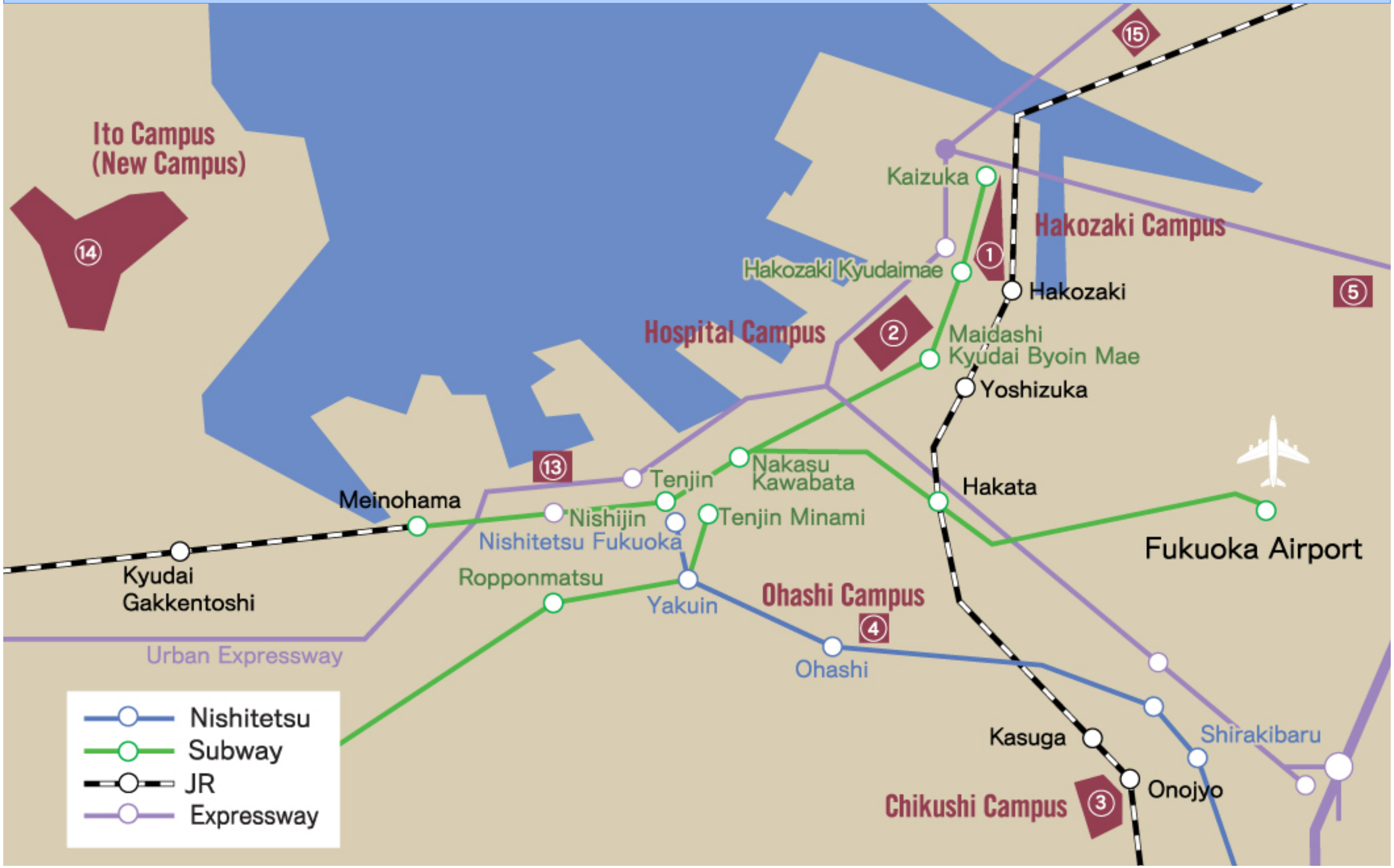

Ito Campus of Kyushu University

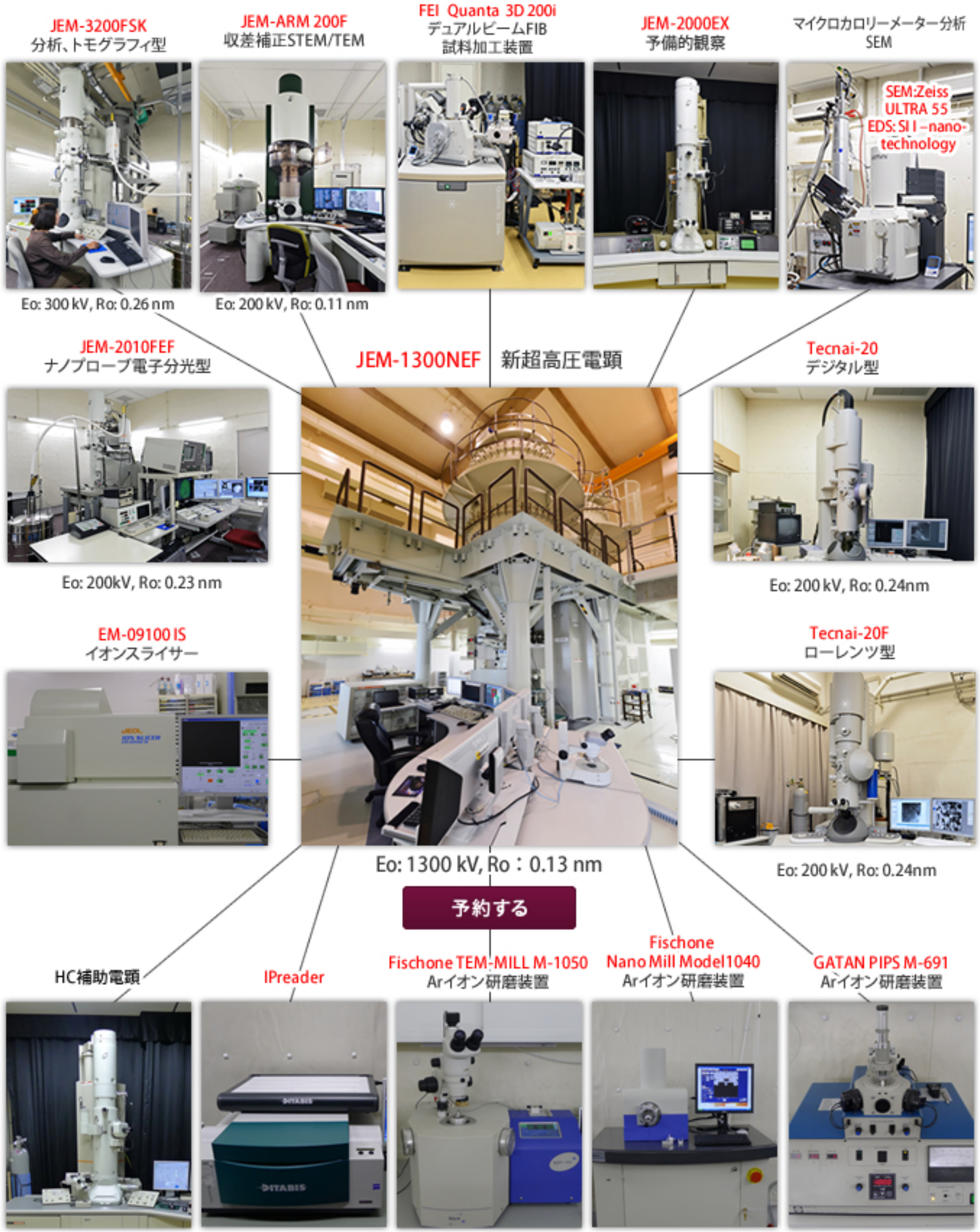

TEMs and related apparatus of HVEM Laboratory in Kyushu University

Chikushi Campus of Kyushu University

Main EMs in Chikushi Campus of Kyushu University

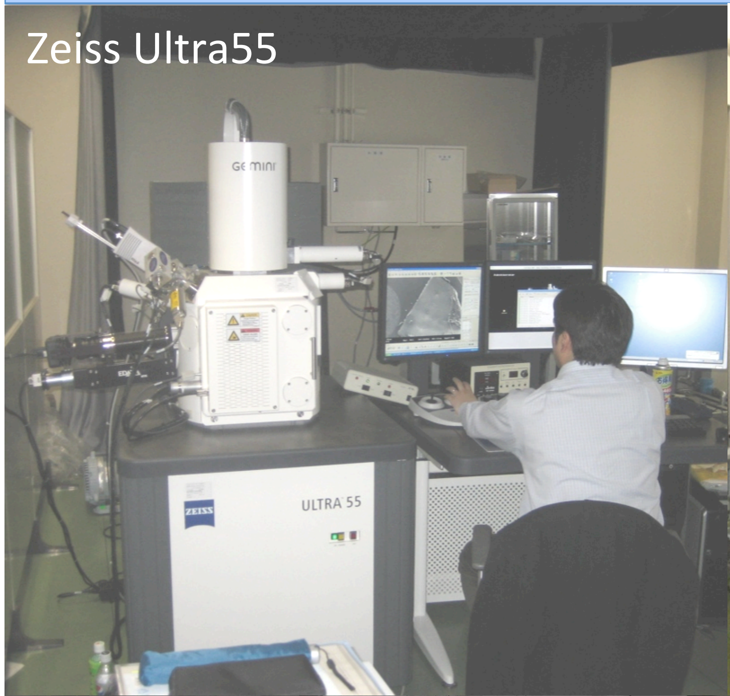

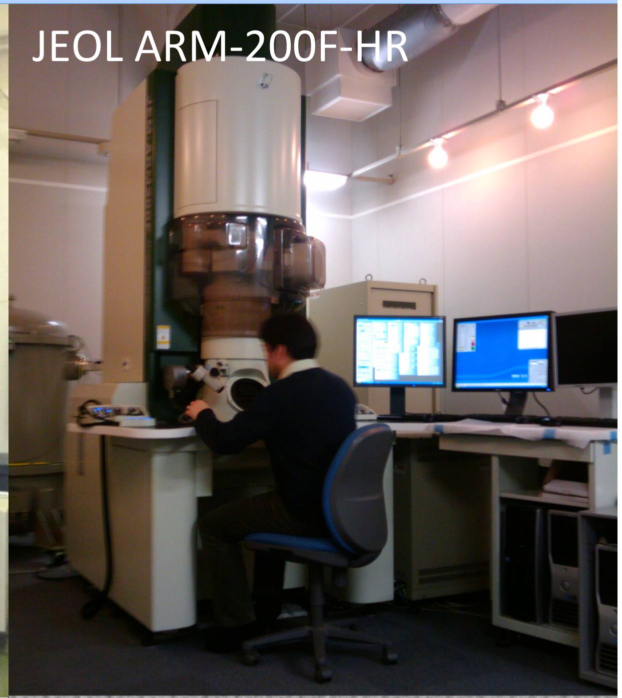

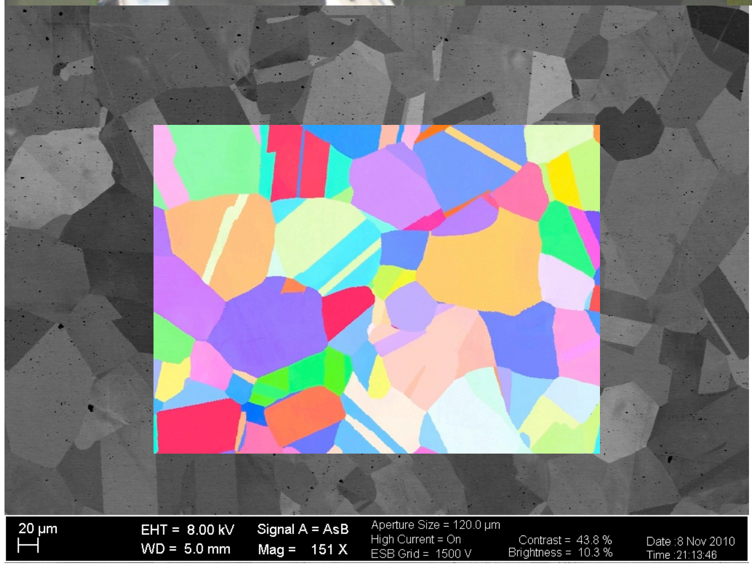

FEI Titan^3 and Dual-Beams coming…

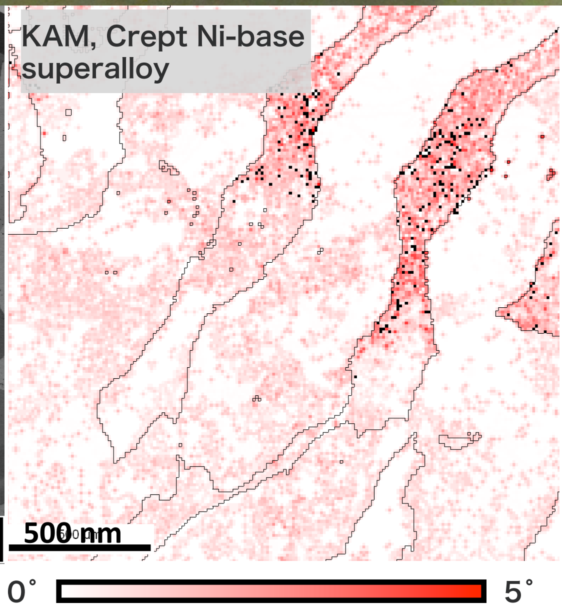

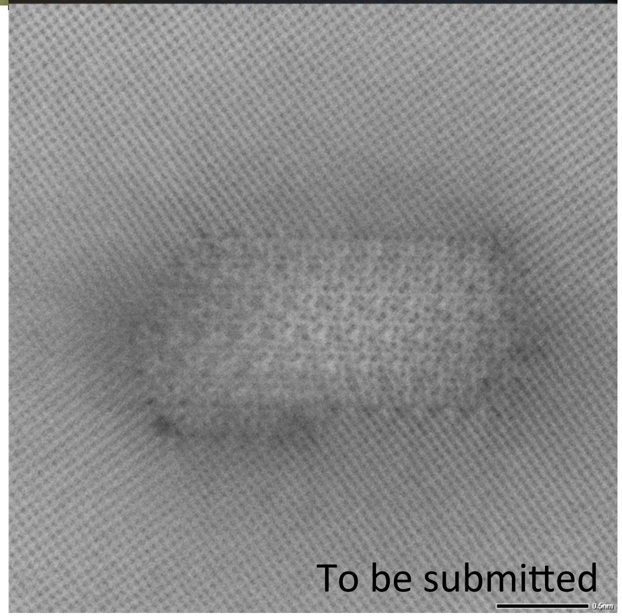

Establishment of International Network of Ultramicroscopy for Real Dimension Analysis and Functional Design of Advanced Materials

"Strategic Young Researcher Overseas Visits Program for Accelerating Brain Circulation"
Sponsored by Japan Society for the Promotion of Science (JSPS),
with Faculty of Engineering Science, Kyushu University, Japan. *2012.10 - 2015.9*

University of Birmingham
I.P. Jones

University of Cambridge
P.A. Midgley

University of Oxford
A.J. Wilkinson

Technical University of Denmark
T. Kasama

Ulm University
C.T. Koch

Helmholtz-Zentrum Berlin
N. Wanderka

University of Antwerp
D. Schryvers

KYUSHU UNIVERSITY **(Lead)**

M. Nishida
K. Higashida
K. Kaneko
S. Matsumura
H. Nakashima

University of Illinois at Urbana-Champaign
I.M. Robertson

VirginiaTech ICTAS
M. Murayama

Technique Development

- Time-resolved 3D Electron Microscopy
- In-situ Electron Microscopy
- Environmental Electron Microscopy
- Sub-Å Electron/ion Microscopy

- Strain Distribution
- Crystal Structure & Orientation
- Magnetic/Electron Structure
- Chemical/Structural Inhomogeneity

Materials Design

Propose contents of today's talk…

- Most of you do not know SH at all.
- There have been many textbooks of electron tomography.
- I would like to talk about my research history for recent 10 years, because you may understand development of electron tomography methods for crystalline materials such as metals and alloys.
- If you would be interested in my talk, I could send you my papers described in better English than my spoken English.

Curriculm vitae of SH

- Born in Osaka on 15 July 1969, 44 years old, male
- Married, two daughters
- 1992 Bachelor of Engineering (Metallurgy), Kyushu University
- 1994 Master of Engineering, Kyushu University
- 1994 Research associate (assistant professor), Kyushu University
- 2001 Doctor of Engineering, Kyushu University (Short-range order and its transformation to long-range order in Ni-Mo alloys)
- 2003 Started electron tomography research
- 2005, 8 Jacquet-Lucas Award of International Metallographic Contest
- 2005, 10-11 Visiting researcher at University of Cambridge (P.A. Midgley)
- 2007 Associate professor (Structural Materials Lab.), Kyushu University
- 2013 Lecturer of ICMR Summer School on Materials in 3D

History of electron tomography (-2001)

Ziese and de Jong: Applied Catalysis A (2004)

1960's: first applications of tomography related technique in electron microscopy in biological sciences (*1982 Nobel Prize for Klug*)

1990's: routine application of TEM tomography in biological sciences

2000: first application of TEM tomography in catalysis by Geus/Janssen/de Jong/Koster [3,4]

2001: routine application of TEM tomography in catalysis by Janssen/de Jong/Koster [6,7].

2001: first applications of electron tomography to HAADF-STEM and spectroscopic (EFTEM, EDX) images by Midgley/Weyland [14] and Möbus [15]

1999: development and application of 3D HAADF-STEM system for nanomaterials by RIKEN, JAEA, Nagoya Univ., Kogakuin Univ., and HITACHI

Timeline

1917: formulation of mathematical base for tomographic techniques by Radon (*Radon Transform*)

1960's: development of X-ray computerized tomography (*1979 Noble Prize for Cormack and Haunsfield*)

1990's: development of automated TEM tomography by Agard [18] and Baumeister [19]

1990: first commercial systems enable data acquisition in ~4 h

2001: development of pre-calibration electron tomography by Koster/Ziese [20,21]

2001: commercial systems making use of pre-calibration enable improved accuracy and data acquisition in ~30–60 min

Computed tomography (CT)

Object (2D) → Projection (1D) → Back projection (2D)

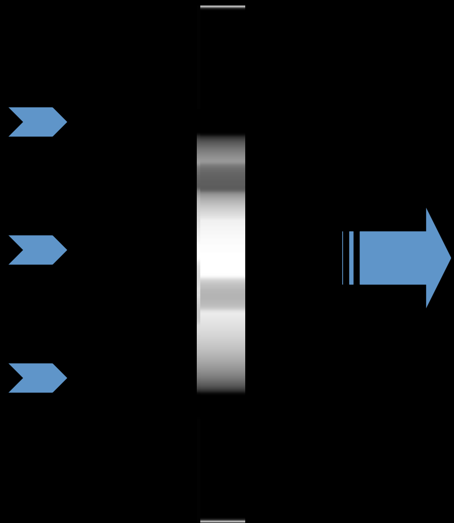

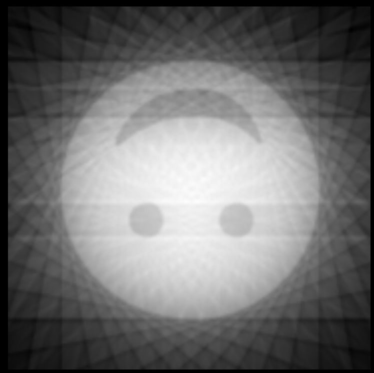

Courtesy of Mr. Furukawa in System In Frontier

Projection requirement

For a correct tomographic 3D reconstruction, the image intensity should be monotonic functions of physical properties of the specimen (density, thickness, degree of order, etc.).

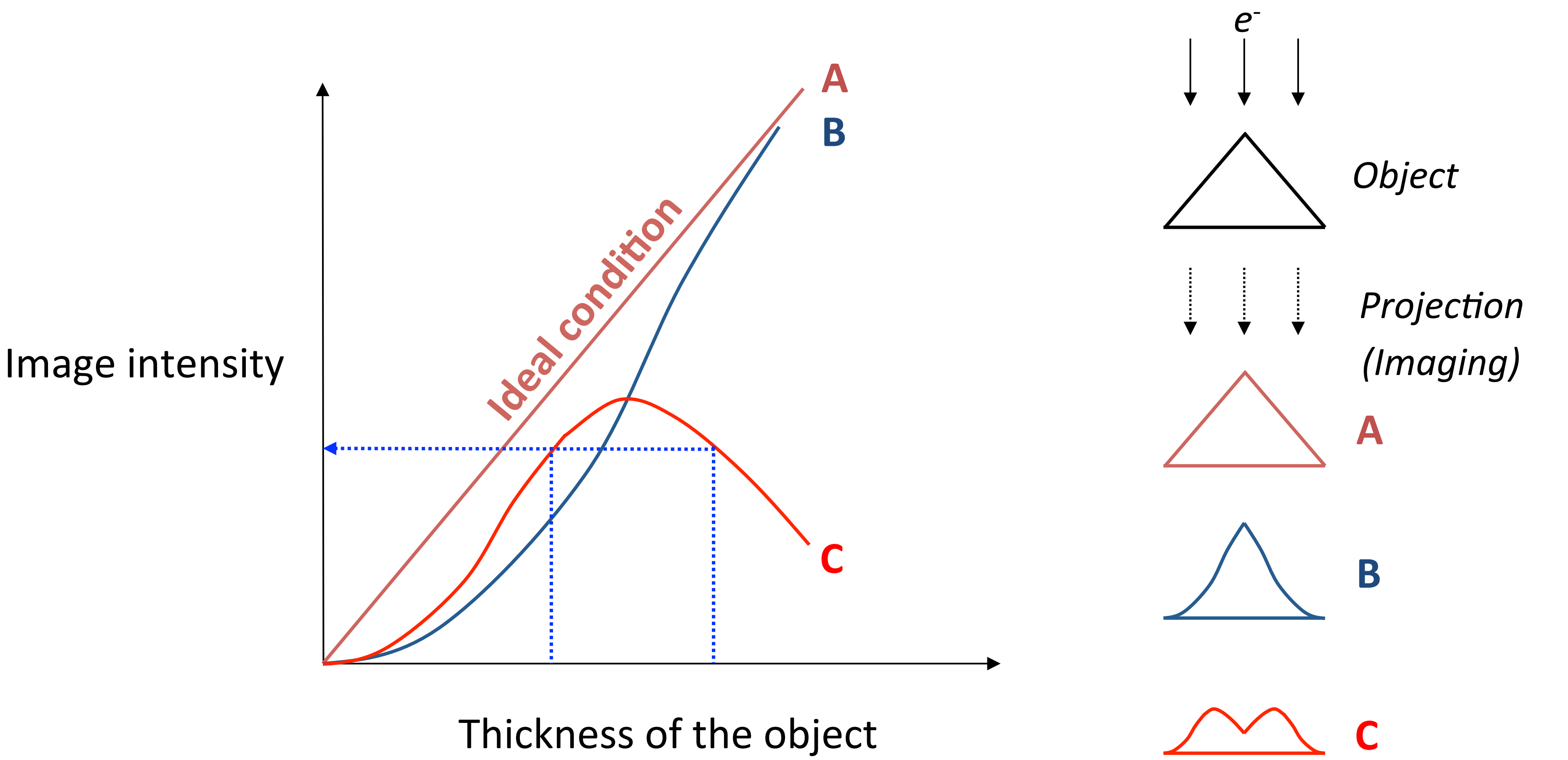

Midgley & Weyland, *Ultramicroscopy*, **96** (2003), 413.

Mass-thickness contrast and diffraction contrast of TEM image

Mass-thickness (absorption) contrast
Heavy, thick ➔ dark
Light, thin ➔ bright

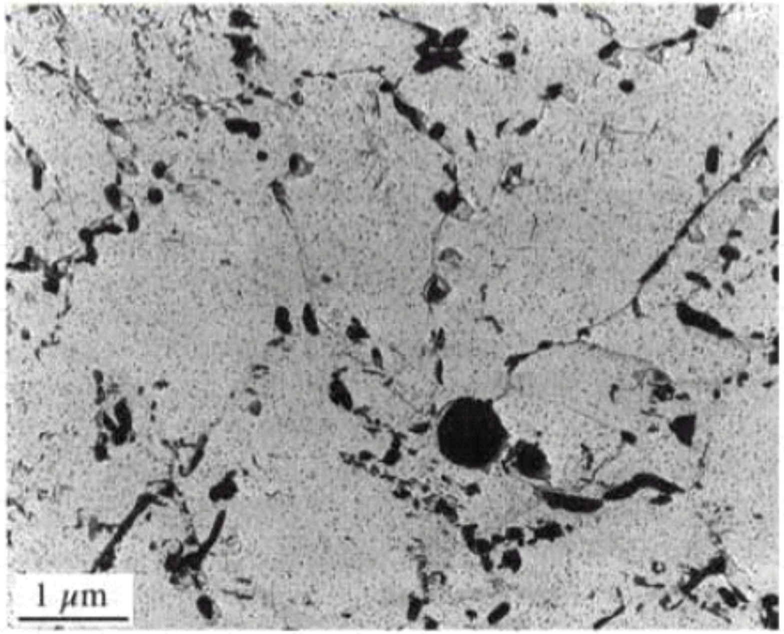

Bright-field TEM image of metal carbides on amorphous carbon film

Diffraction contrast
On Bragg condition ➔ dark
Off Bragg condition ➔ bright

Bright-field TEM image of polycrystalline aluminum (Direct mag.: x15,000)

HVEM Laboratory, Kyushu University

Diffraction contrast tilt-series

Nano-grained Cu by high-pressure torsion process

Even if the Bragg condition is satisfied (central grain), the projection requirement is violated.

To be submitted

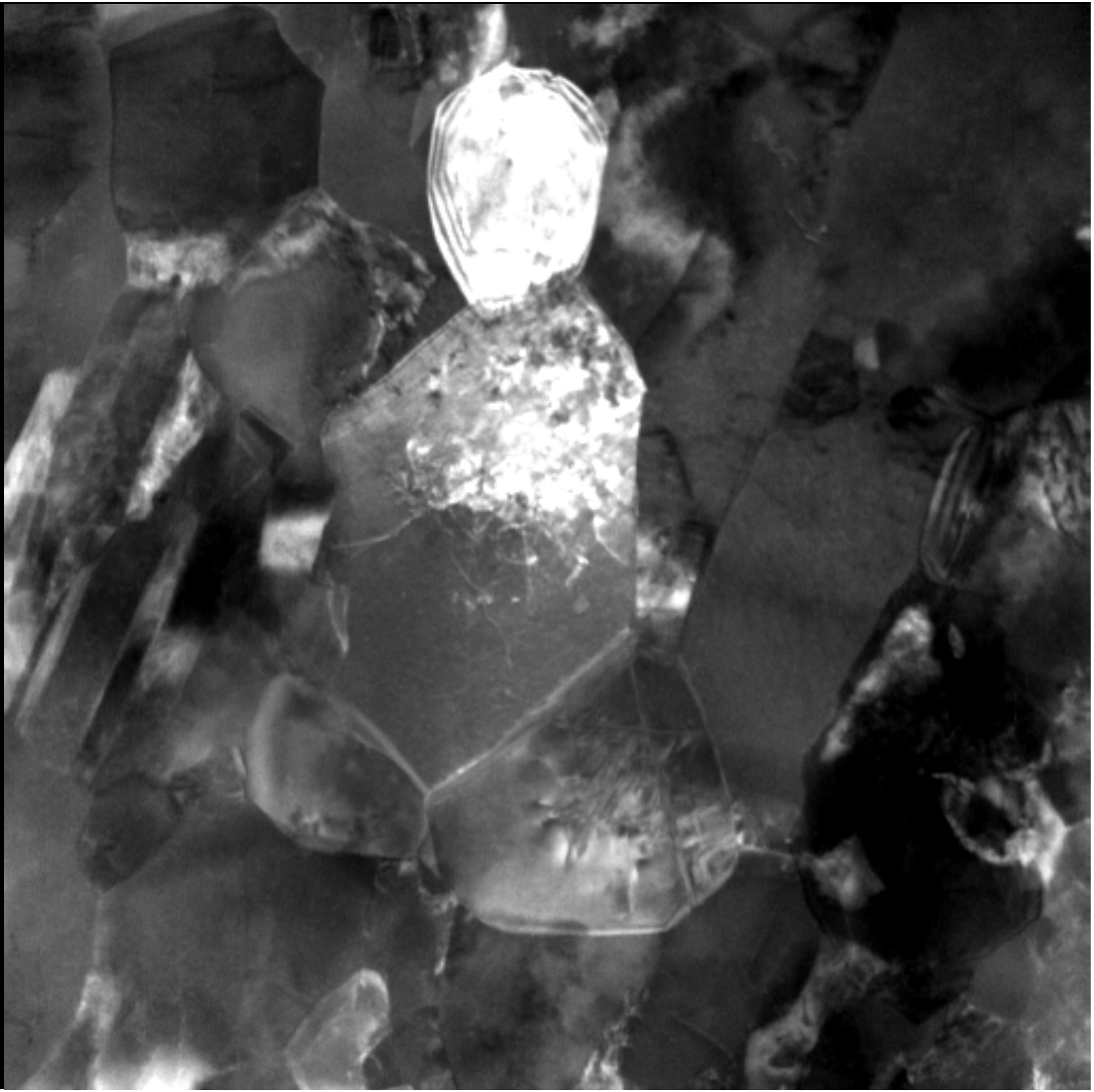

Scanning transmission electron microscopy (STEM)

Convergent-beam electron diffraction pattern formed on STEM detectors

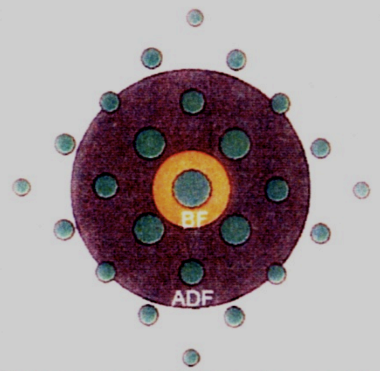

Alignment of diffraction pattern on BF/DF

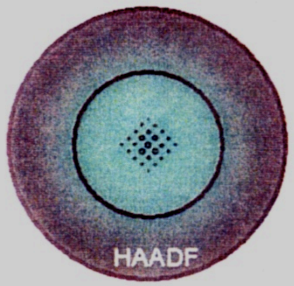

Alignment of diffraction pattern on HAADF

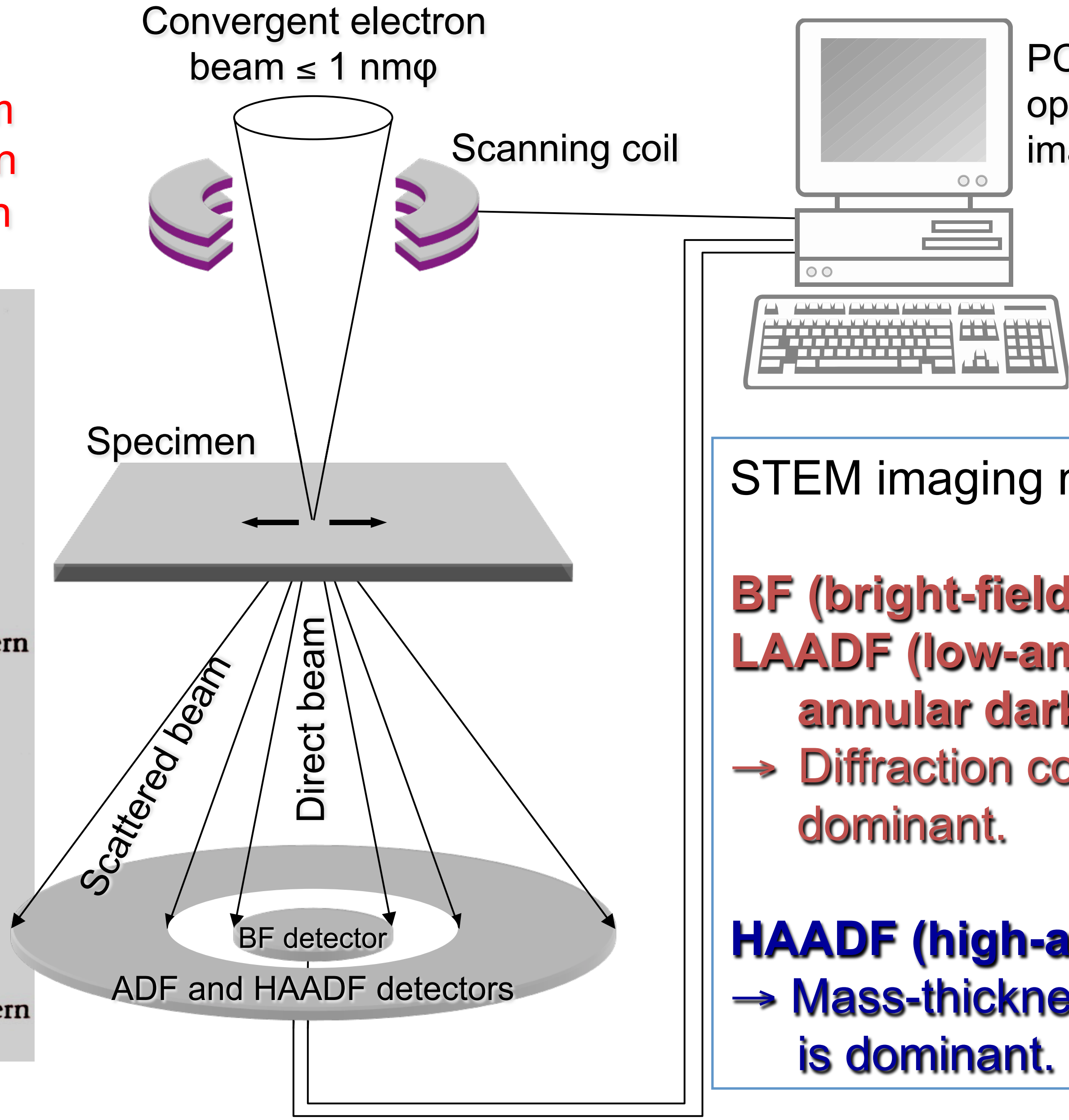

STEM imaging modes:

BF (bright-field)
LAADF (low-angle annular dark-field)
→ Diffraction contrast is dominant.

HAADF (high-angle ADF)
→ Mass-thickness contrast is dominant.

STEM imaging

Fe-3 mass% Cu alloy

BF (Diffraction)

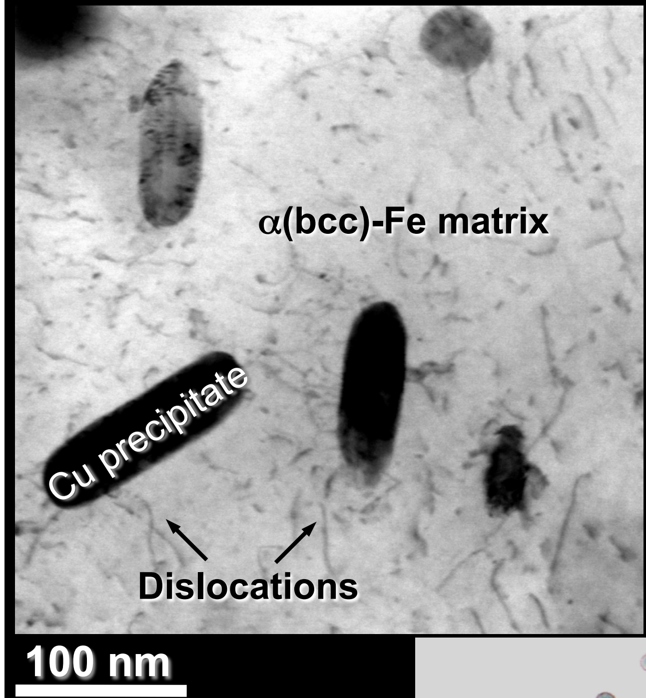

LAADF (Diffraction)

HAADF (Mass-thickness)

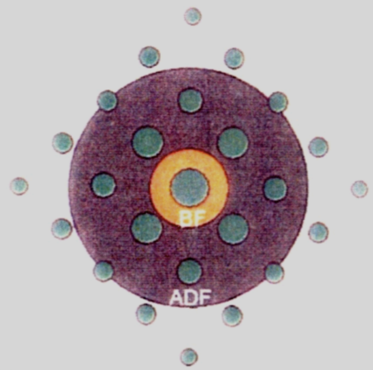

Alignment of diffraction pattern on BF/DF

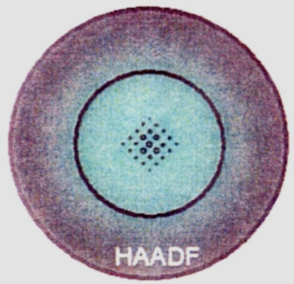

Alignment of diffraction pattern on HAADF

HAADF STEM tomography

ZrO_2 particles in Pt-Rh alloy

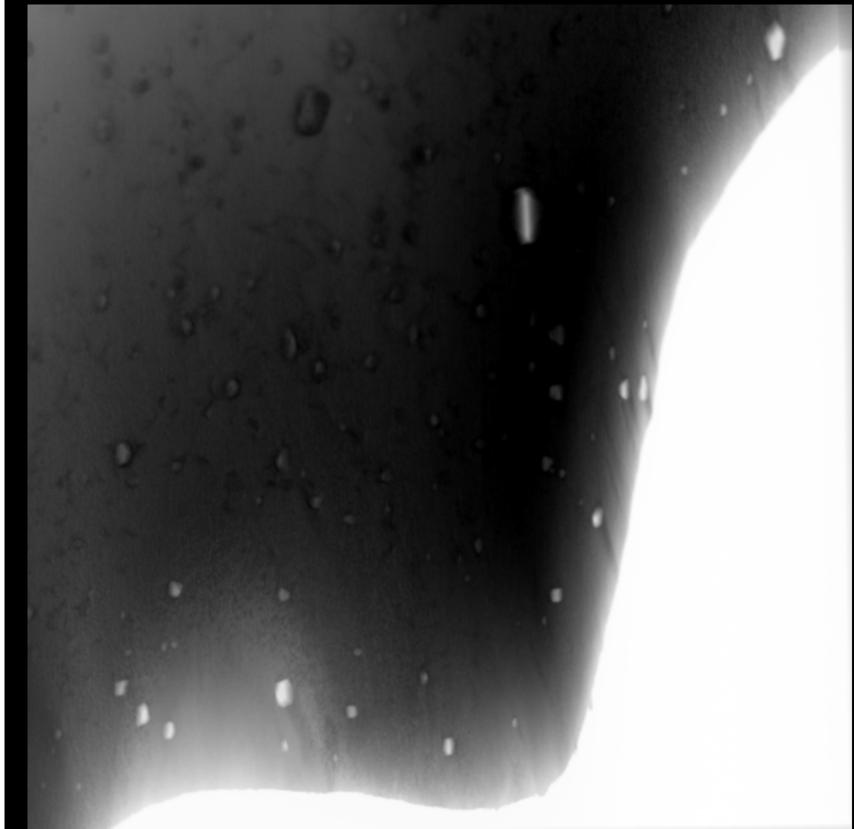

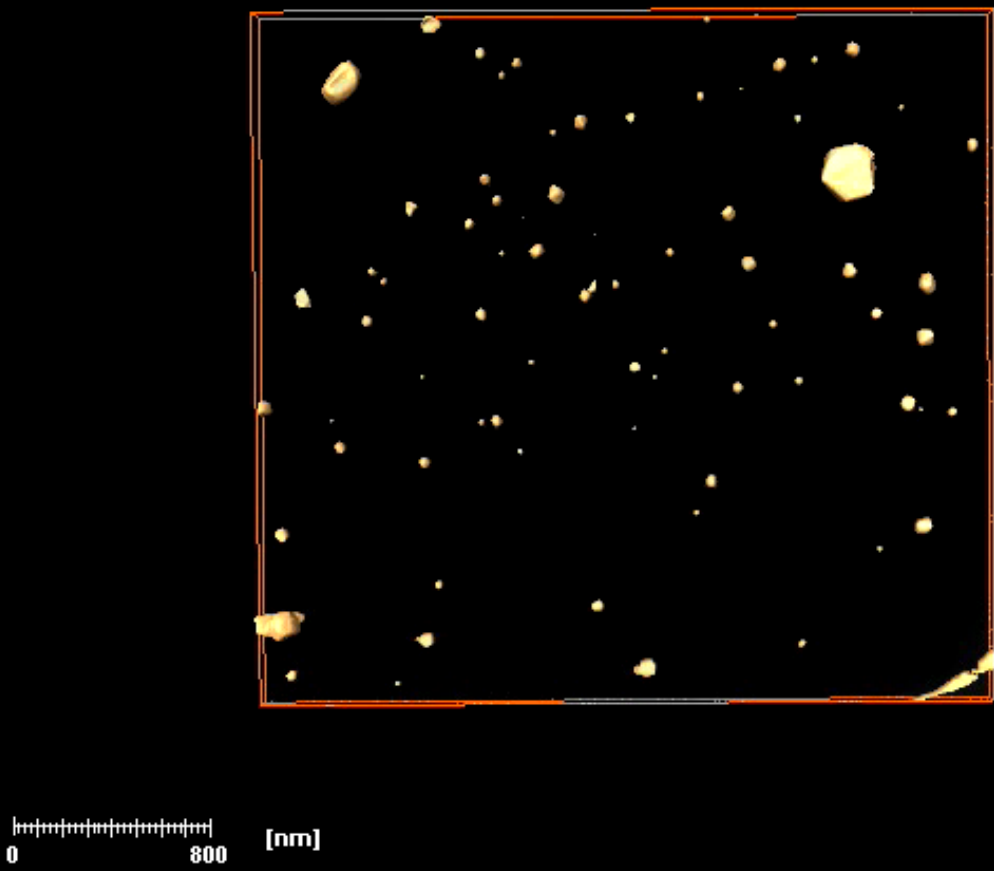

Contrast reversed

Strong mass-thickness contrast

Weak diffraction contrast

Mitsuhara and Tomita, *in preparation*

HAADF-STEM tomography (Cambridge)

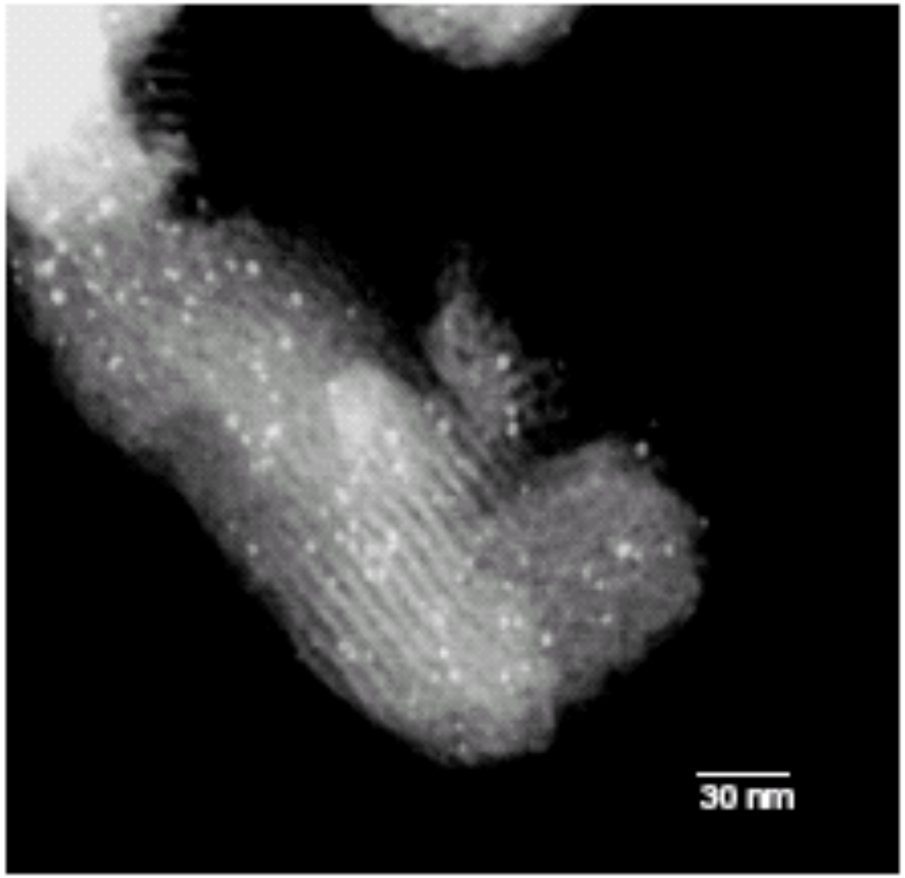

Fig. 7. A typical STEM HAADF image of a heterogeneous catalyst composed of Pd_6Ru_6 nanoparticles (about 1 nm diameter) and an MCM-41 mesoporous silica support with mesopores of approximately 3 nm diameter.

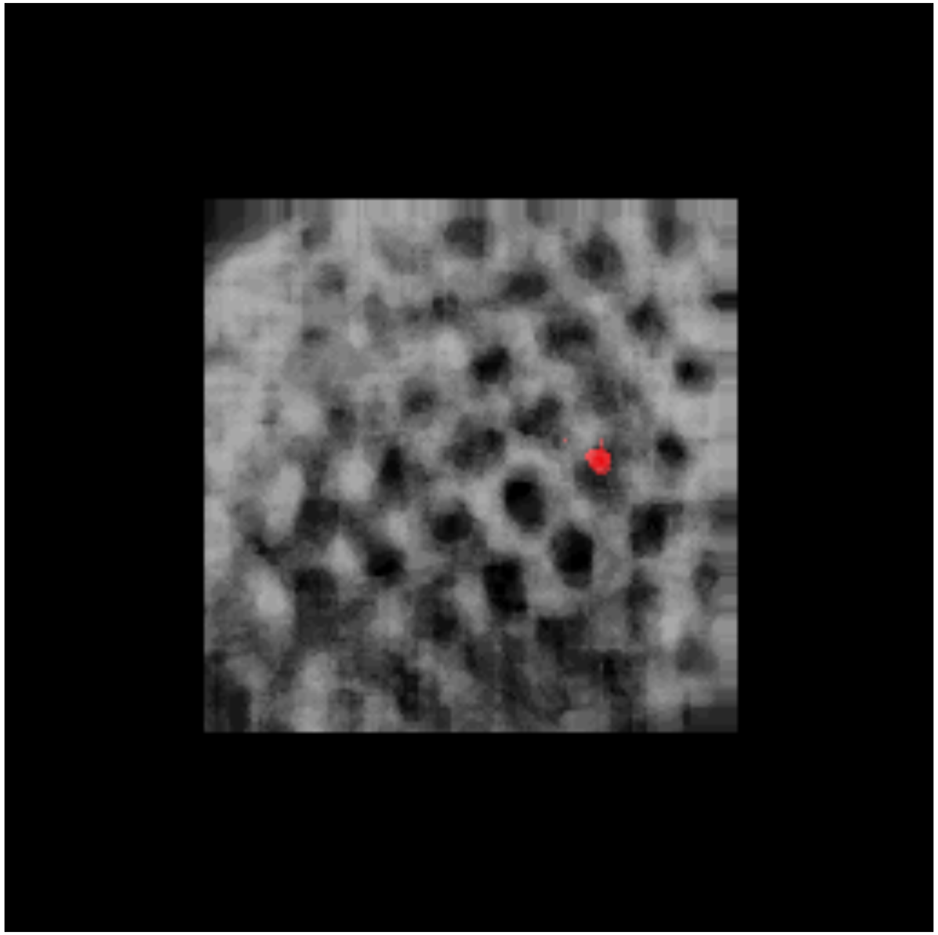

Midgley & Weyland, *Ultramicroscopy*, **96** (2003), 413.

HAADF-STEM tomography (National project in Japan from 1997)

Three-dimensional STEM for observing nanostructures
M. Koguchi, H. Kakibayashi, R. Tsuneta, M. Yamaoka, T. Niino, N. Tanaka, K. Kase and M. Iwaki
Journal of Electron Microscopy, 50, 235-241 (2001)
See PDF (copyright protected)

Koguchi *et al.*, *J. Electron Microscopy*, **50** (2001), 235.

ET for metallic materials

Measuring shear deformation of precipitates in Al-Ag alloy after severe plastic deformation by ECAP process

Inoke *et al.* Acta Mater. (2006)

STEM-HAADF Z-contrast imaging

Resolution
5~10 nm

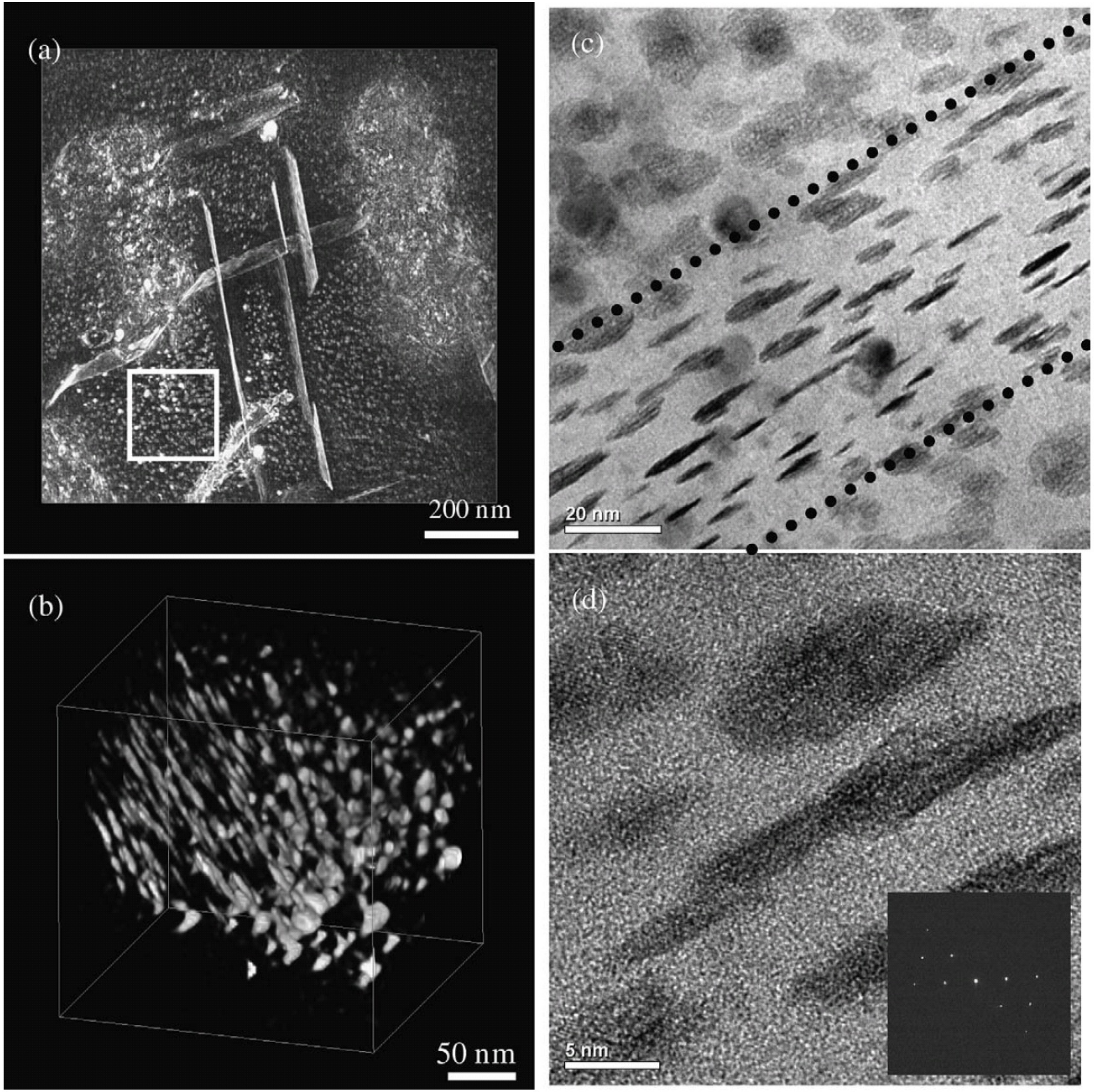

Diffraction contrast imaging

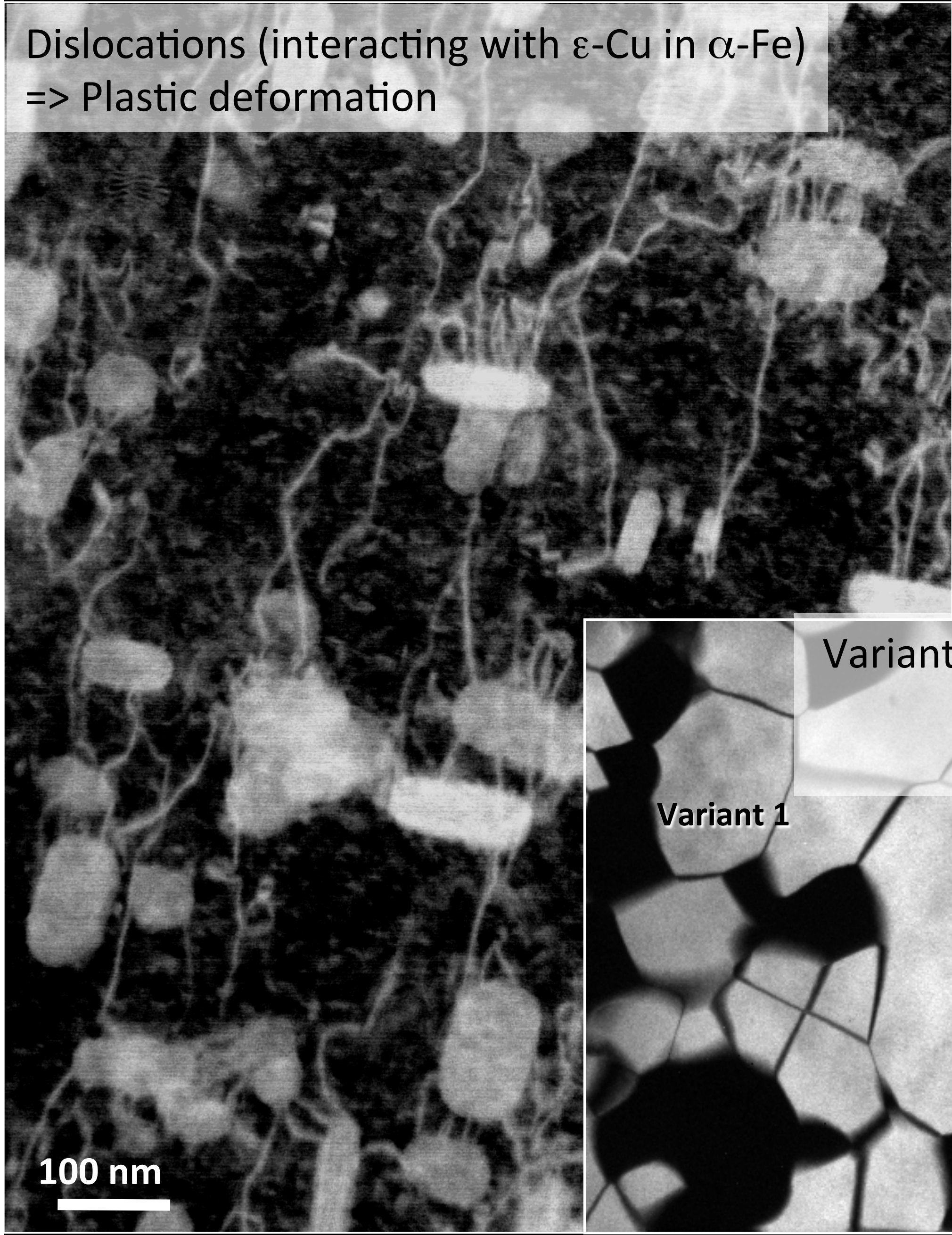

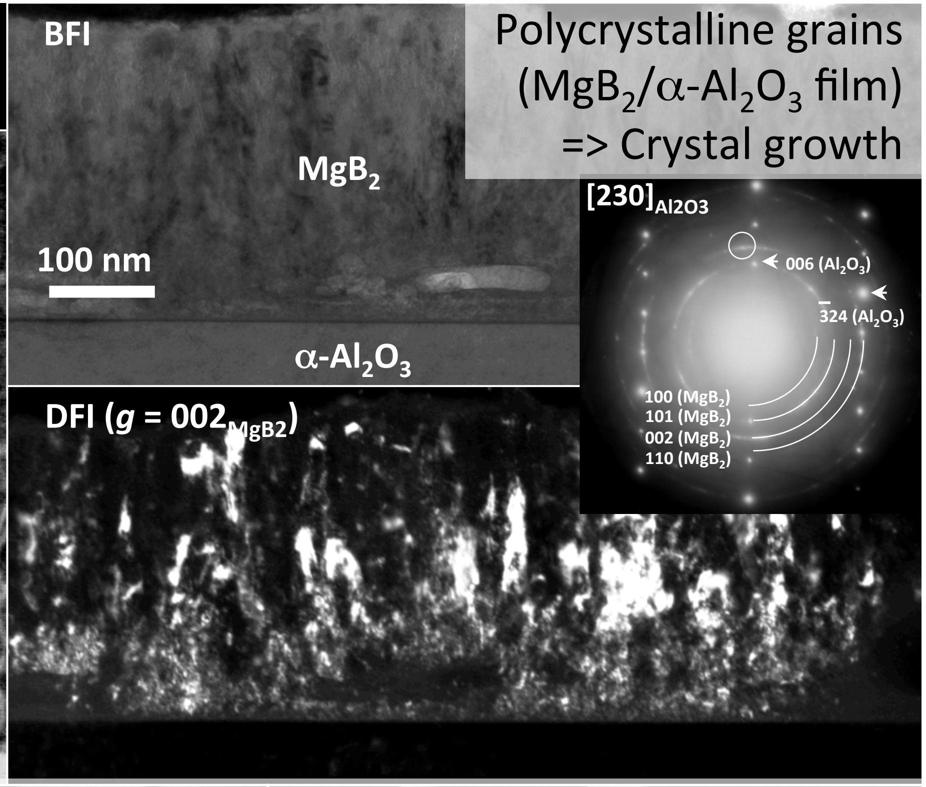

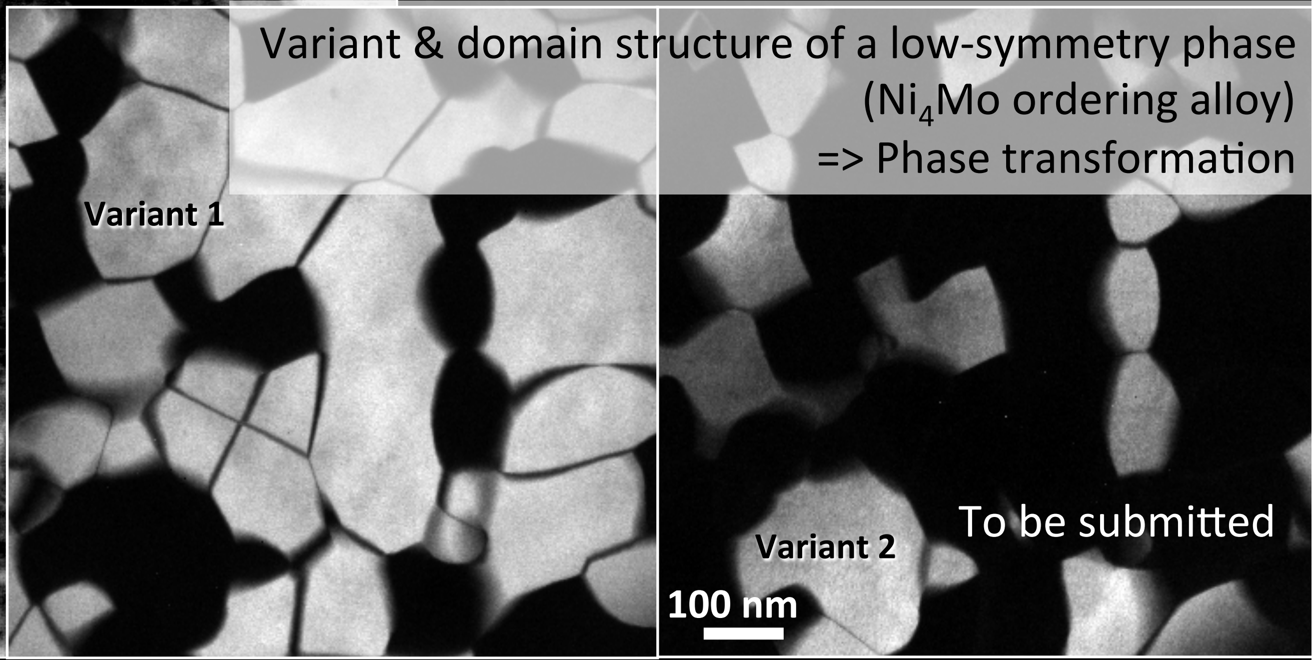

Imaging a variant of tetragonal Ni_4Mo ($D1_a$ ($I4/m$)) in Ni-Mo alloy using dark-field TEM

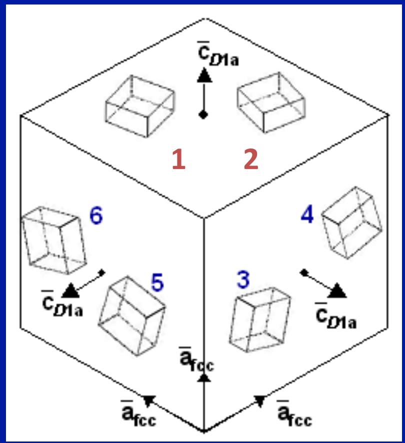

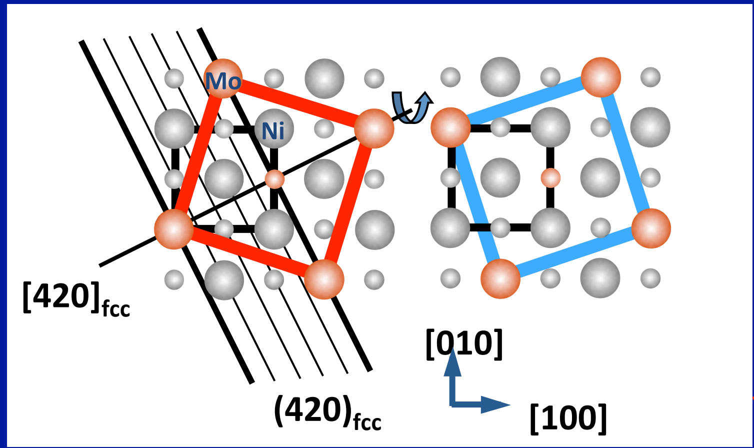

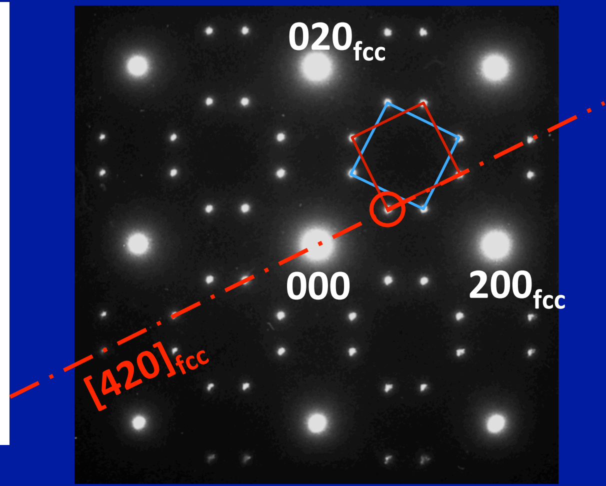

Solid solution -> 800 ℃-0.2 h

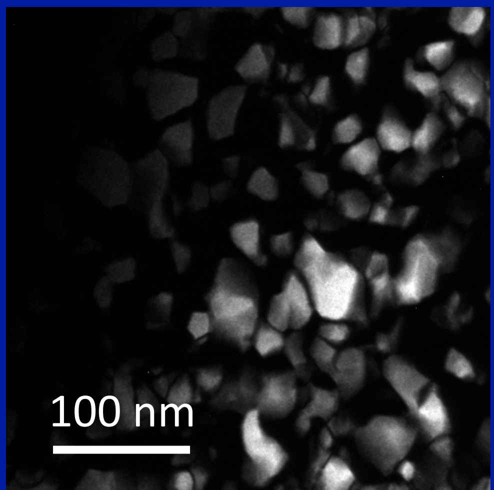

800 ℃-2 h

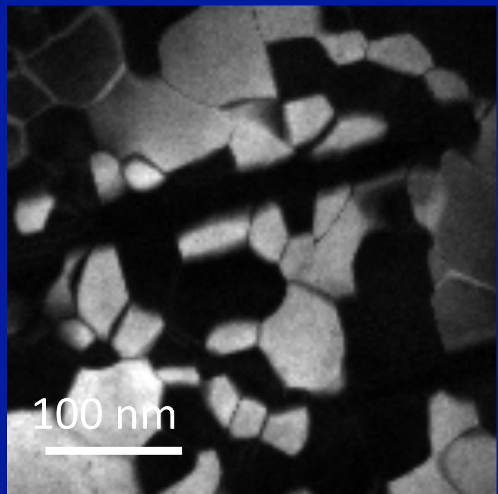

800 ℃-24 h

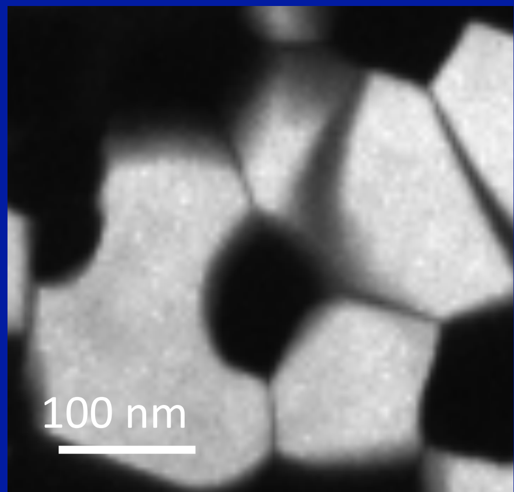

To be submitted

Superlattice reflection imaging (calculation)

$D1_a$ (Tetragonal, $I4/m$) type Ni_4Mo superlattice structure

Bragg condition under systematic excitation, 5% absorption of fast electrons

g = 200 (fundamental lattice reflection)

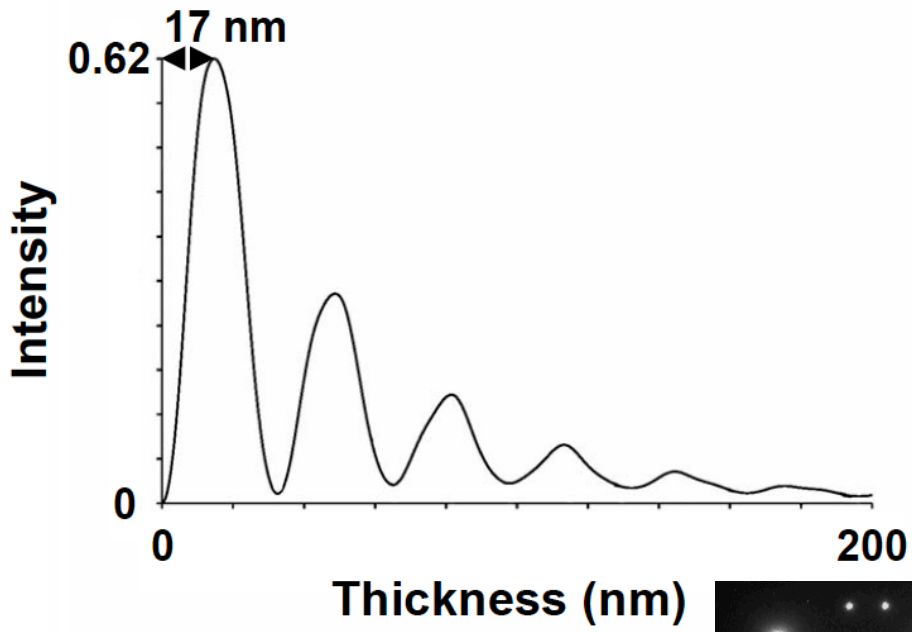

g = 4/5,2/5,0 ($D1_a$ superlattice reflection)

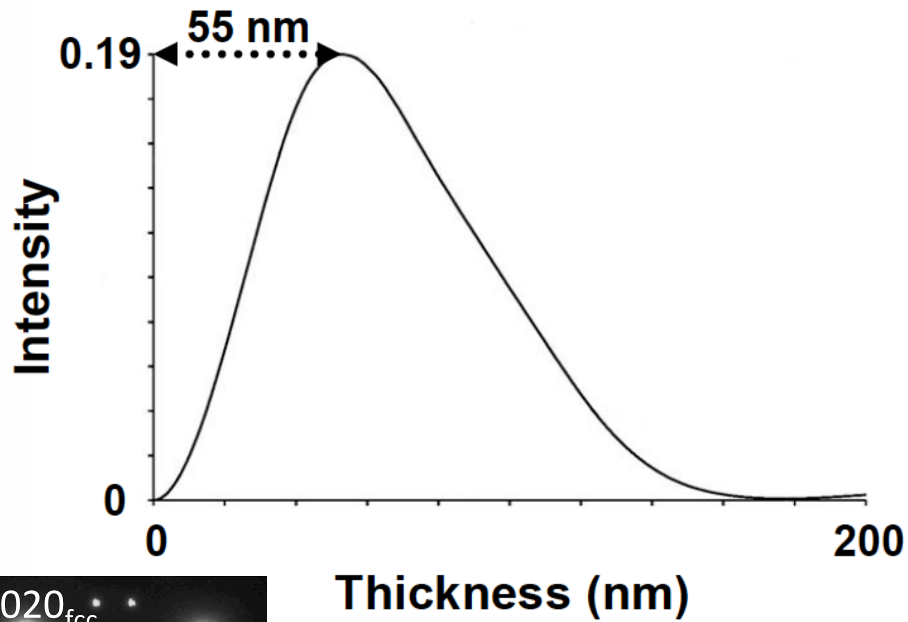

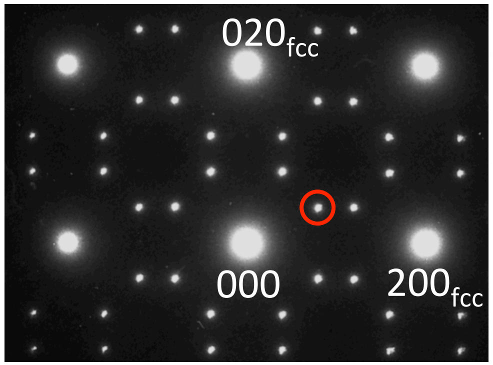

To be submitted

Steps of diffraction-contrast tilt-series acquisition

[001] diffraction pattern

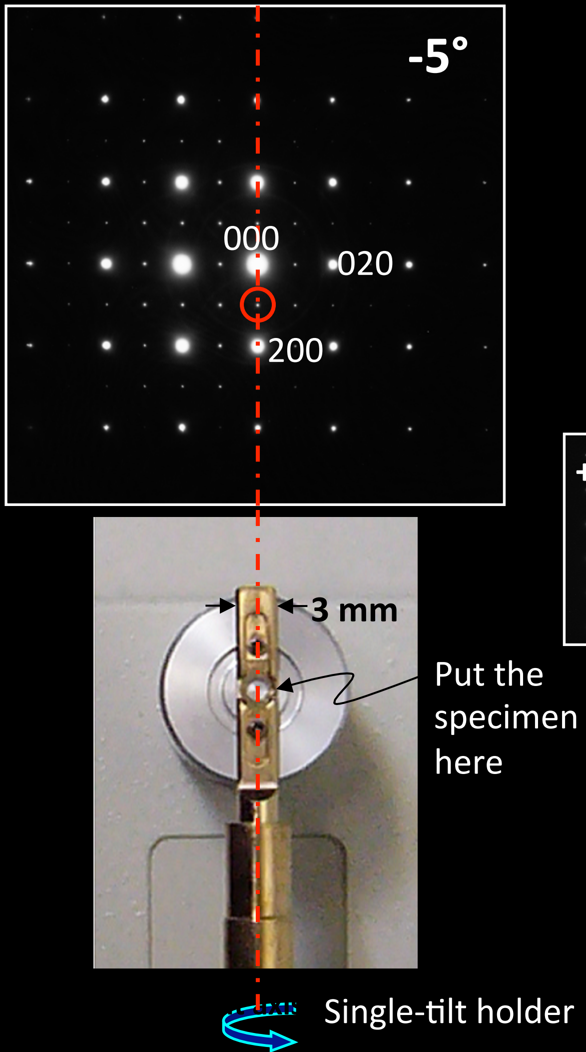

Set a specimen. The diffraction vector should be parallel to the specimen-tilt axis. Here, a superlattice reflection (○) is always excited during a tilt-series acquisition.

→ A rotation stage is convenient for the specimen setting.

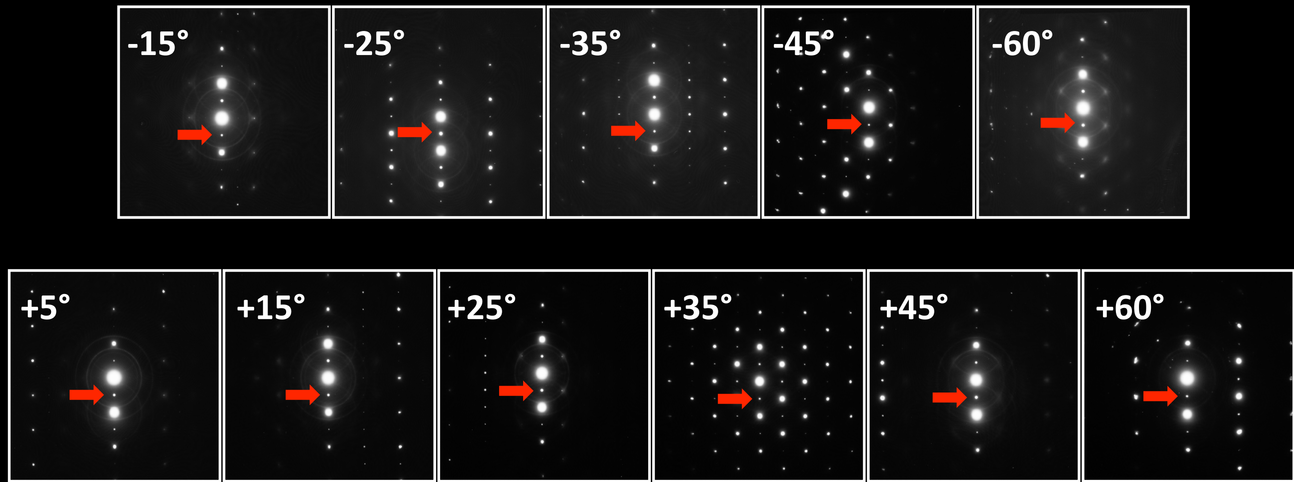

For the single-tilt (& rotation) tomography holder, a perfect setting of the diffraction condition is difficult due to the lack of a double-tilt function.

Kimura, Hata, Matsumura, Horiuchi: *J. Electron Microscopy* (2005)

DF TEM tilt series with unsatisfactory diffraction alignment

Ni_4Mo superlattice domains (tetragonal, *I*4/*m*) in Ni-18 at% Mo (fcc, $Fm\bar{3}m$) alloy

Projection requirement violated due to deviation from Bragg condition

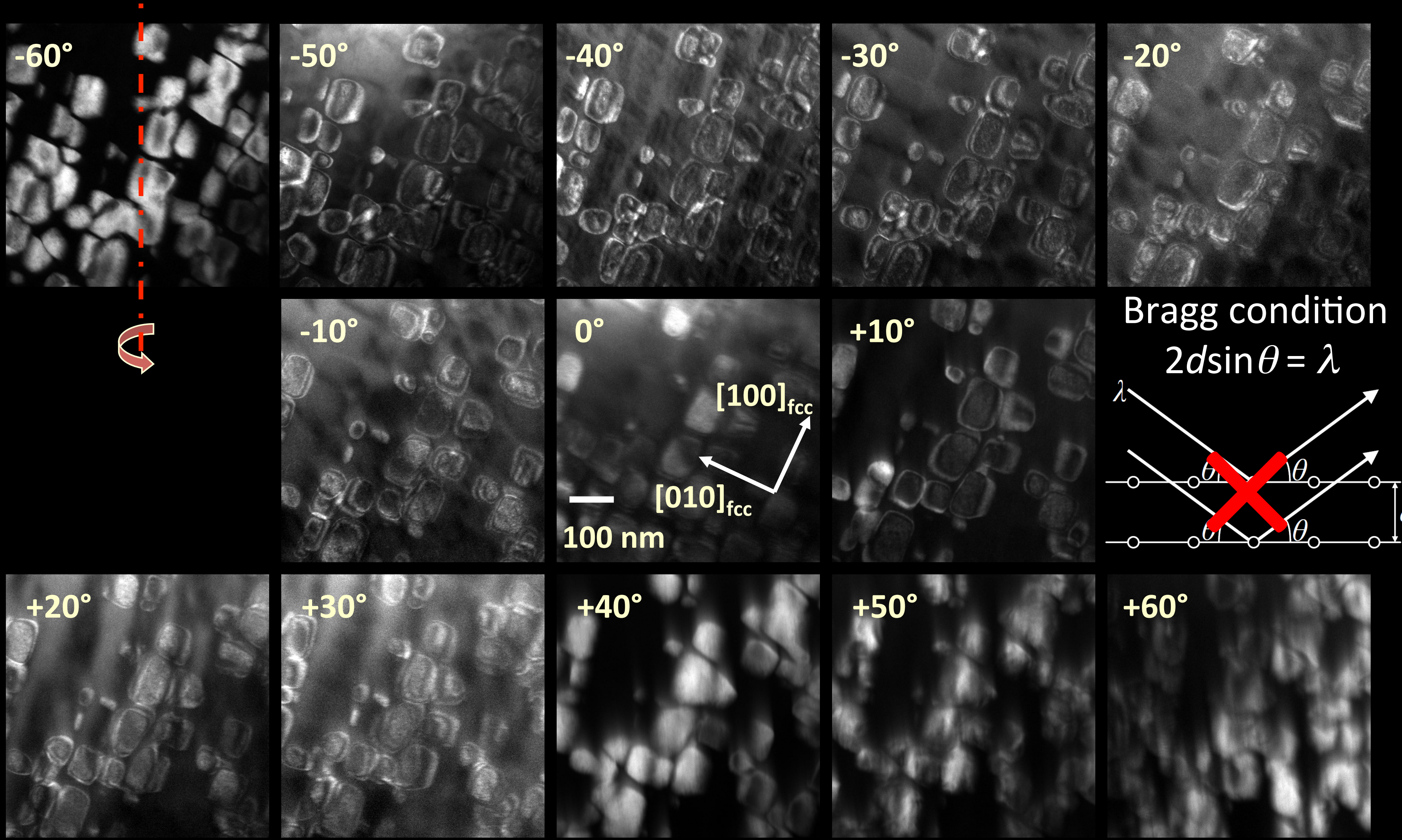

Realignment of the diffraction condition by tilting the incident electron beam

To keep the exact Bragg condition

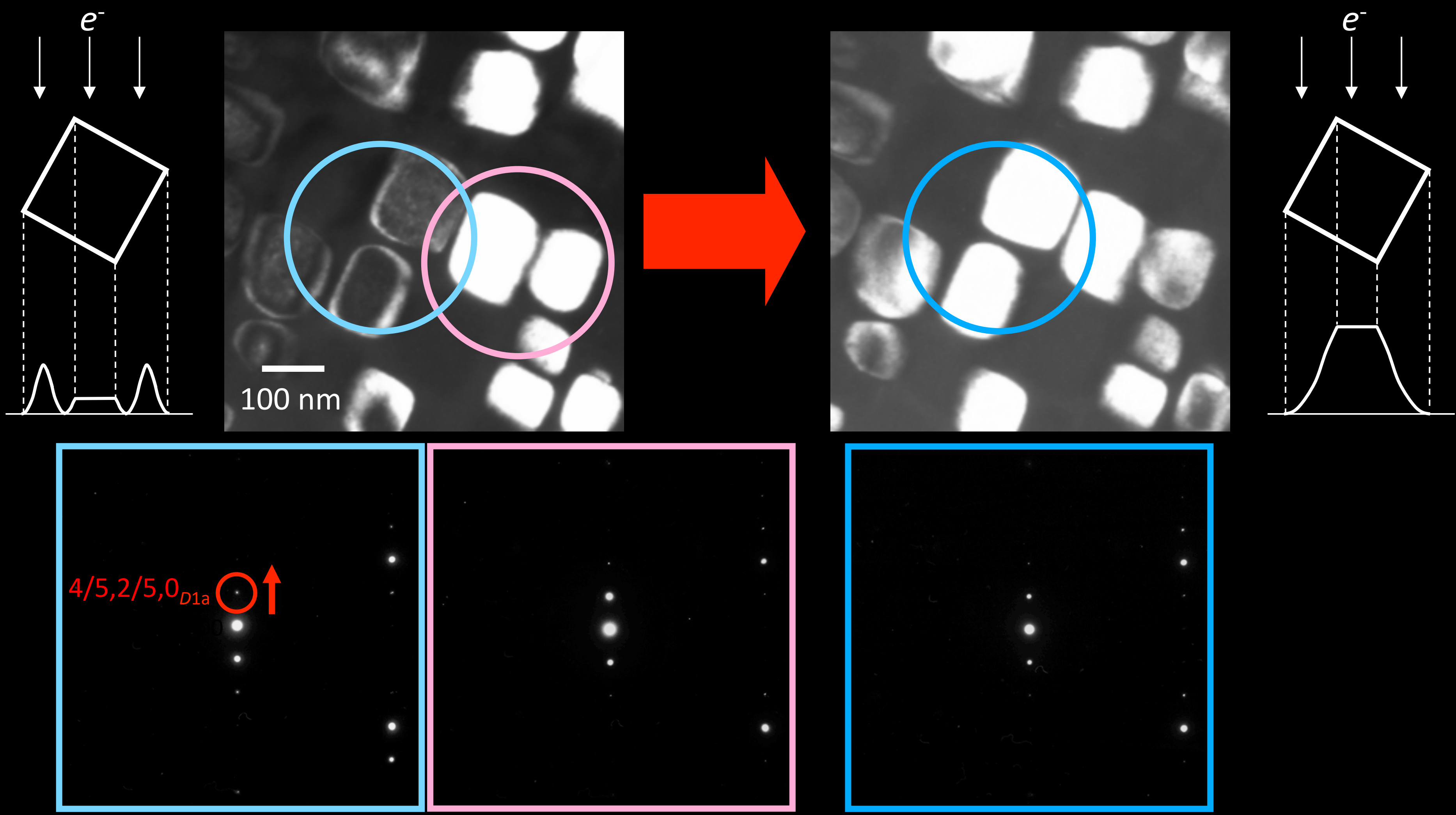

Kimura, Hata, Matsumura, Horiuchi: *J. Electron Microscopy* (2005)

Violation of the projection requirement (Ni_4Mo precipitates)

Thickness contours under a zone-axis illumination condition

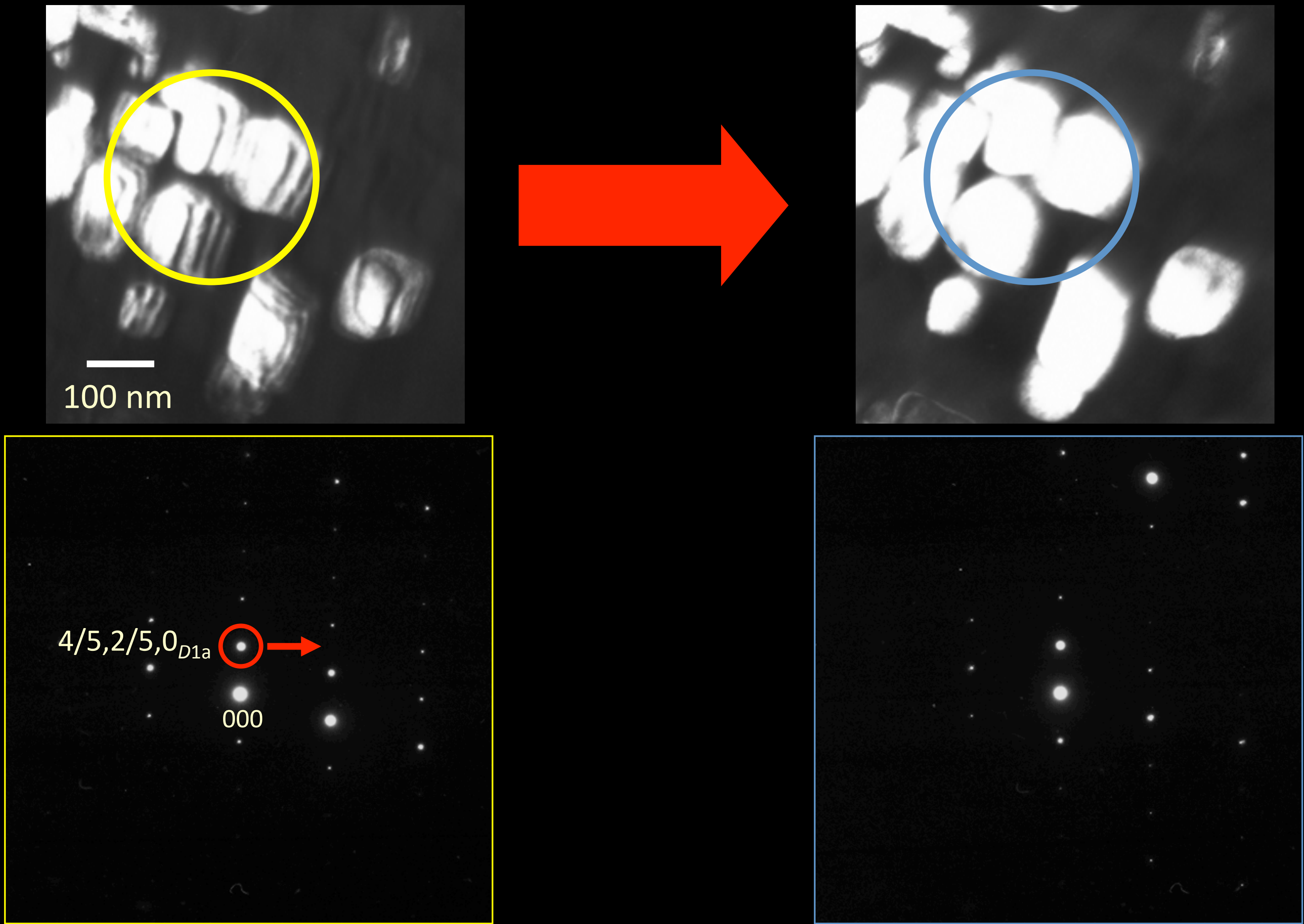

Near $[1\text{-}23]_{fcc}$

Kimura, Hata, Horiuchi, Matsumura: *JEM* (2005)

DF TEM tilt series with fine diffraction alignment

Image intensity may be nearly a monotonic function of crystal thickness.

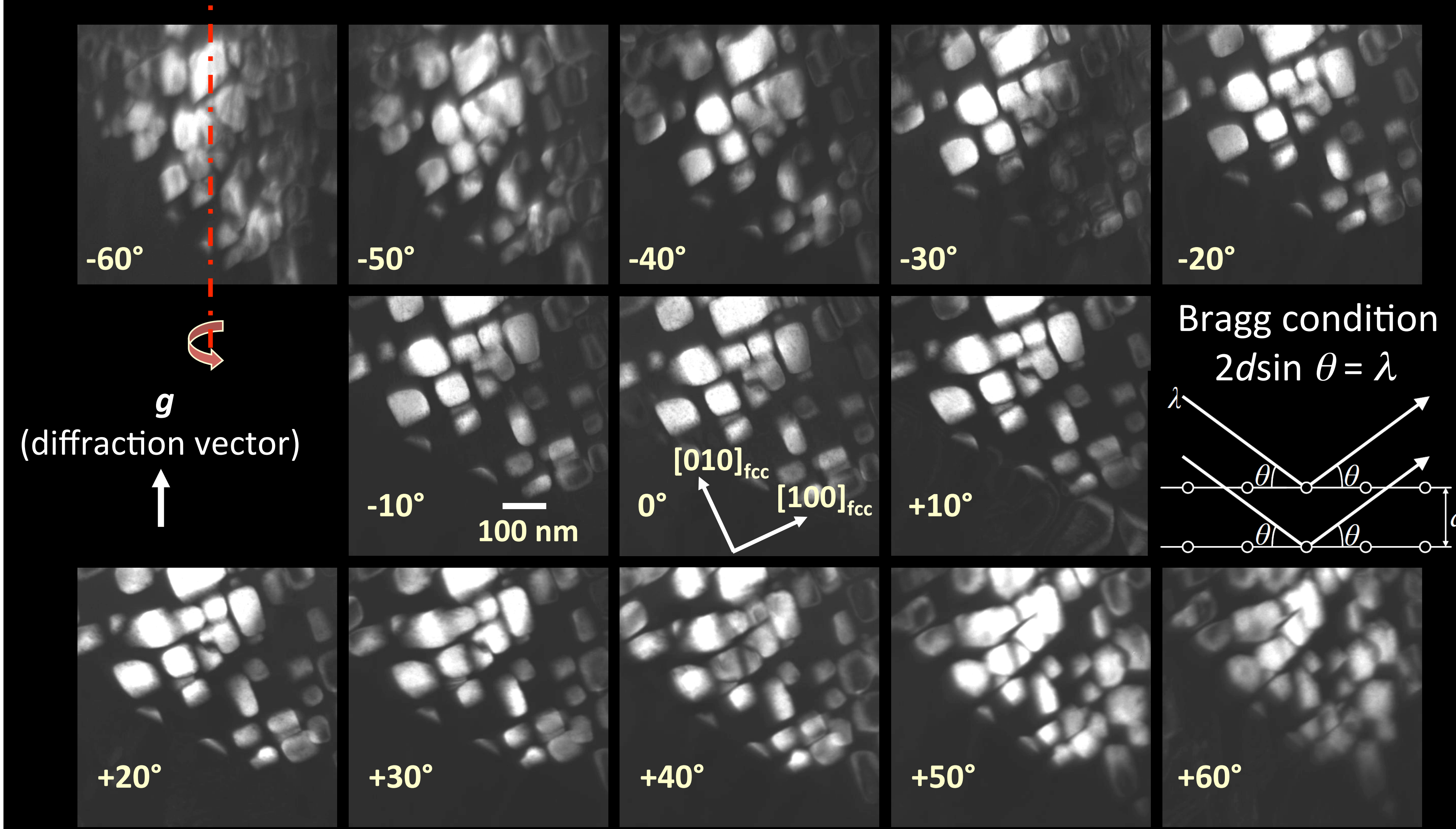

Kimura, Hata, Matsumura, Horiuchi: *J. Electron Microscopy* (2005)

Diffraction alignment important for reliable tomographic reconstructions

Ni_4Mo superlattice domains (tetragonal, $I4/m$) in Ni-Mo (fcc, $Fm\bar{3}m$) alloy

With unsatisfactory diffraction alignment

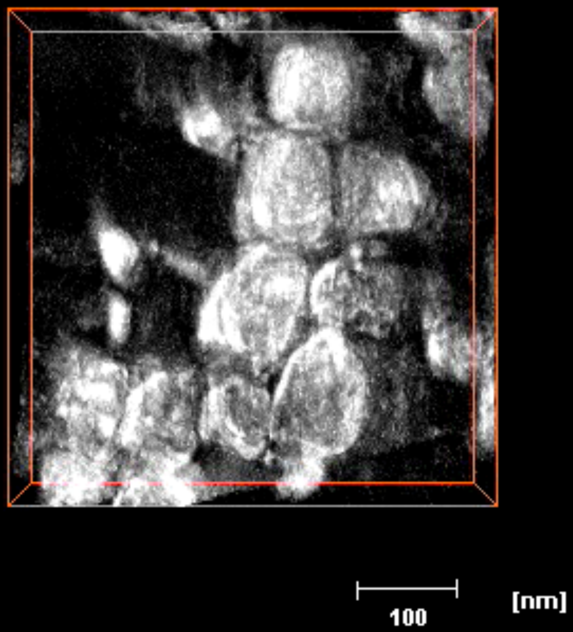

With fine diffraction alignment

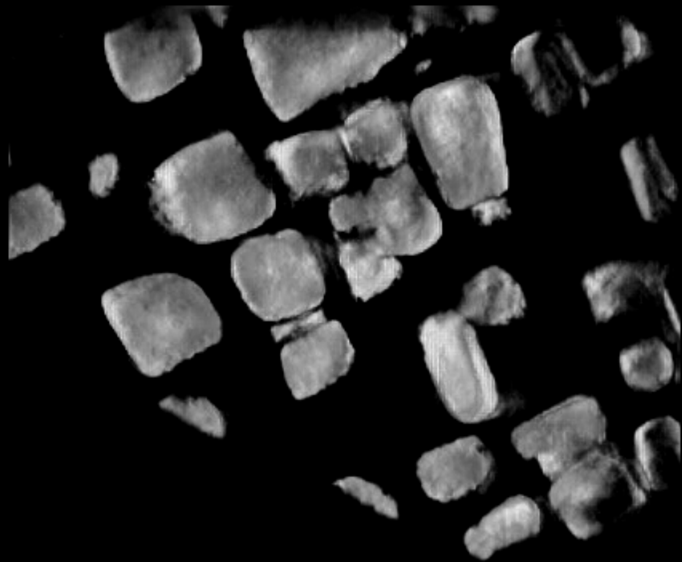

2005 JACQUET-LUCAS AWARD

Tomographic Dark-Field TEM Observation of Ordered Precipitates in a Ni–Mo Alloy

Kosuke Kimura, Takao Horiuchi, Satoshi Hata, Syo Matsumura
Kyushu University, Japan

A solution-treated Ni-Mo alloy (18 at.% Mo) was annealed at 1073K for 24 hours to obtain a two-phase nanostructure composed of the nickel matrix with a face-centered cubic (fcc) structure, and Ni_4Mo precipitates with a *D*1a body-centered tetragonal superstructure (Fig. 1(a)) .When the Ni4Mo precipitates are formed in the nickel matrix, six types of orientation relationships exist between the precipitates and the matrix (Fig.1(b)).

- The etchant was an electrolysis polishing solution with composition $CH_3OH : H_2SO_4 = 3:1$.
- The magnification of the dark-field image was 26000X.

Visualization of nanostructures

Figures 2, 3, and 4 show the first successful visualization of three-dimensional (3D) crystalline nanostructures. Made by an electron tomography technique, these images show the orientation variants of ordered domains in a nickel-molybdenum alloy.

Up to now, the electron tomography of such crystalline nanostructures has been considered impossible because of the diffraction effects of electrons in crystals. We succeeded in obtaining a tilt series of dark-field transmission electron microscopy (DF-TEM) images by accurately controlling the diffraction condition and by reconstructing the 3D views of the orientation variant. This work would be informative to scientists and engineers working in various fields, who are interested in 3D nanostructures in crystalline materials and devices.

The Jacquet-Lucas Award is presented to the best entry in the annual International Metallographic Contest, by the International Metallographic Society, an Affiliate Society of ASM International.
The award consists of $3000.
Deadline for entries in the 2006 competition is July 17.
For more information, please visit www.internationalmetallographicsociety.org.

Detailed procedures

Figure 1: A crystal structure of *D*1a-ordered Ni_4Mo precipitates.

- **(a)** [001] projection views of the fcc-based *D*1a superstructure. Large and small circles indicate different (002) layers in the fundamental fcc lattice. The *D*1a unit cells of variants 1 and 2 and the fcc unit cells are marked with red, blue, and black open squares, respectively.
- **(b)** Six orientation variants of the *D*1a structure.

Figure 2: Part of a tilt series of electron diffraction patterns in a Ni–18 at.% Mo alloy annealed at 1073K for 24 hours, and a photograph of the single-tilt specimen holder. The [420]fcc systematic row is set parallel to the tilt axis of the holder. As a result, the *D*1a superlattice reflection at *hkl* =4/5, 2/5, 0 is always excited in the tilt series, as indicated by the red arrows.

Figure 3: Part of a tilt series of DF-TEM images of the Ni_4Mo precipitates with one *D*1a variant. After realignment of the diffraction condition using a beam tilt function, the Ni_4Mo precipitates are clearly imaged at every step.

Figure 4 (a): Tomographic reconstructions from the tilt series in Fig. 3. Bright areas correspond to the Ni_4Mo precipitates with one *D*1a variant.

- **(b):** Enlarged Ni_4Mo precipitates in the selected area indicated with the red square viewed from different directions (a).
- **(c):** Schematic illustration of the Ni_4Mo precipitates with one *D*1a variant. Yellow objects and blue broken lines show the Ni_4Mo precipitates and the specimen edge, respectively.

For more information: Kosuke Kimura, Department of Applied Science for Electronics and Materials, Kyushu University, Fukuoka 816-8580, Japan; tel: 8192-583-7536; fax: 8192-583-7534; e-mail: kimurak4@asem.kyushu-u.ac.jp.

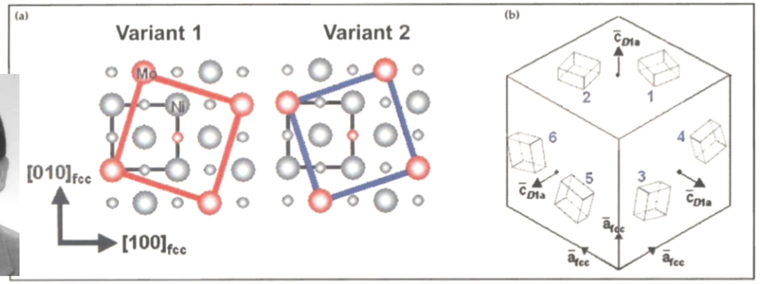

Figure 1

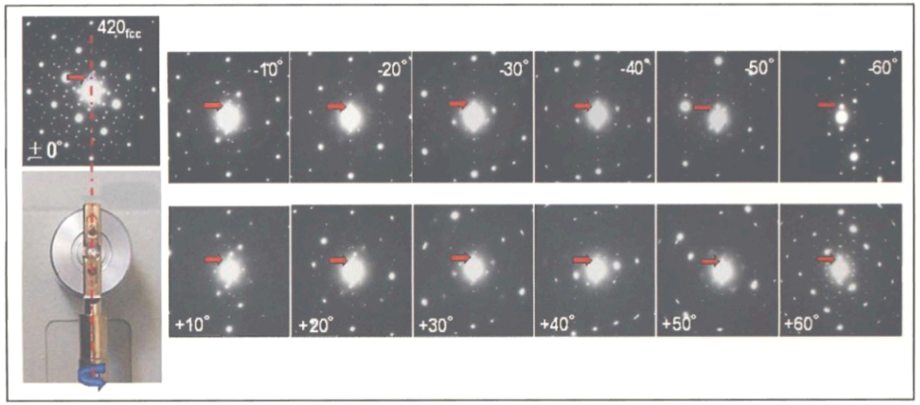

Figure 2

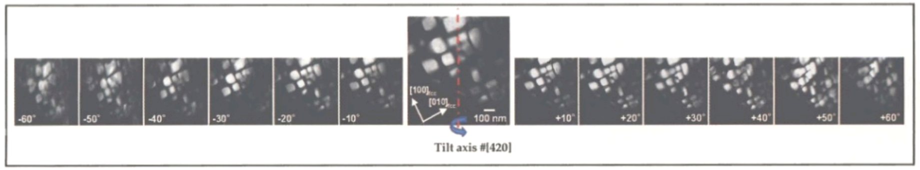

Figure 3

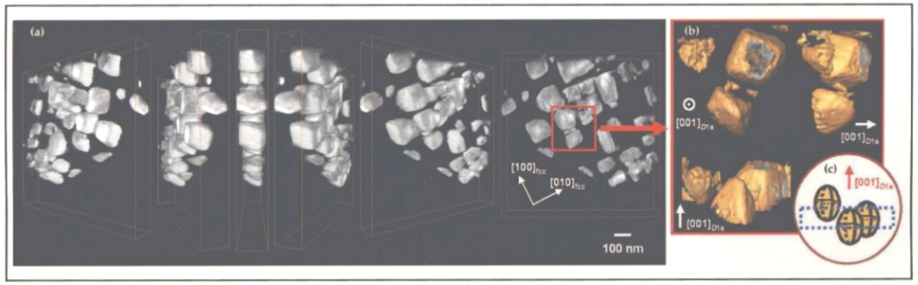

Figure 4

Weak-beam DF TEM tomography imaging of dislocations in GaN film

Use of image processing to reduce dynamical diffraction contrast

Unsatisfactory diffraction alignment during tilt-series acquisition

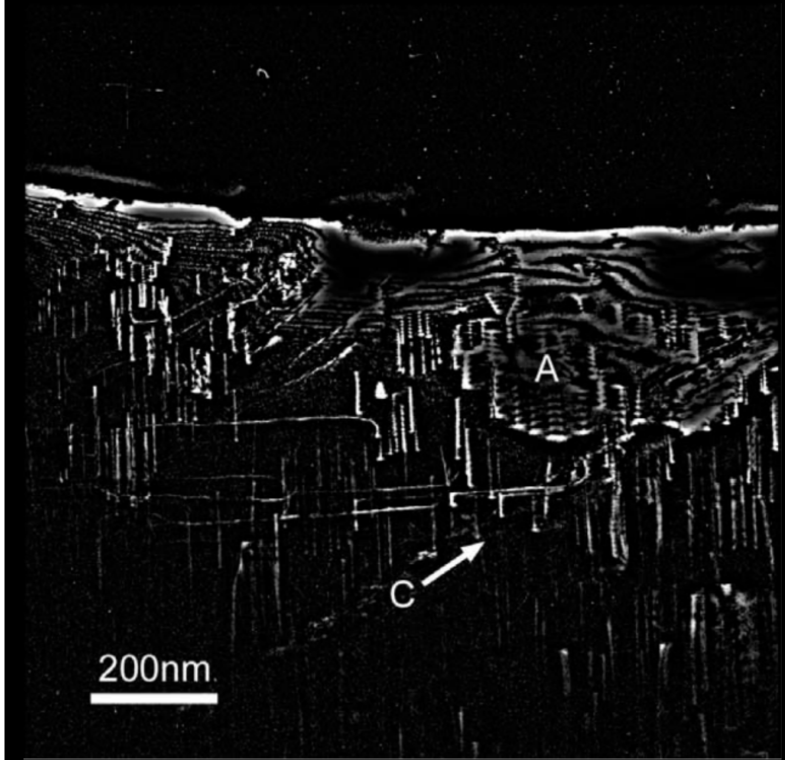

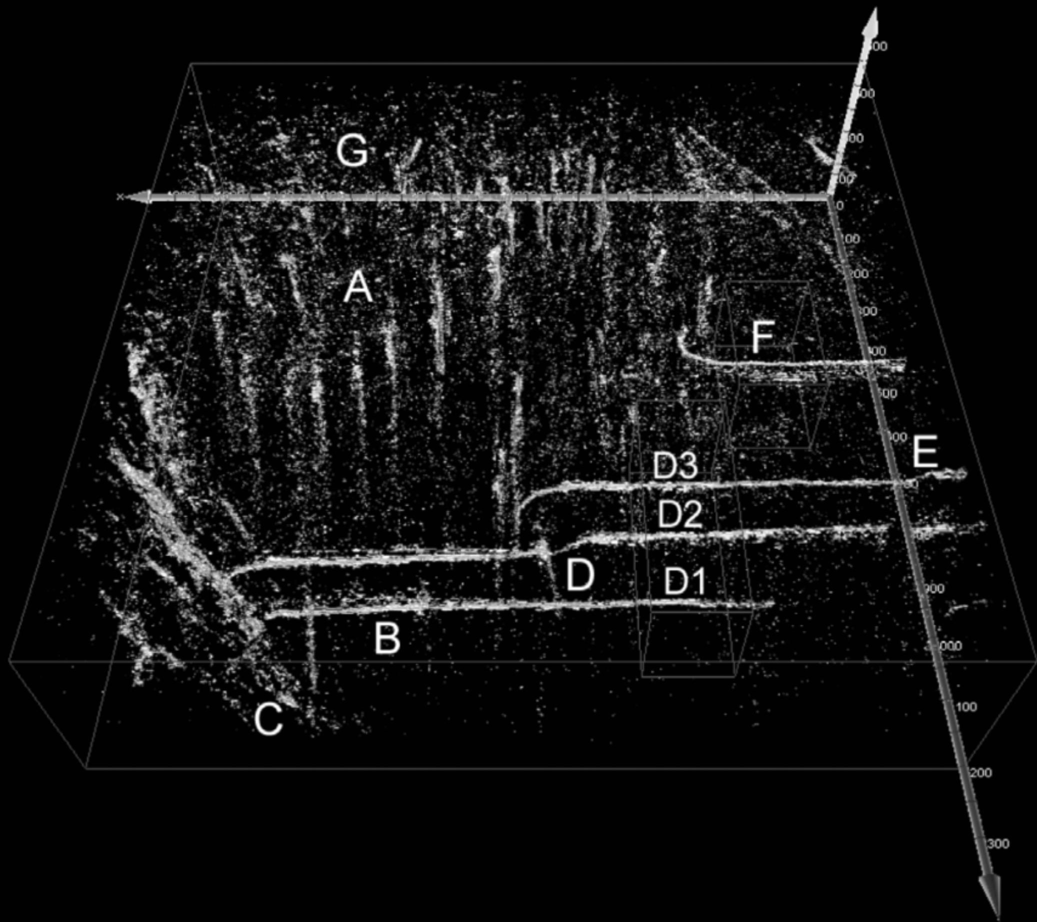

Barnard, Sharp, Tong, Midgley: *Science* (2006); *Philos. Mag.* (2006)

Collaboration on electron tomography for crystals with EM Group in University of Cambridge

17 October – 18 November 2005

P. A. Midgley, J. S. Barnard, J. R. Tong, J. Sharp, S. Hata

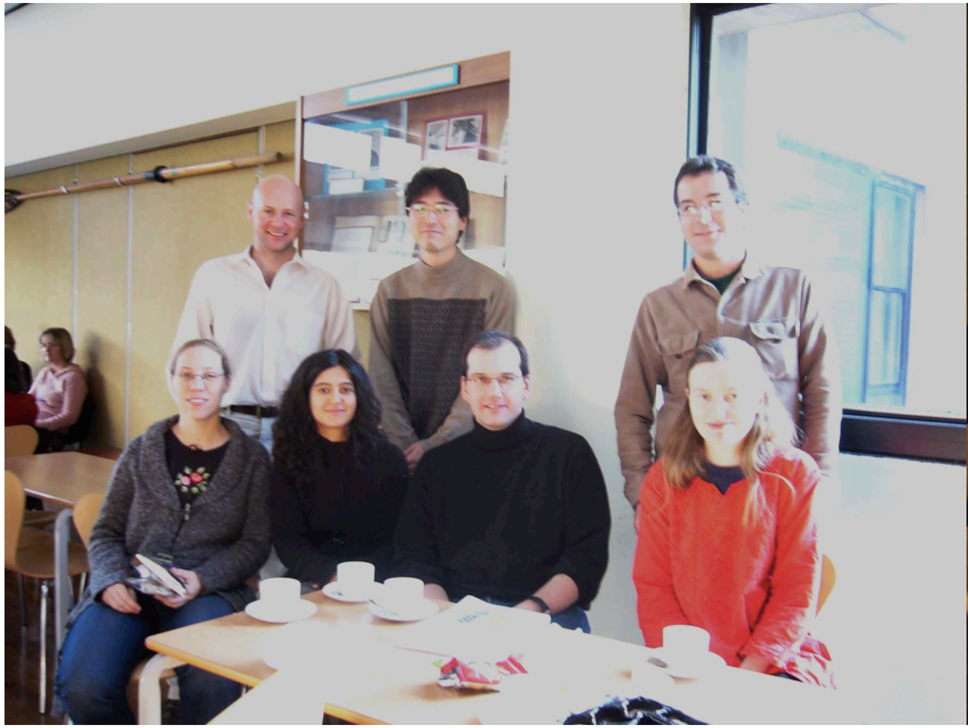

Phase separation of γ' in Ni-Al-Ti alloy

3D morphology and arrangements of fine γ in γ' visualized by DFTEM tomography

Hata *et al*: *Adv. Mater.* (2008)

○ Very high contrast using diffraction in crystals

△ Difficulty in setting a constant diffraction condition (sample dependent, single-tilt ET holder)

△ Influence of strain contrast at γ/γ' interfaces (serious for imaging nanoparticles)

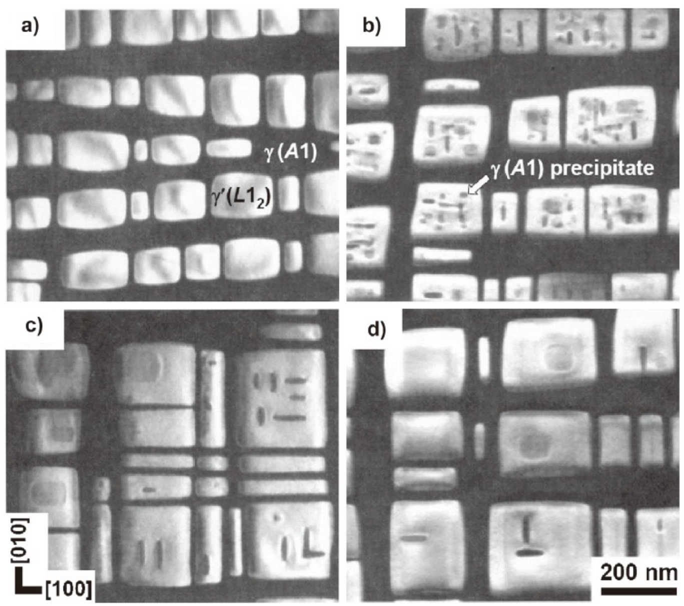

ges of Ni–8.5 at% Al–5.4 at% Ti alloys aged at 1213 K for a) 45 minutes, and subsequently aged at 1

DFTEM tilt series, ***k*** = ***g***$(001)_{L12}$

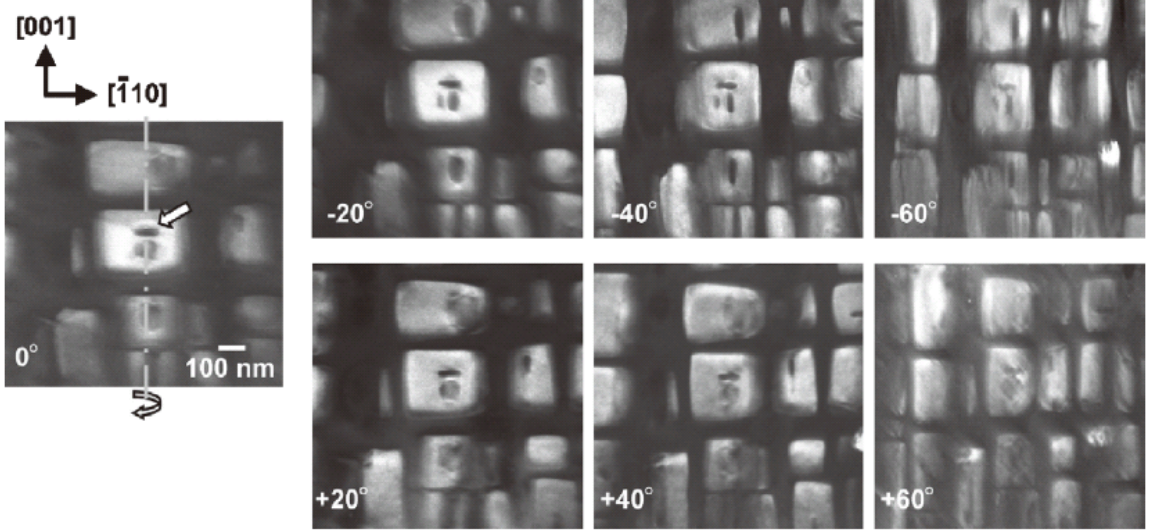

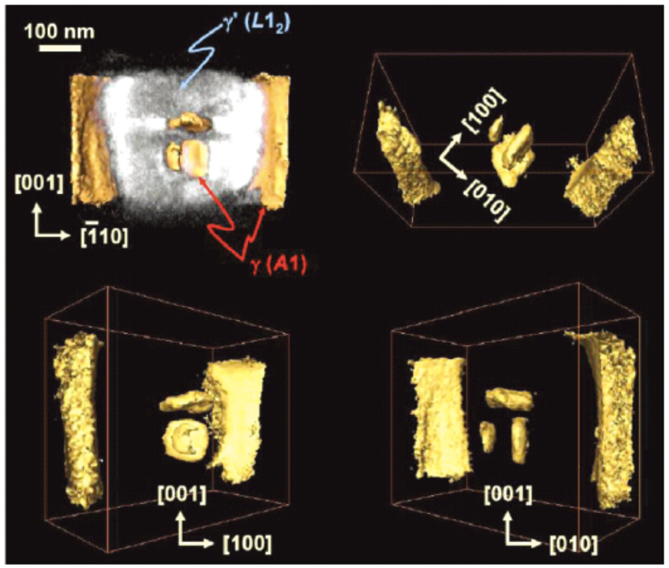

Figure 3. Surface-rendered views of the γ'/γ interfaces reconstructed from the DFTEM tilt series in Figure 2. The γ precipitates are rectangular plates in shape and parallel to the {100} planes.

Acquire diffraction-contrast tilt-series

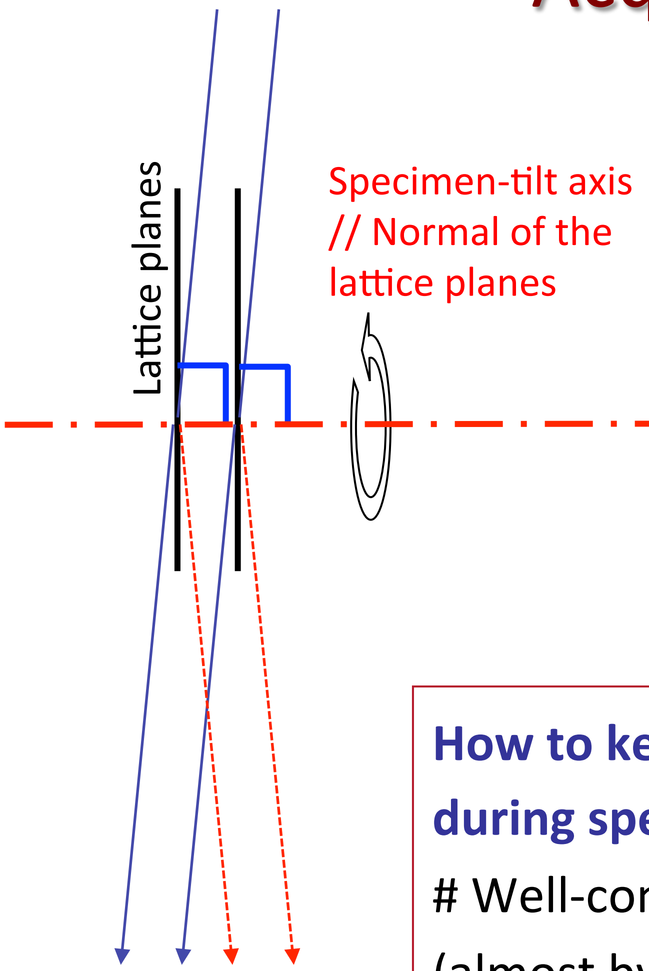

High-angle (> 60°) single-tilt
Specimen holder (Fischione™)

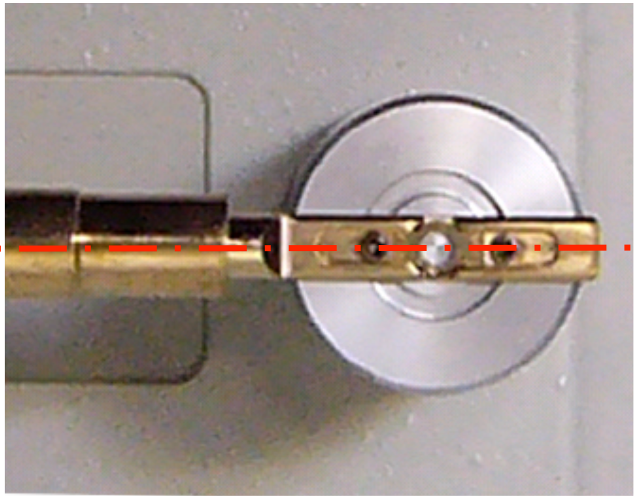

Two-beam condition

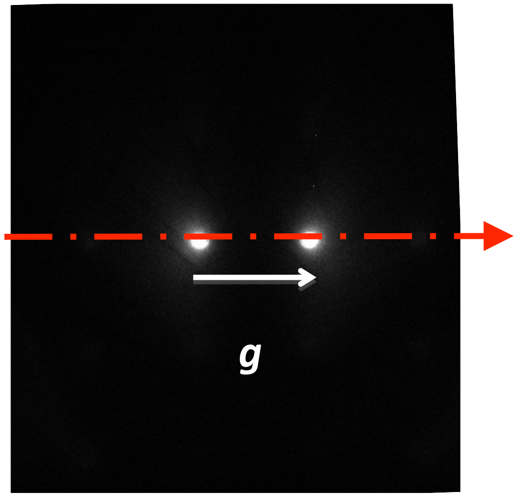

How to keep the diffraction condition during specimen tilt?

Well-controlled sample preparation (almost by chance)

Incident beam-tilt (causes image distortion due to aberration)

High-angle double-tilt holder (not commercially available)

Example diffraction tilt-series
under a two-beam condition

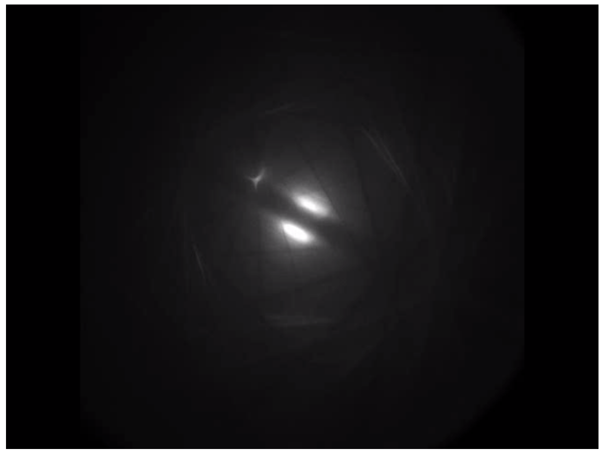

High-angle triple-axis（HATA）specimen holder

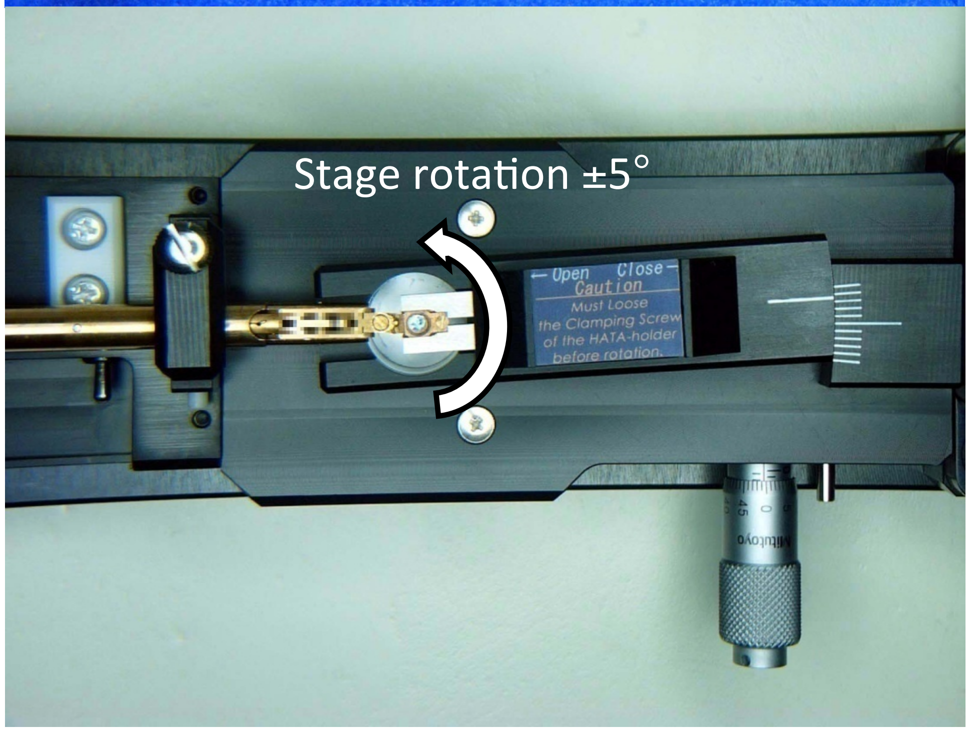

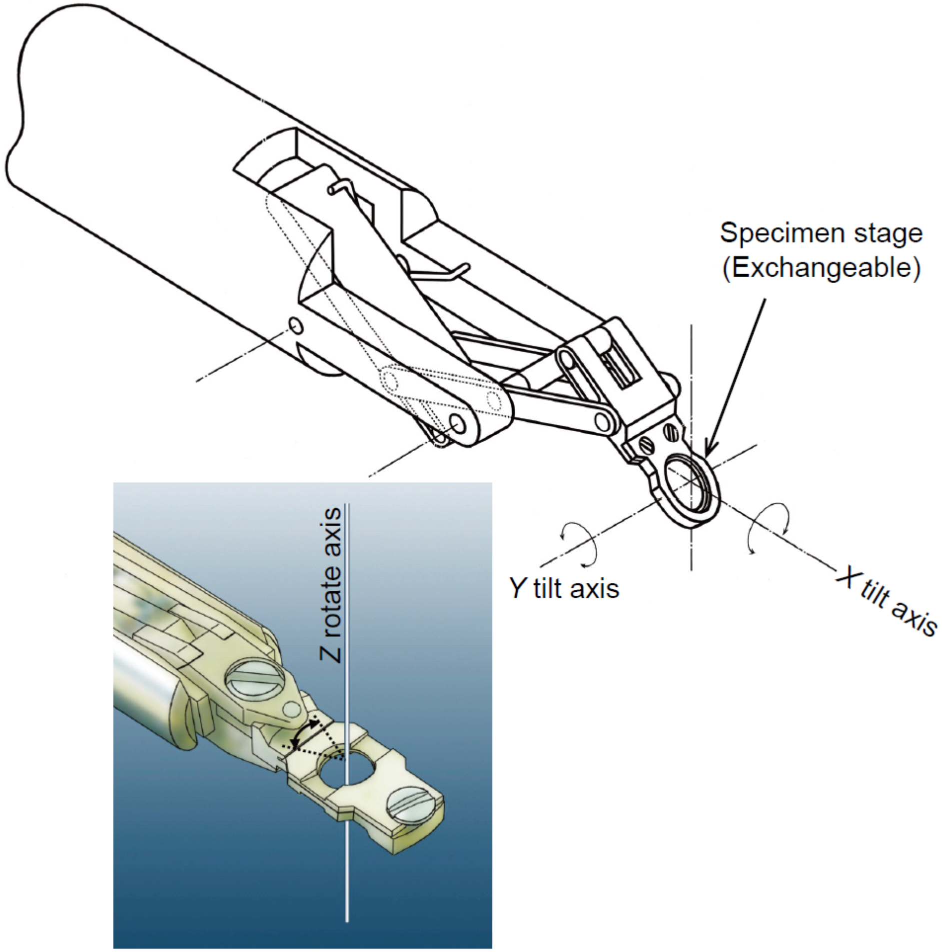

Hata *et al. Ultramicroscopy* (2011)
http://www.melbuild.com/

Movement of high-angle triple-axis holder

http://www.melbuild.com/

Mel-Build

KYUSHU UNIVERSITY

HATA holder for JEOL TEM (2011)

\# 360° tilt on x-axis

for a needle sample

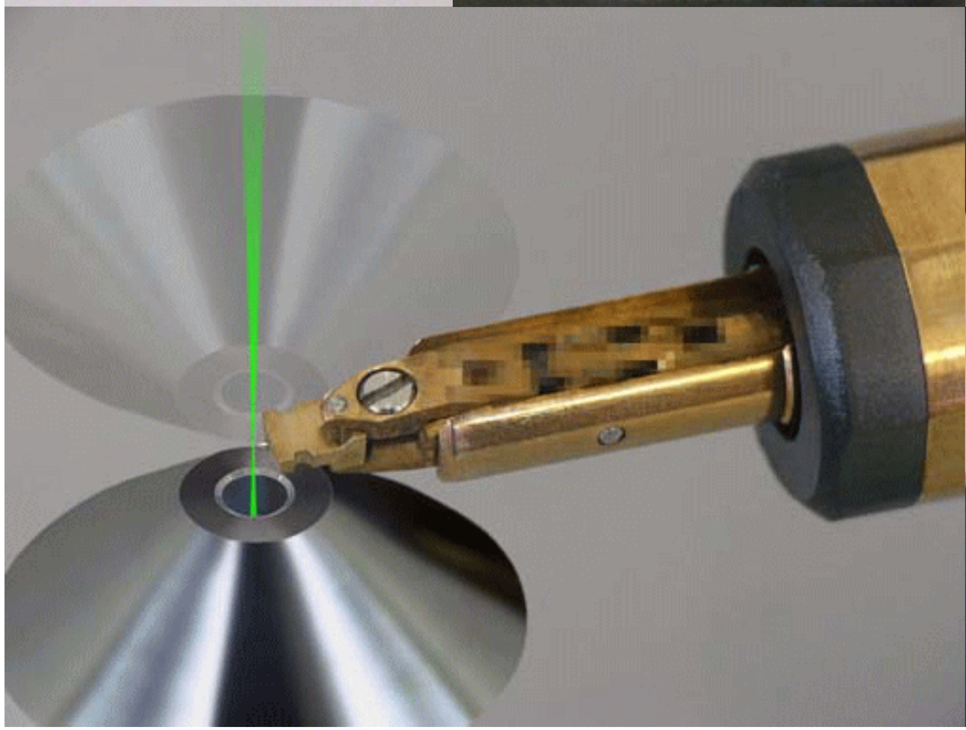

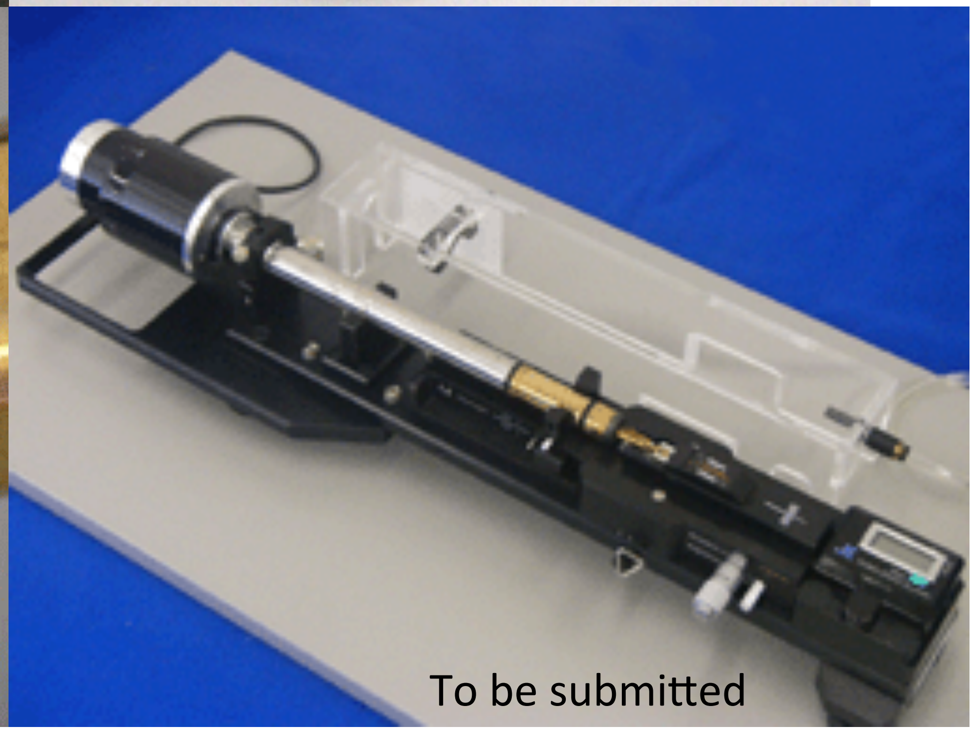

To be submitted

Crack tip dislocations revealed by electron tomography in silicon single crystal

Vickers indent and heated at 873 K

Tanaka, Higashida, Kaneko, Hata, Mitsuhara, *Scripta Mater.* (2008)

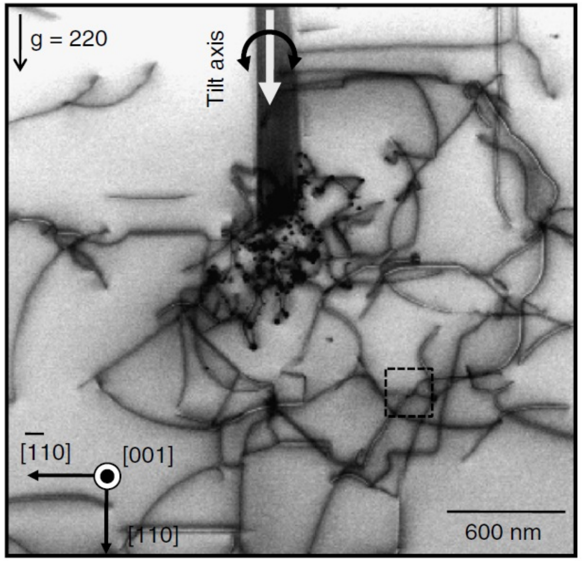

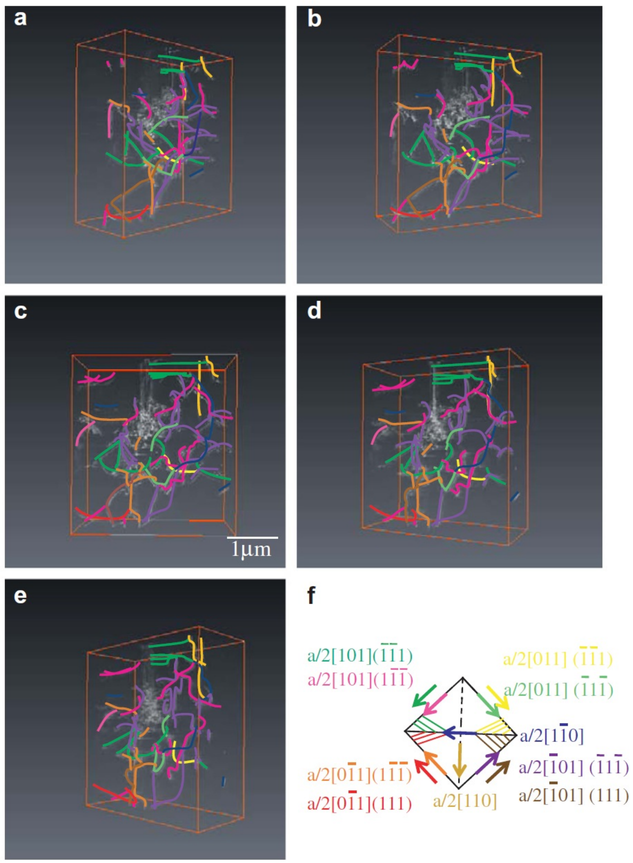

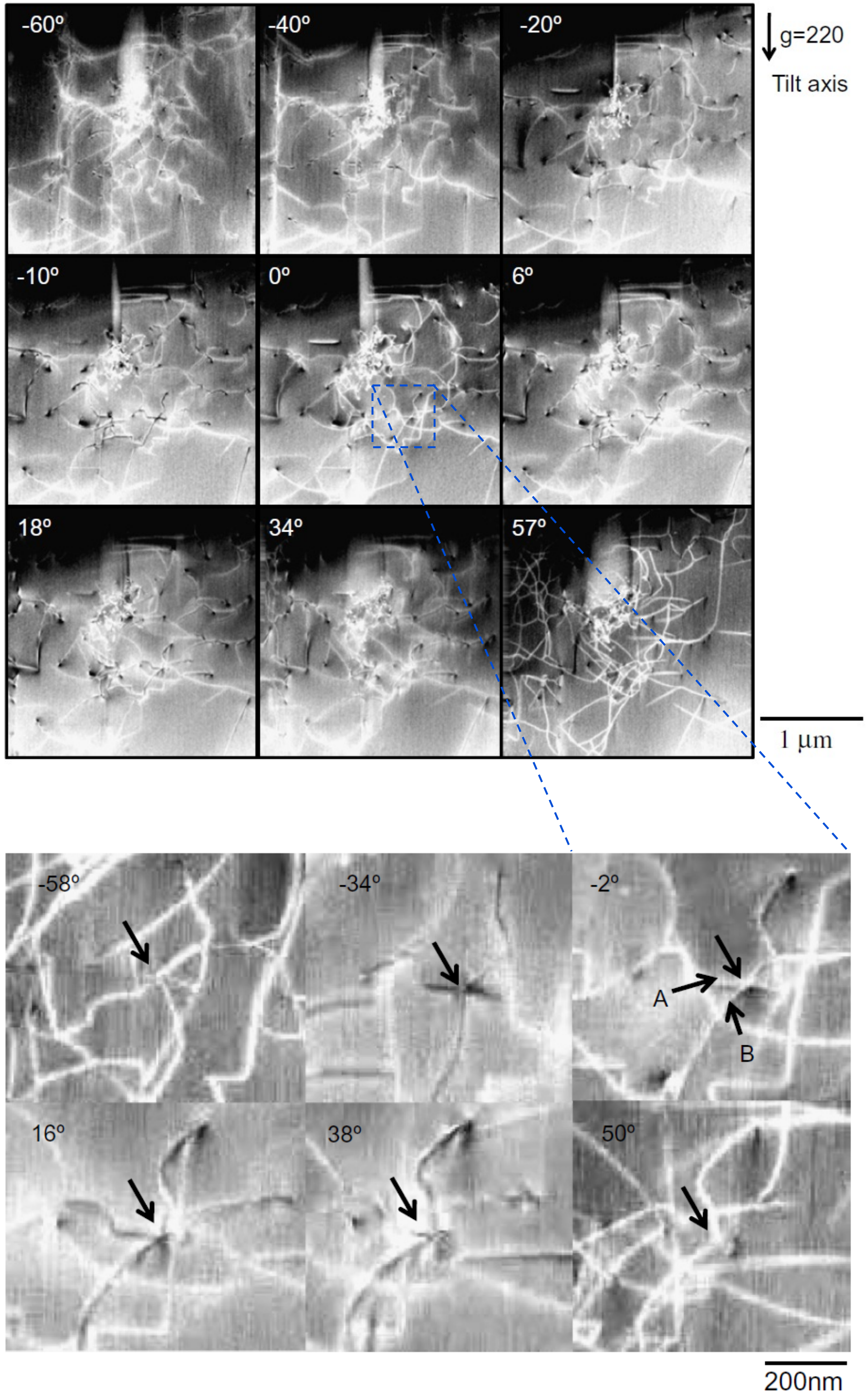

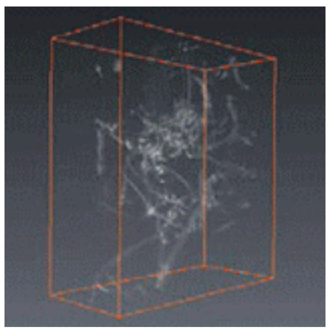

Test a HATA holder

9. 2007, University of Cambridge

WBDF-TEM dislocation tomography for Si crystal with crack

J. S. Barnard, J. Sharp, P. A. Midgley,

S. Miyazaki (Mel-Build & FEI, Japan), H. Miyazaki (Mel-Build), S. Hata

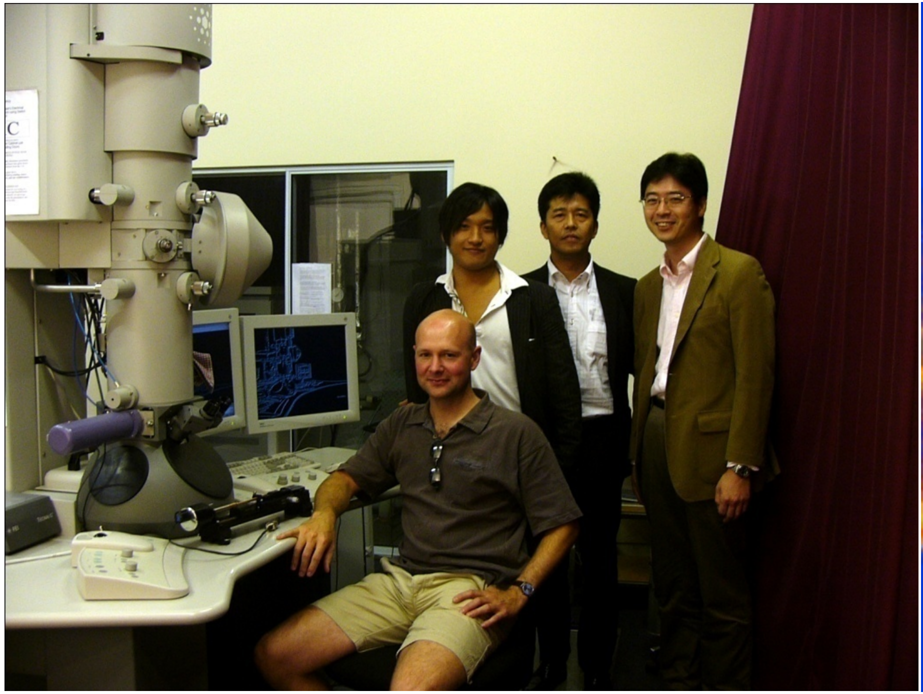

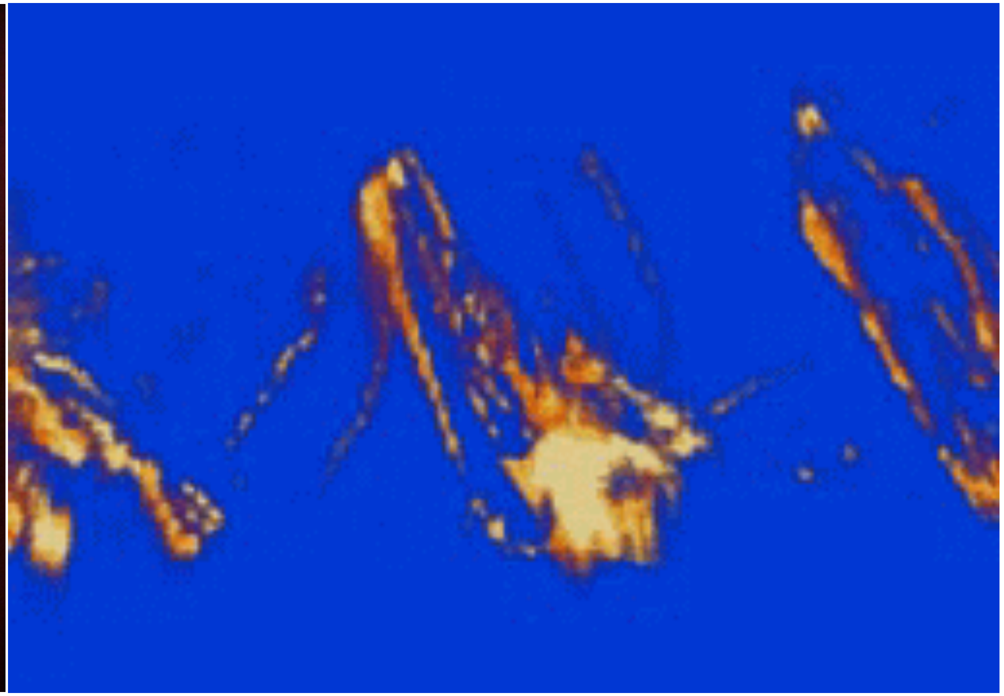

Ultramicroscopy 111 (2011) 1168–1175

Contents lists available at ScienceDirect

Ultramicroscopy

journal homepage: www.elsevier.com/locate/ultramic

High-angle triple-axis specimen holder for three-dimensional diffraction contrast imaging in transmission electron microscopy

S. Hata [a,*], H. Miyazaki [b], S. Miyazaki [c], M. Mitsuhara [a], M. Tanaka [d], K. Kaneko [d], K. Higashida [d], K. Ikeda [a], H. Nakashima [a], S. Matsumura [e], J.S. Barnard [f], J.H. Sharp [g], P.A. Midgley [f]

[a] *Department of Electrical and Materials Science, Kyushu University, Kasuga, 6-1 Kasugakoen, Kasuga, Fukuoka 816-8580, Japan*
[b] *Mel-Build, Nishi-ku, Fukuoka 819-0052, Japan*
[c] *FEI Company Japan Ltd., Minato-ku, Tokyo 108-0075, Japan*
[d] *Department of Materials Science and Engineering, Kyushu University, Nishi-ku, Fukuoka 819-0395, Japan*
[e] *Department of Applied Physics and Nuclear Engineering, Kyushu University, Nishi-ku, Fukuoka 819-0395, Japan*
[f] *Department of Materials Science and Metallurgy, University of Cambridge, Pembroke Street, Cambridge CB2 3QZ, UK*
[g] *Department of Materials Science and Engineering, Sir Robert Hadfield Building, Mappin Street, Sheffield, S1 3JD, UK*

ARTICLE INFO

Article history:
Received 1 October 2010
Received in revised form
25 March 2011
Accepted 29 March 2011
Available online 9 April 2011

Keywords:
Electron tomography
Specimen holder
Diffraction contrast

ABSTRACT

Electron tomography requires a wide angular range of specimen-tilt for a reliable three-dimensional (3D) reconstruction. Although specimen holders are commercially available for tomography, they have several limitations, including tilting capability in only one or two axes at most, e.g. tilt–rotate. For amorphous specimens, the image contrast depends on mass and thickness only and the single-tilt holder is adequate for most tomographic image acquisitions. On the other hand, for crystalline materials where image contrast is strongly dependent on diffraction conditions, current commercially available tomography holders are inadequate, because they lack tilt capability in all three orthogonal axes needed to maintain a constant diffraction condition over the whole tilt range. We have developed a high-angle triple-axis (HATA) tomography specimen holder capable of high-angle tilting for the primary horizontal axis with tilting capability in the other (orthogonal) horizontal and vertical axes. This allows the user to trim the

Two-beam diffraction tilt series using HATA holder
STEM (convergent illumination) mode

First, find the specimen-tilt (*X*) axis on the screen/camera of your TEM!

Austenitic (fcc) steel

Diffraction condition
K = ***g***(200)

Specimen-tilt angle
-70° ~ +70°

Misorientation angle between specimen-tilt axis and ***g***(200) < 1°

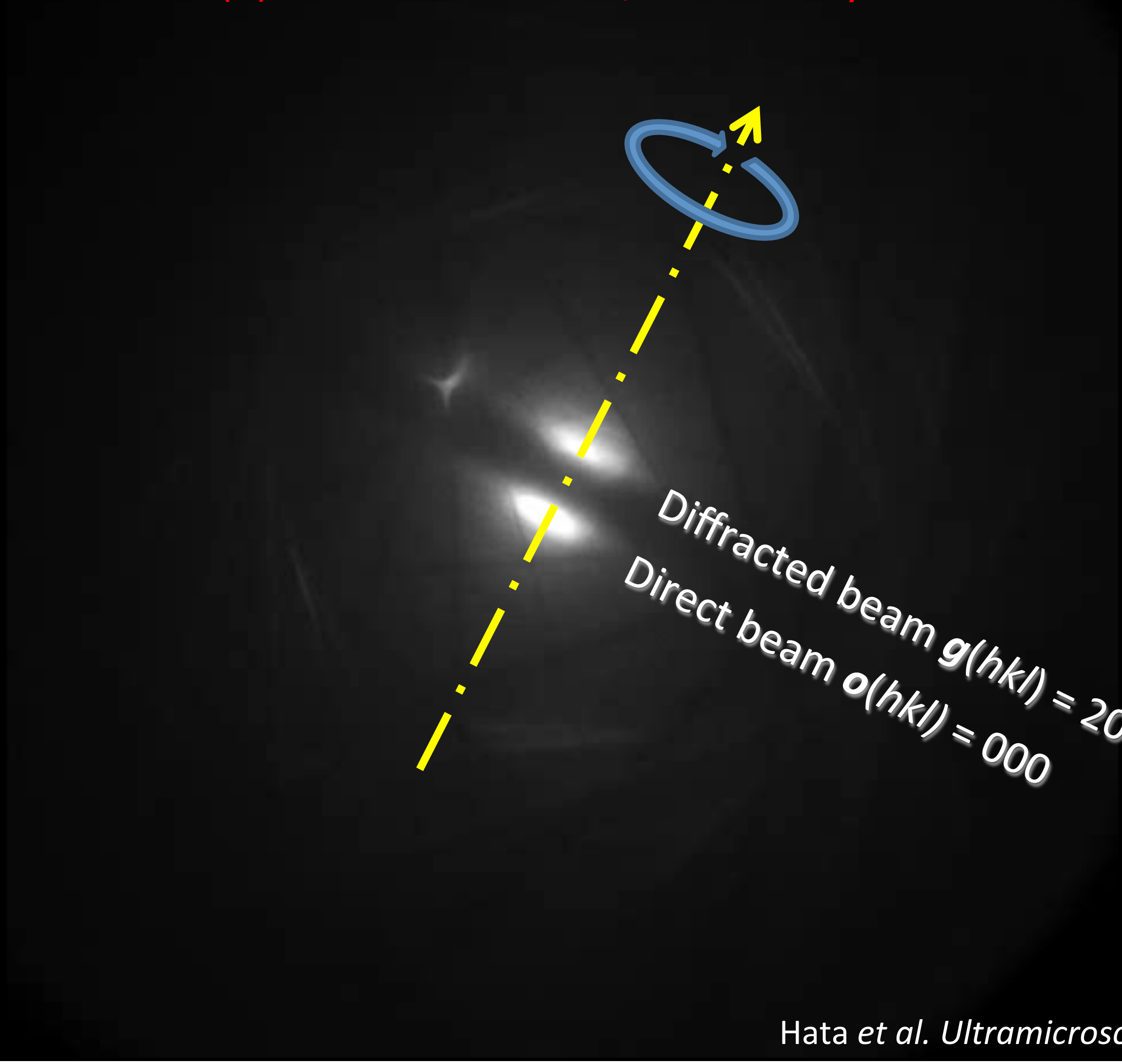

Hata *et al. Ultramicroscopy* (2011)

STEM tilt-series of dislocations in austenitic steel

After 3% compressive deformation at room temperature

STEM-BF
（Contrast reversal）
Specimen-tilt angle
-70° ~ +70°

HATA holder

Tilt axis // $\boldsymbol{g}(hkl) = 200_{fcc}$

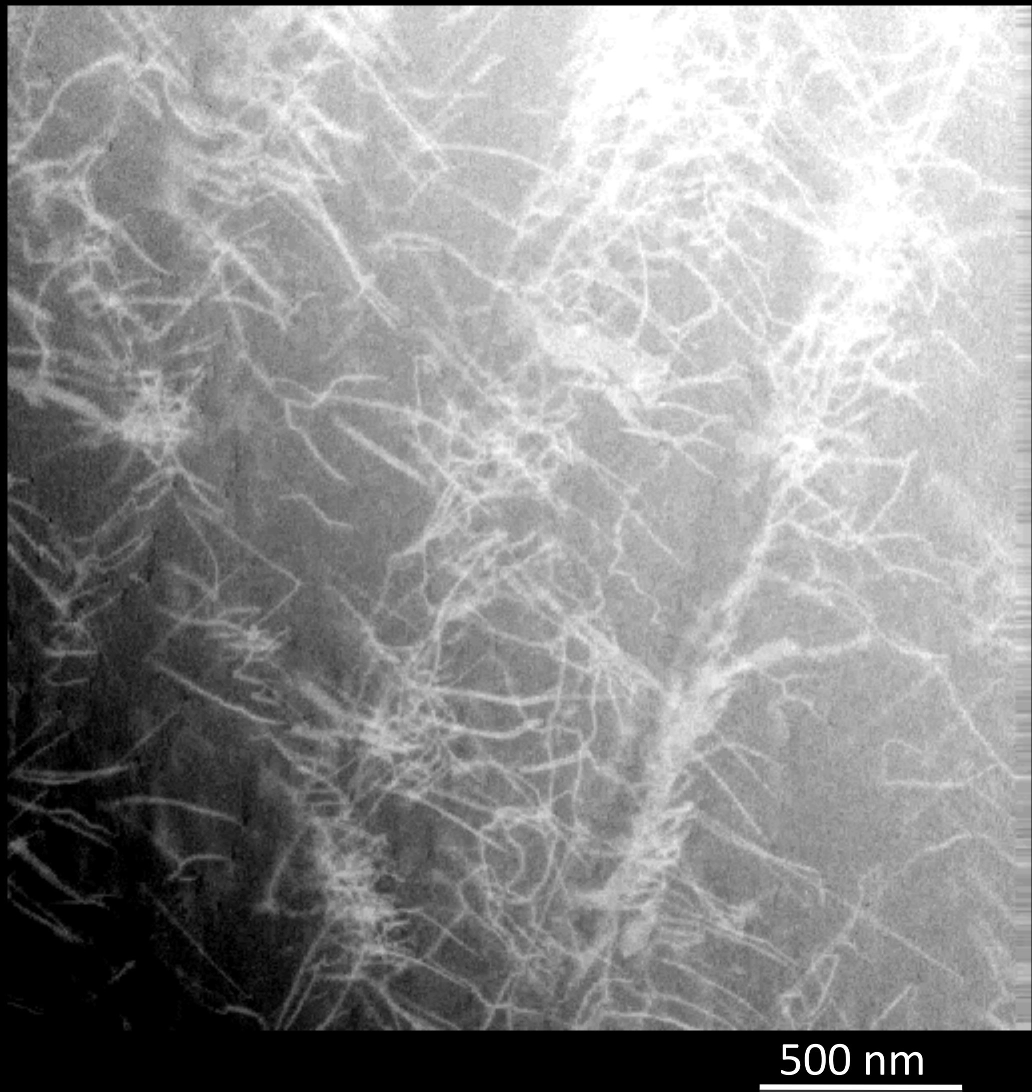

Hata *et al. Ultramicroscopy* (2011)

3D reconstruction of dislocations

SUS316 austenitic steel after 3% compressive deformation at R. T.

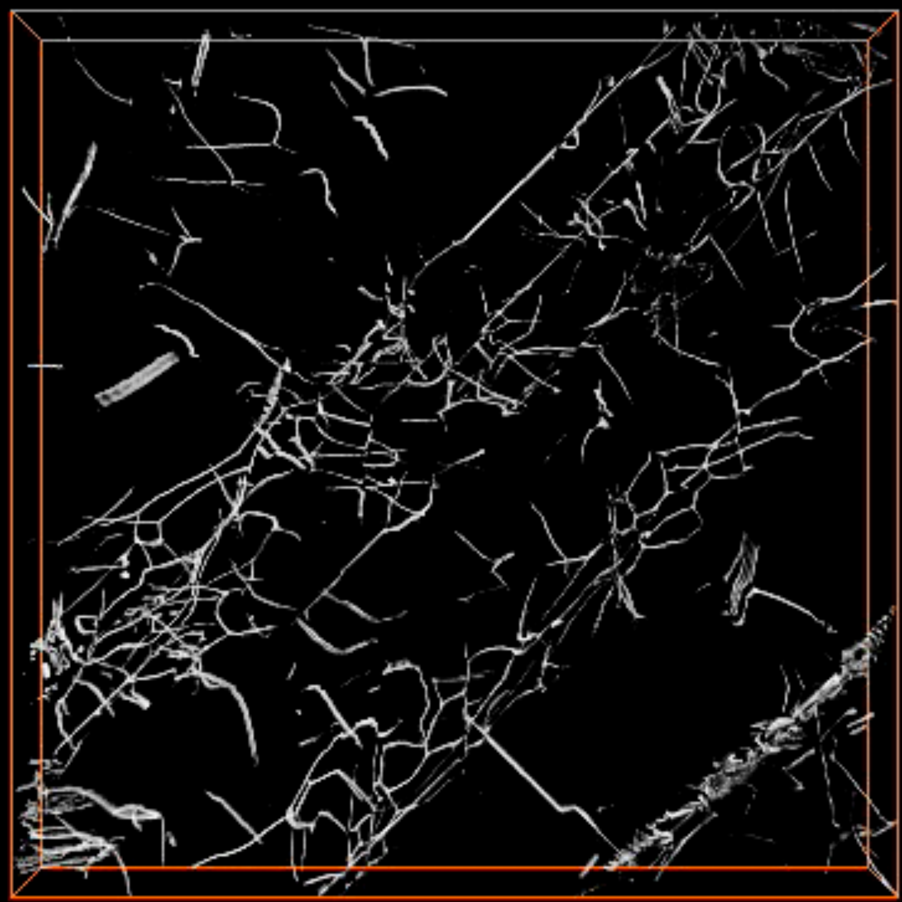

Hata *et al. Ultramicroscopy* (2011)

500 nm

Dual-axis STEM dislocation tomography

SUS316 austenitic steel, 3% compression at R.T., BF-STEM (contrast reversal)

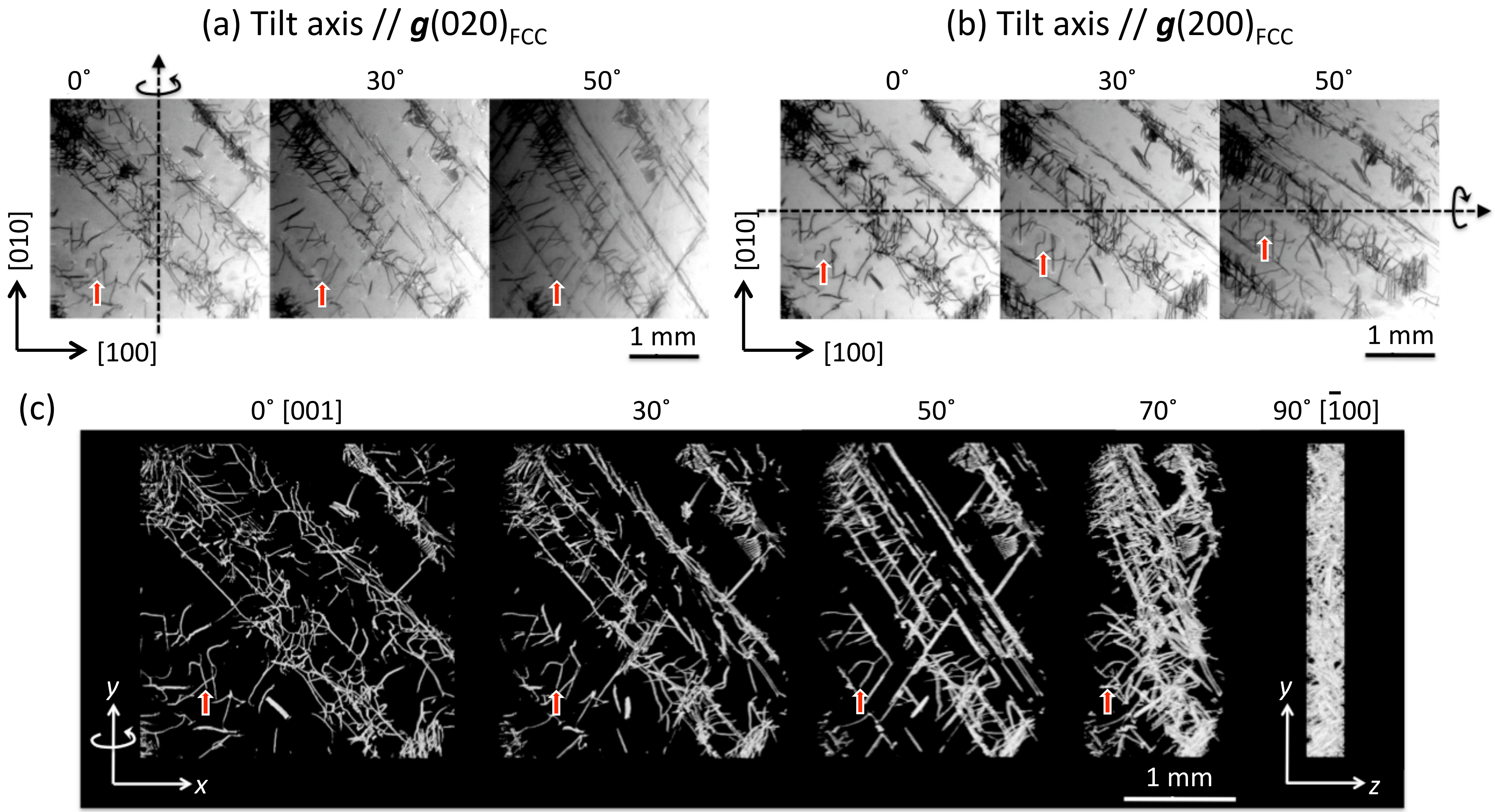

Dislocation density: $\rho = 4.0 \times 10^{13}$ m^{-2}

Hata *et al. Ultramicroscopy* (2011)

Number of dislocations in 2D tomograms

Austenitic steel, 3% strained at R. T., (001) foil

20-30% reduction of dislocation density near the specimen surface

Reconstructed 3D volume (1 pixel = 3 nm)

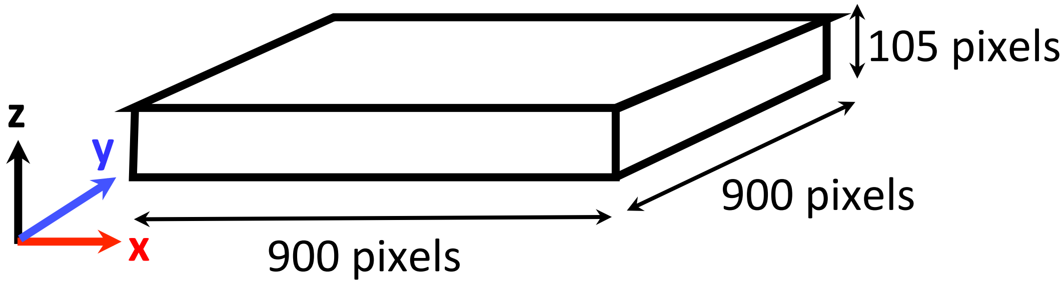

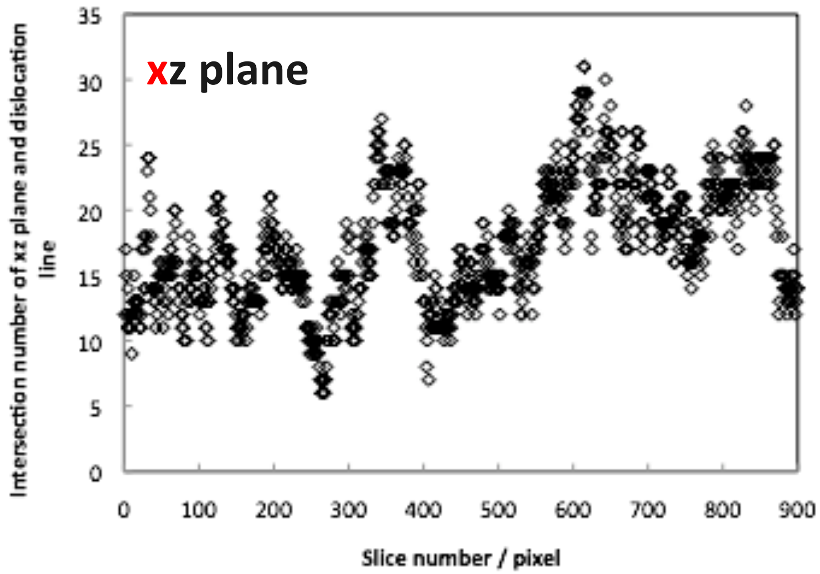

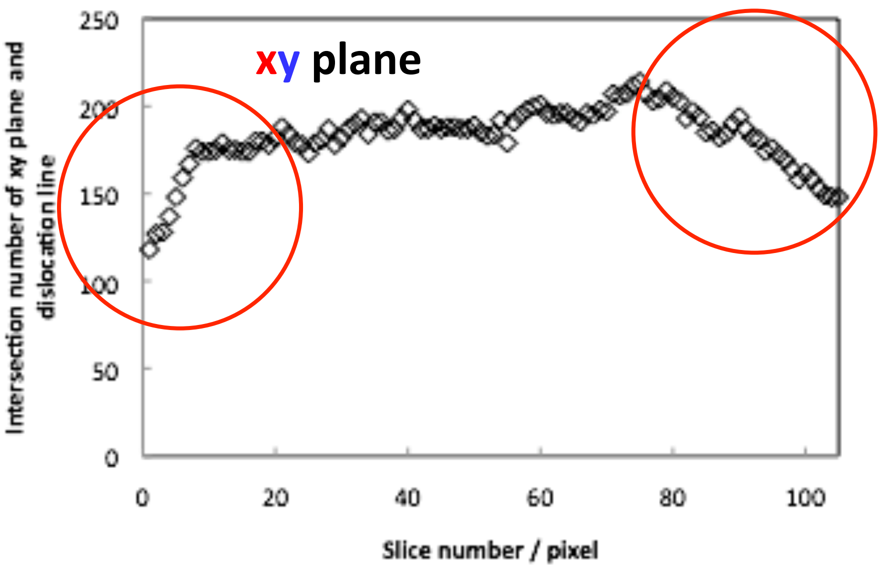

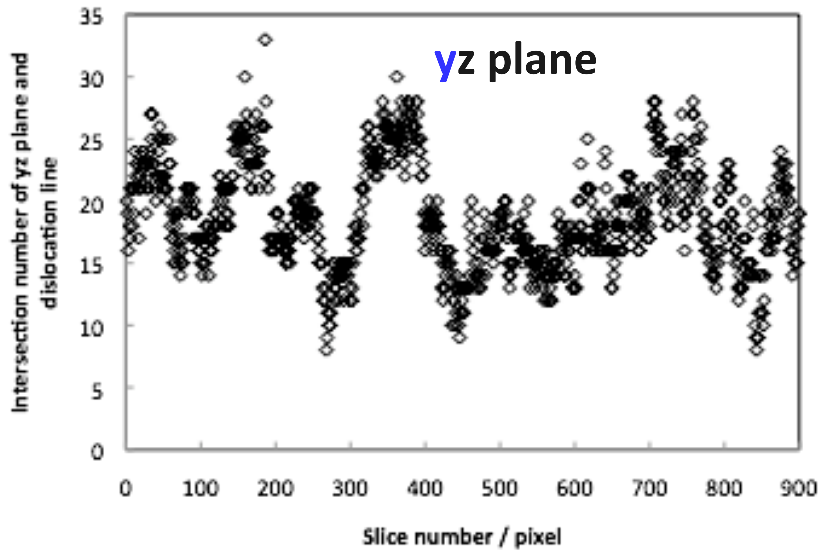

Hata, Mitsuhara *et al.*: Ultramicroscopy (2011)

Dislocation density evaluated from 2D image and 3D volume

Austenitic steel, 10% compressive deformation at R. T.

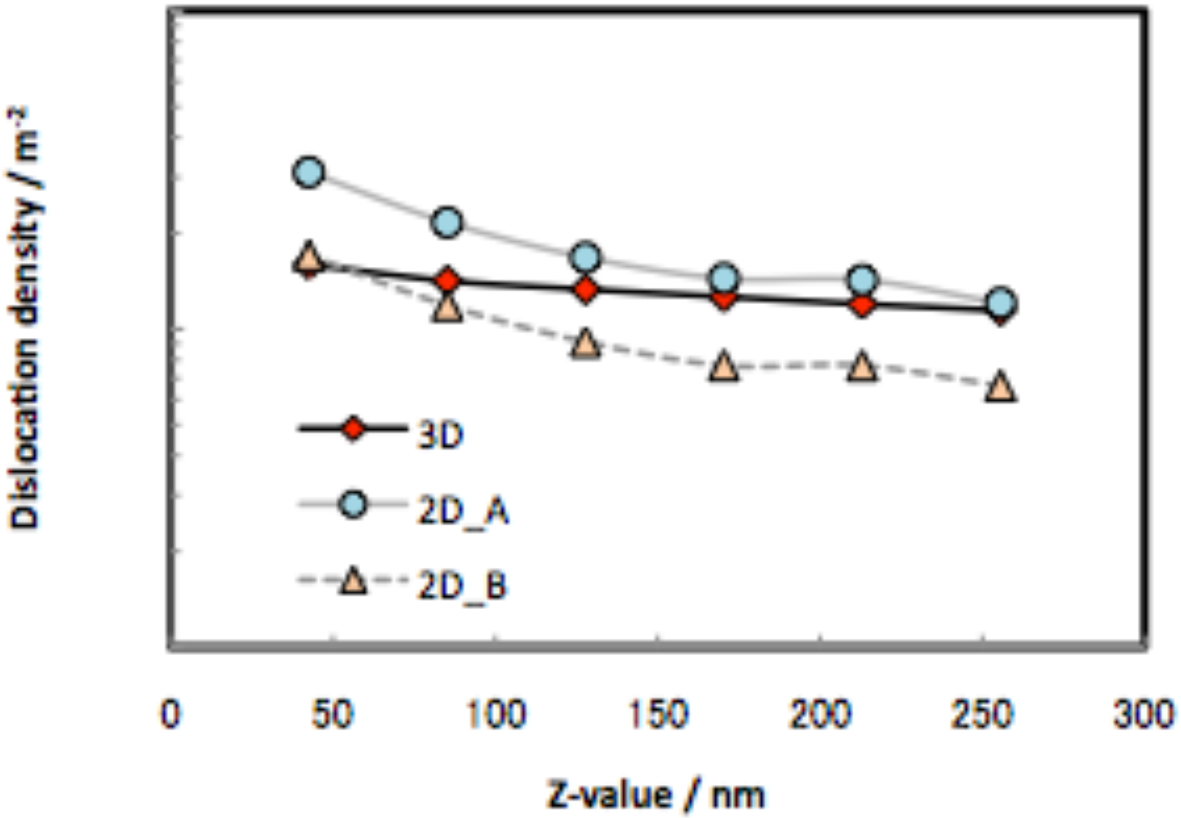

2D_A

$$\rho = \frac{2N}{Lt}$$

L: total length of straight lines on 2D image
N: intersection number of straight lines and dislocations
t: specimen thickness

2D_B

$$\rho = \left(\frac{n_1}{L_1} + \frac{n_2}{L_2}\right)\frac{1}{t}$$

L_1: total length of vertical lines
n_1: intersection number of vertical lines and dislocations
L_2: total length of horizontal lines
n_2: intersection number of horizontal lines and dislocations

Mitsuhara, *to be submitted*

Collaboration using HATA holder

3. 2009~, EMAT, University of Antwerp

STEM dislocation tomography for nano-grained metals and FIB induced defects

H. Idrissi, M. Mitsuhara, S. Hata, D. Schryvers

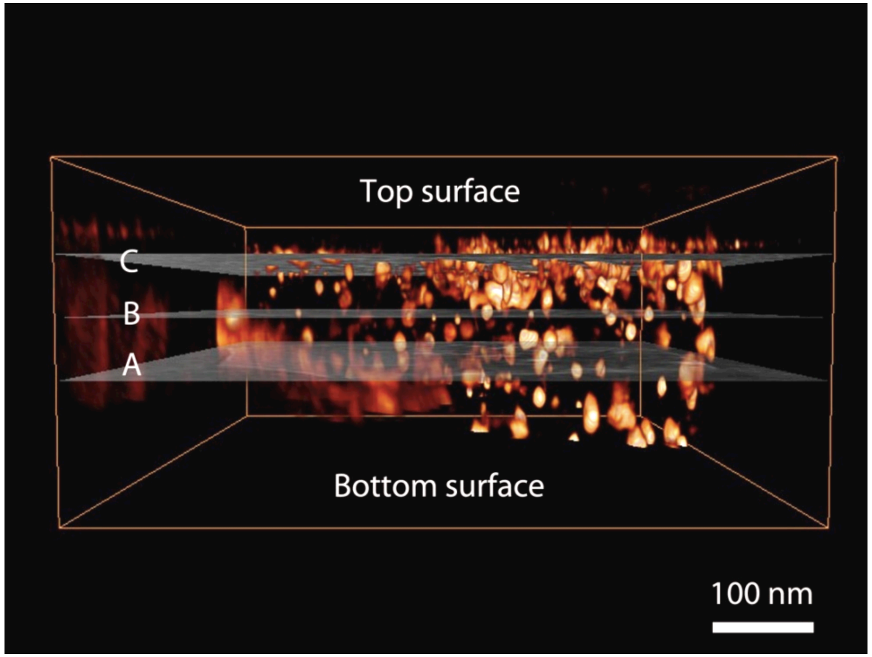

3D reconstruction of a single Al nanograin viewed along the thickness of the film, revealing multiple dislocation loops especially near to the top surface (indications of top & bottom surfaces relate to the FIB sample surfaces).

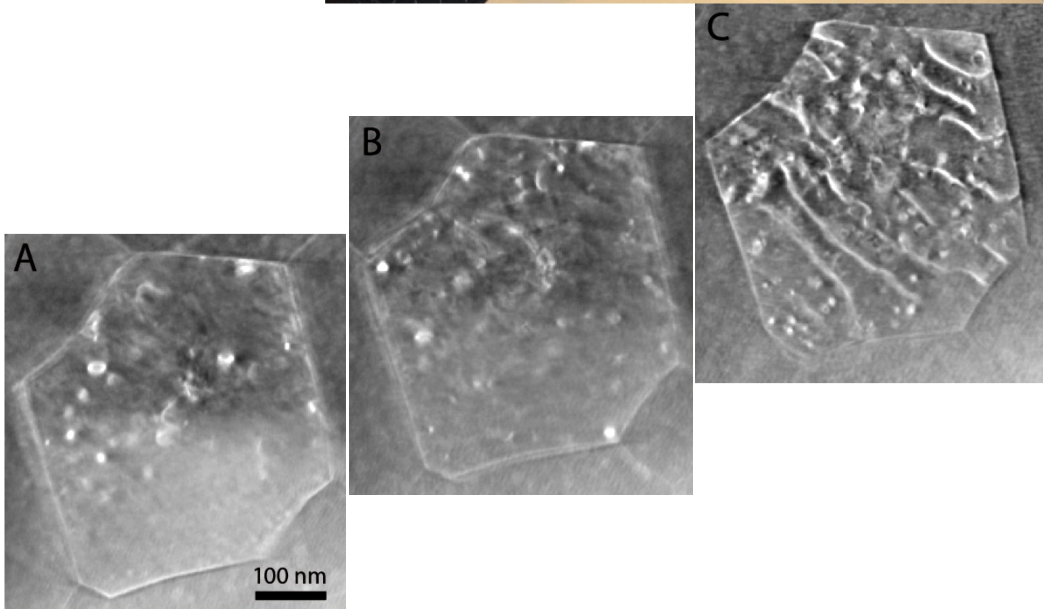

Three orthoslices selected at depth positions A, B and C in the grain shown in the left figure. Only the top slice C shows long dislocation lines pinned near the surface of the film by point defect clusters created during FIB milling.

Collaboration using HATA holder

5. 2010~, CEN, RISØ, Technical University of Denmark

Dislocation tomography for grain refinement process in pure Al

<u>A. Ramar</u>, S. Hata, <u>T. Kasama</u>, R. E. D.-Borkowski,
<u>X. Huang</u>, G. Winther, N. Hansen

Ramar *et al. RISØ Symp. Proc.* (2010)

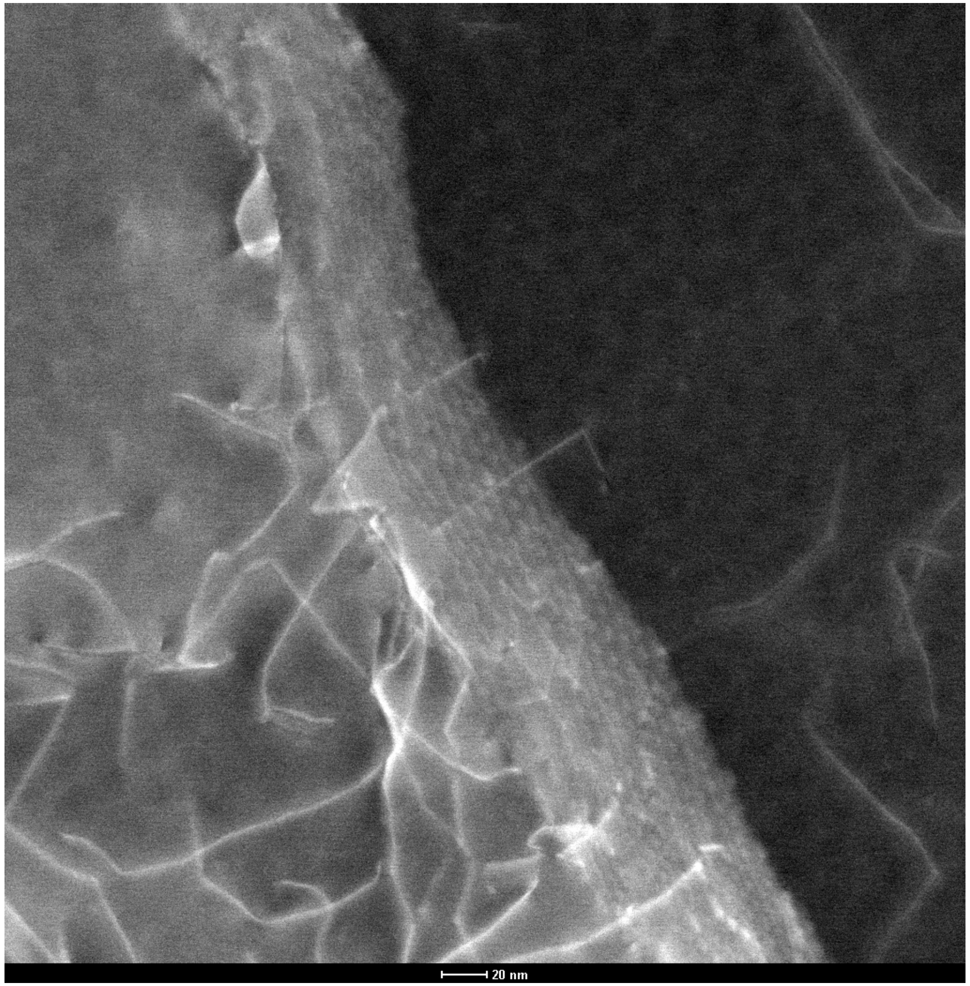

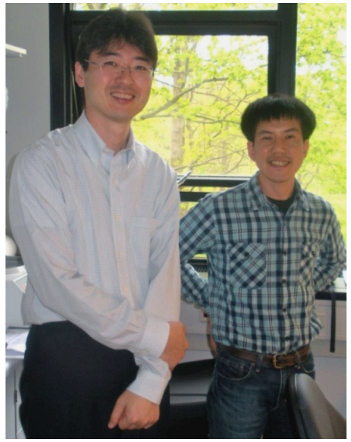

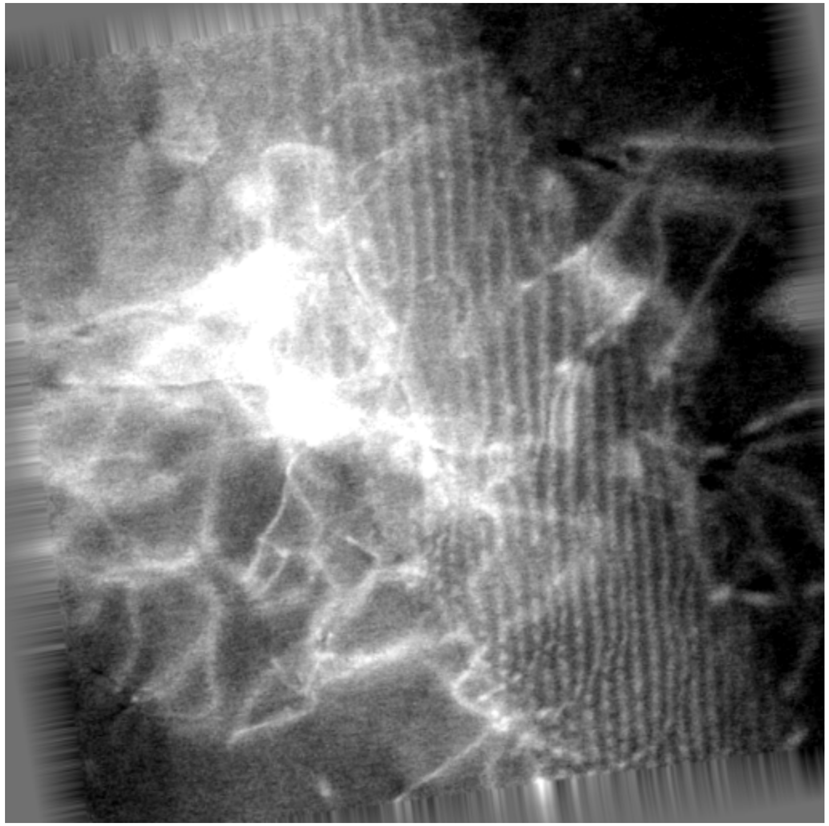

Dislocation tomography attracts structural materials researchers

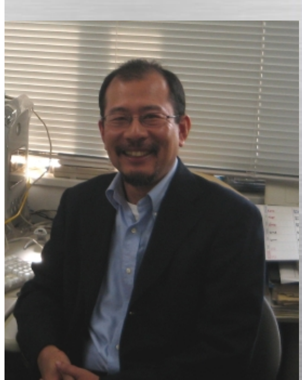

Prof.
Nobuhiro TSUJI
Kyoto University

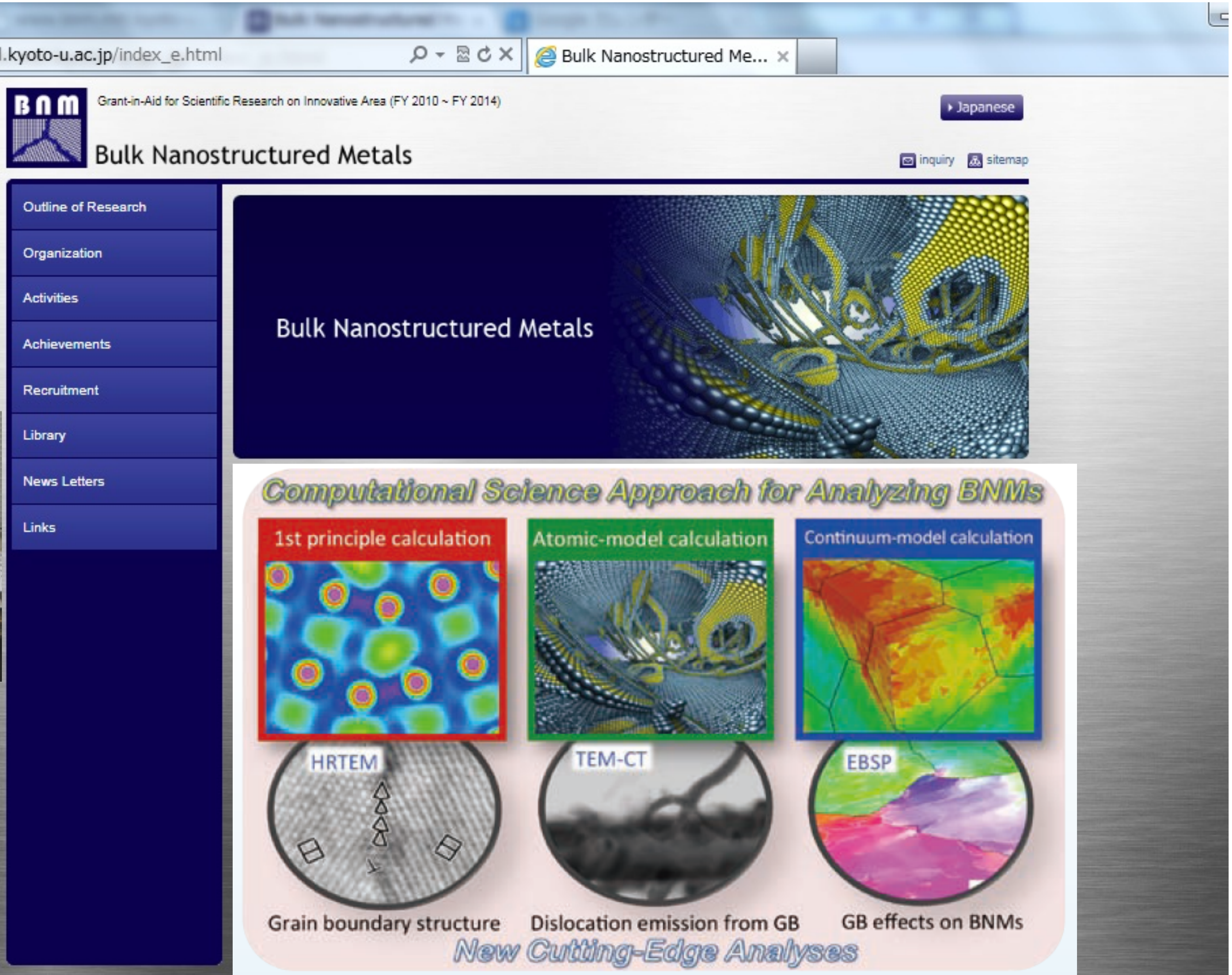

"Bulk Nanostructured Metals (BNM)" are the bulky polycrystalline materials composed of matrix grains or phases having sizes smaller than 1 μm; hence BNMs are considered as the materials "full of grain boundaries".

Tomographic 3D imaging of GB/dislocation interaction

Dislocations at Σ3 twin boundary of austenitic steel

Tilt-series acquisition with excitation of two (parallel) diffracted beams: ***g*** **=** 1-1-1 (for grain with incoming dislocations) & -11-1 (for other grain)

Available for limited types of GBs, Limited specimen-tilt angles of double-tilt holder

Drawing dislocations based on 3D TEM data and theoretical background for dislocation

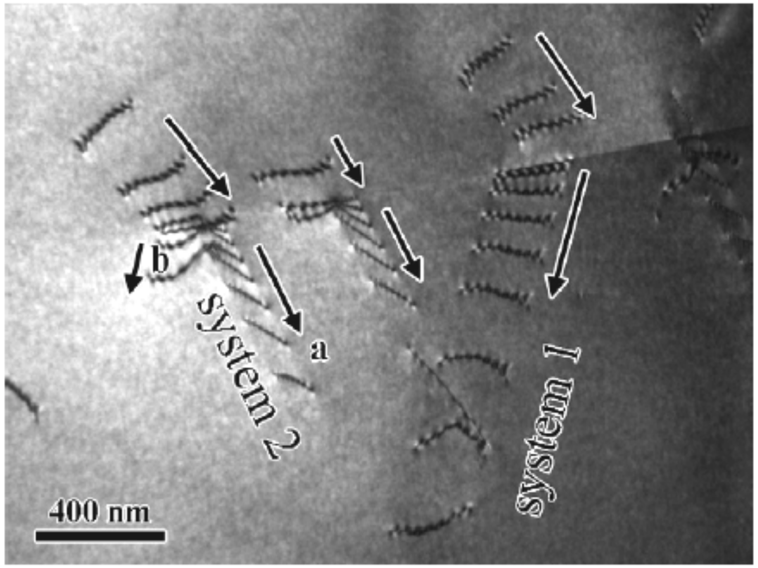

Fig. 1. Bright-field image of a dislocation system, with arrows indicating the direction of motion of the dislocations and labels identifying the slip systems.

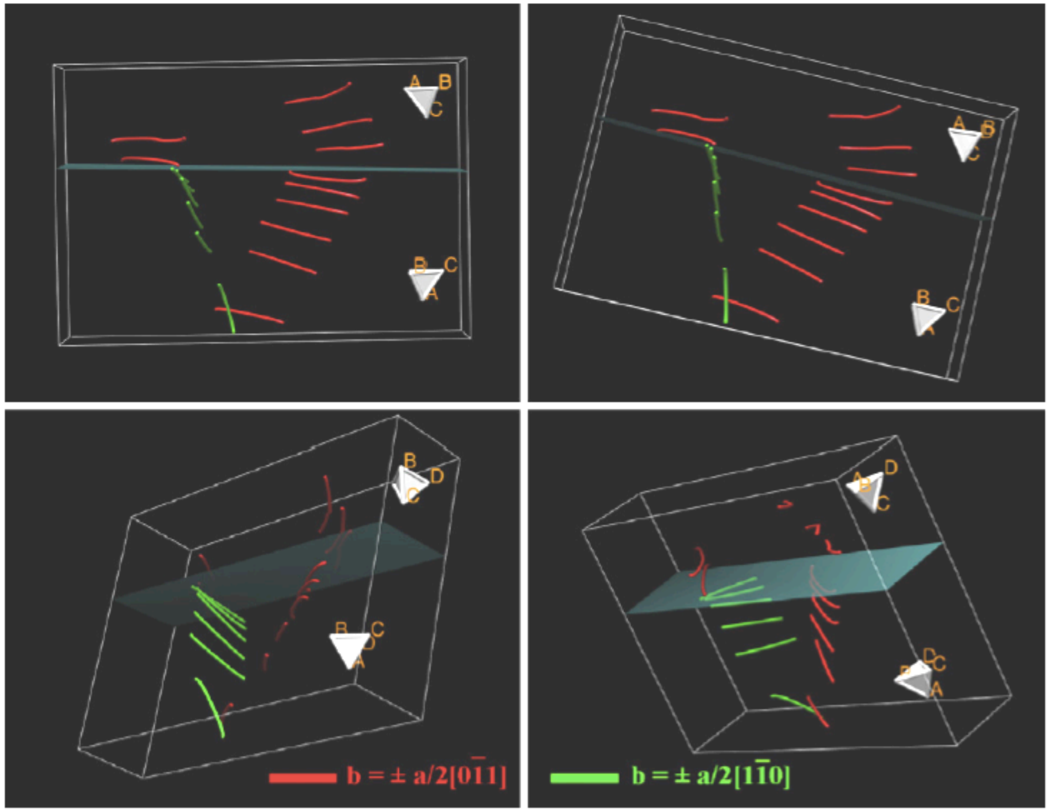

Fig. 3. Reconstructed model of dislocation system at different tilts. Thompson tetrahedra placed in each grain allows for easy identification of the slip planes on which the dislocations reside.

J. P. Kacher, G. S. Liu and I. M. Robertson: *Scripta Mater.* 64 (2011) 677-680.

Sample preparation

Sample 1: Mo bicrystal

Sample 2: Mo single crystal

[001](210)Σ5 symmetric tilt boundary

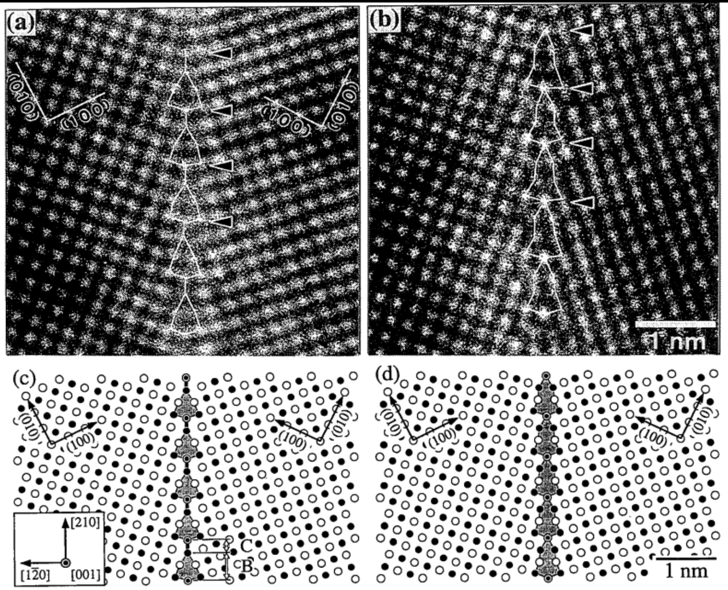

Fig. 2 Atomic structures of [001](1$\bar{2}$0)$\Sigma 5$(ϕ=53.13°) coincidence boundaries; (a) and (b) HRTEM images of purified and not-purified specimens, respectively, (c) and (d) calculated structures using the MD method of most stable structure (E=1.66 J/m^2) and metastable structure (E=2.16 J/m^2), respectively.

Morita *et al.*: *J. Jpn. Inst. Metals.* (1997)

Table 1 Impurity contents of C, O and N in not-purified and purified molybdenum.

Sample	Impurity contents (ppm)		
	C	O	N
Starting material	<10	<10	<10
Not-purified specimen	10.8	13.8	3.4
Purified specimen	<5.0	2.0	2.2

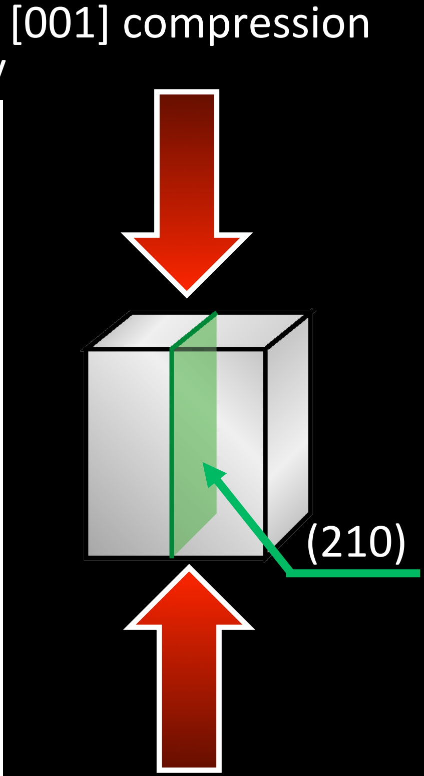

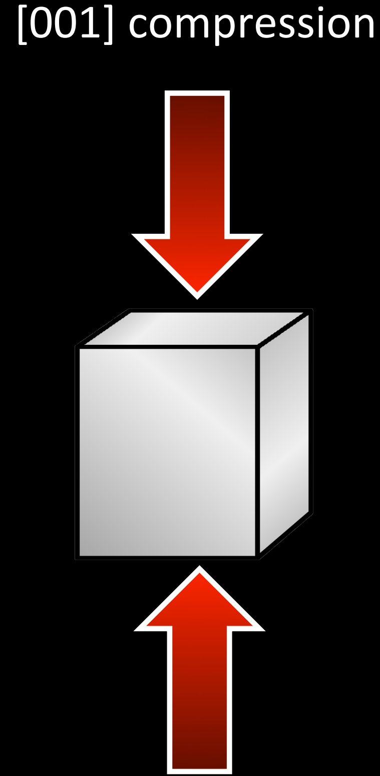

2 mm x 2 mm x 3 mm in sample size

Compressive deformation with 1% plastic strain

TEM specimens: foil parallel to (001), electropolishing

To be submitted

Dislocation tilt series for each crystal in Mo[001](210)Σ5 boundary

Crystal 1: $\boldsymbol{K} = \boldsymbol{g}(200)$

Crystal 2: $\boldsymbol{K} = \boldsymbol{g}(200)$

200 nm

Crystal 1: $\boldsymbol{K} = \boldsymbol{g}(020)$

Crystal 2: $\boldsymbol{K} = \boldsymbol{g}(020)$

FEI Tecnai F20, HATA holder

STEM BF, -70° to +70°, 2° step, SIRT algorithm

To be submitted

Dual-axis tomographic reconstruction for crystals 1 and 2 → Combine crystals 1 and 2

Four 3D reconstructions

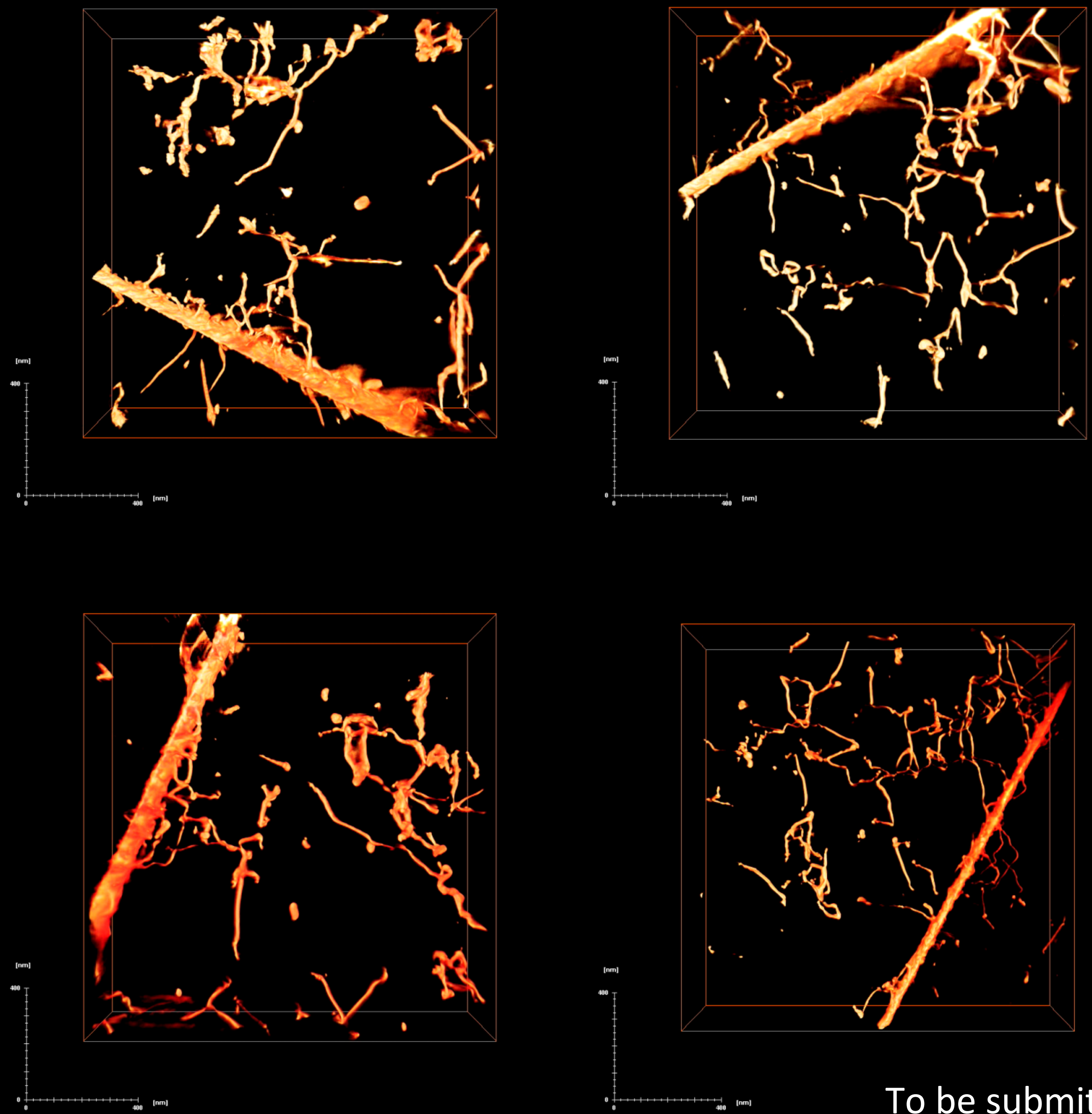

To be submitted

3D reconstruction of Mo[001](210)Σ5 boundary, 1% compression

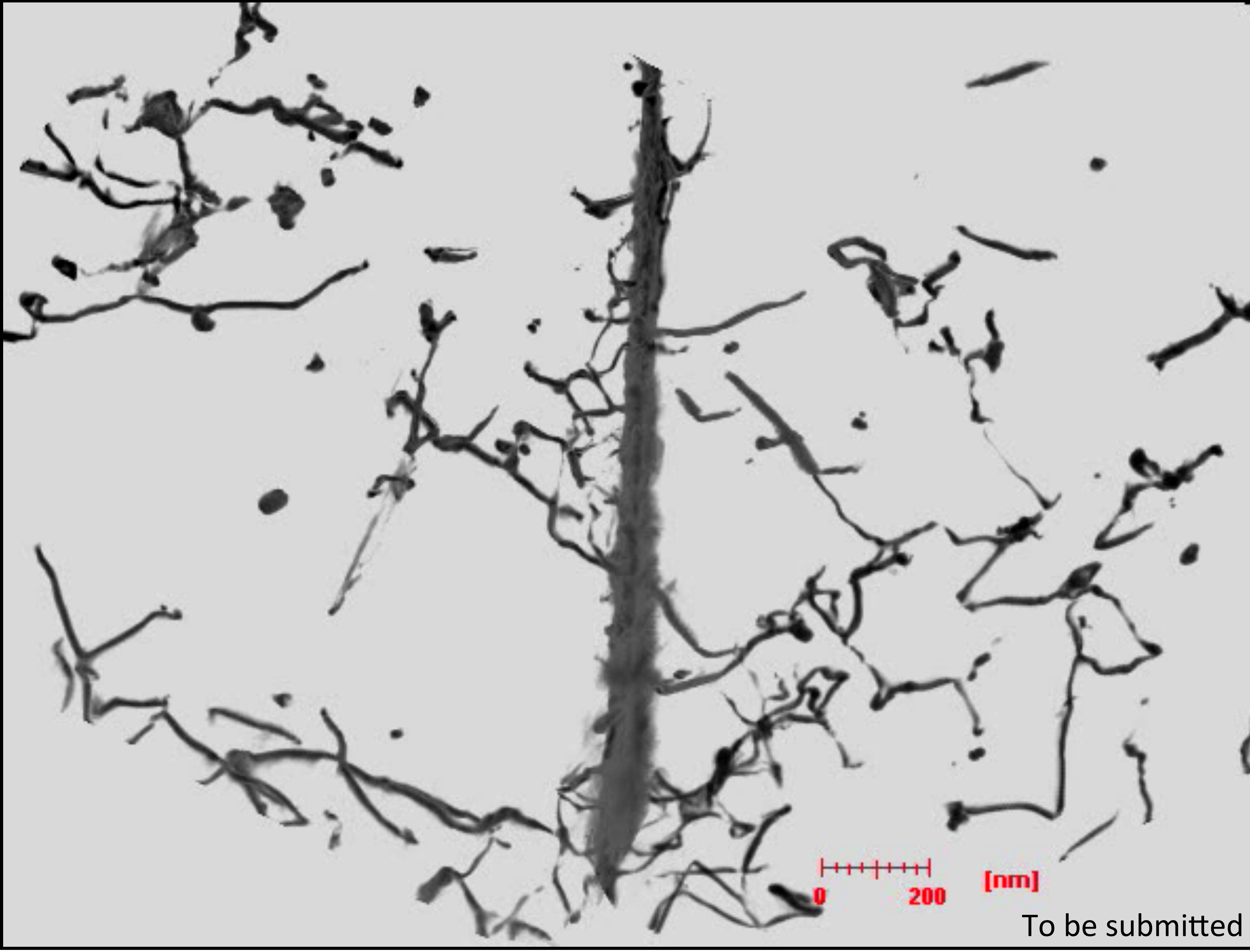

To be submitted

Slip plane distribution in Mo[001](210)Σ5 bicrystal

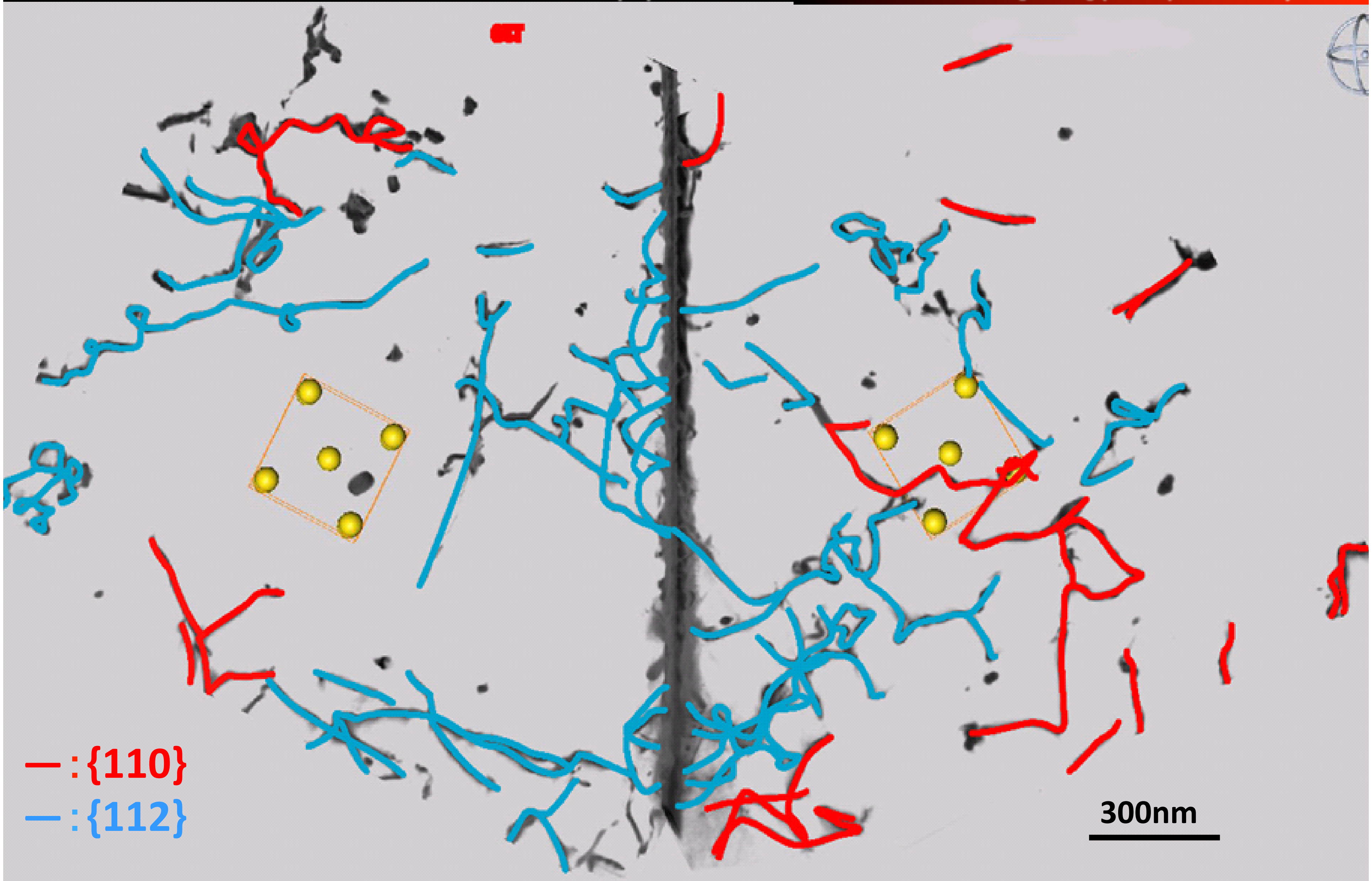

GB influences active slip-plane distribution.

To be submitted

Back projection algorithm

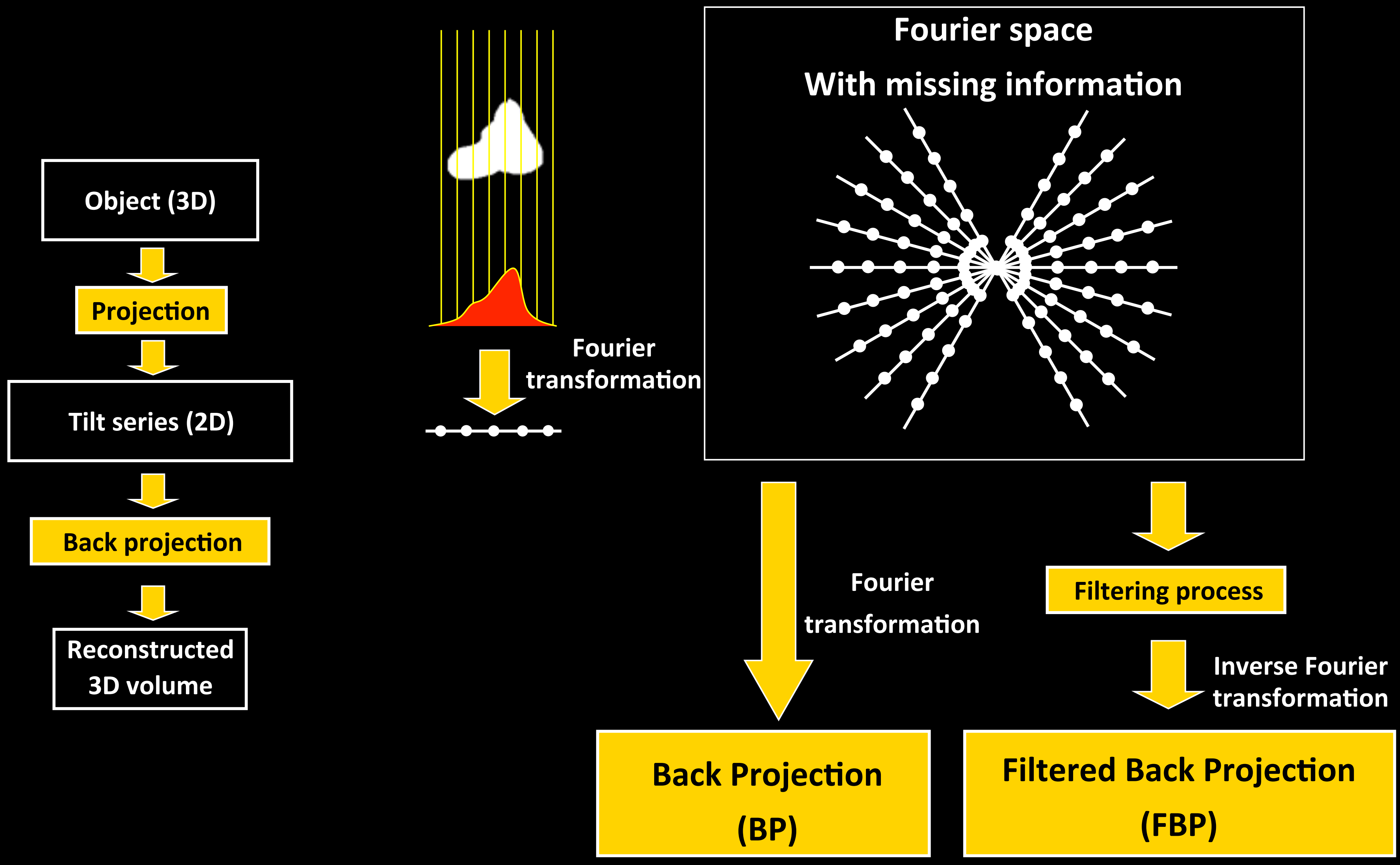

Rod-shape specimen

Zirconia-polymer composit

Kawase *et al. Ultramicroscopy (2007)*

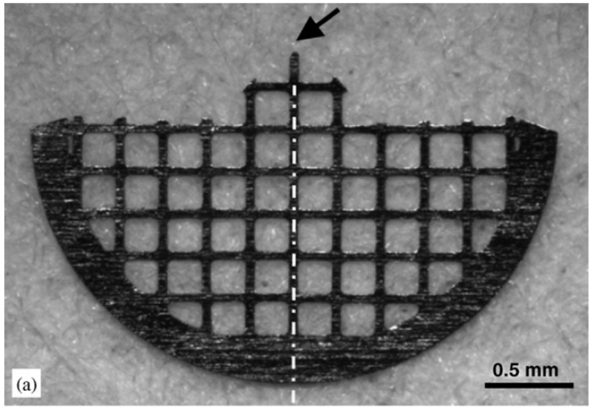

ELSEVIER

Ultramicroscopy 107 (2007) 8–15

www.elsevier.com/locate/ultramic

Transmission electron microtomography without the "missing wedge" for quantitative structural analysis

Noboru Kawase[a], Mitsuro Kato[a], Hideo Nishioka[b], Hiroshi Jinnai[c,*]

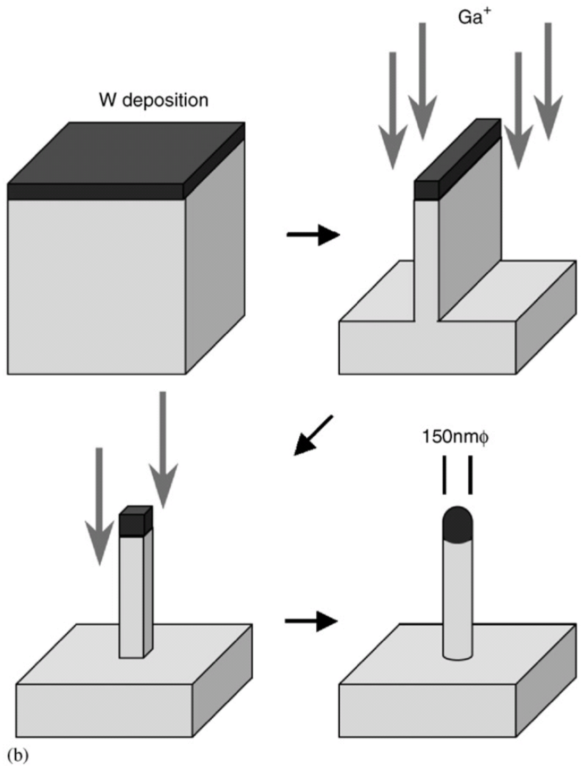

Fig. 1. (a) A modified molybdenum specimen grid with the fixing position of the rod-shaped specimen indicated by an arrow. (b) Schematic illustrations of procedures to form the rod-shaped specimen. After a tungsten deposition for the purpose of protection against the gallium ion irradiation, the specimen was first fabricated in a plate form, a prism form next, and finally a rod form by FIB.

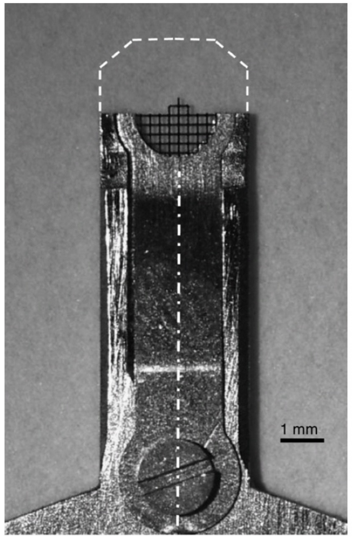

Fig. 2. A modified JEM2200FS specimen holder allowing ±90° tilt. The original profile is marked by the dashed line.

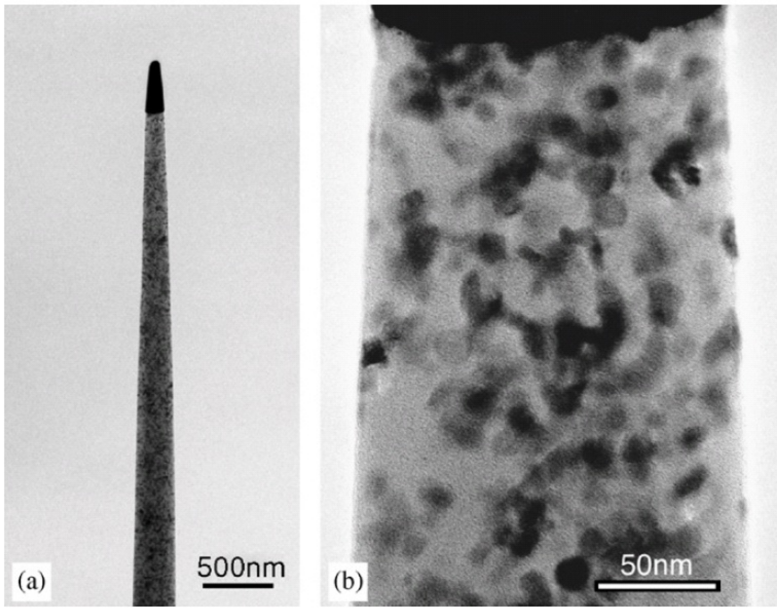

Fig. 3. (a) An electron micrograph of a rod-shaped polymer nanocomposite containing zirconia fillers. (b) An enlarged electron micrograph of the thinnest region of the rod-shaped specimen.

3D reconstruction of rod-shape specimen (FBP)

Zirconia-Polymer composite, Kawase *et al. Ultramicroscopy* (2007)

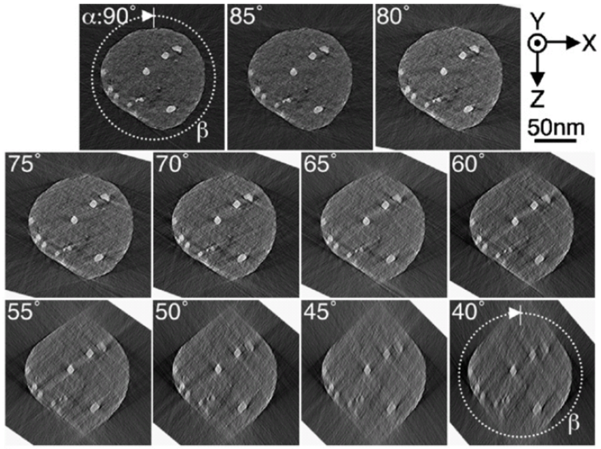

(a)

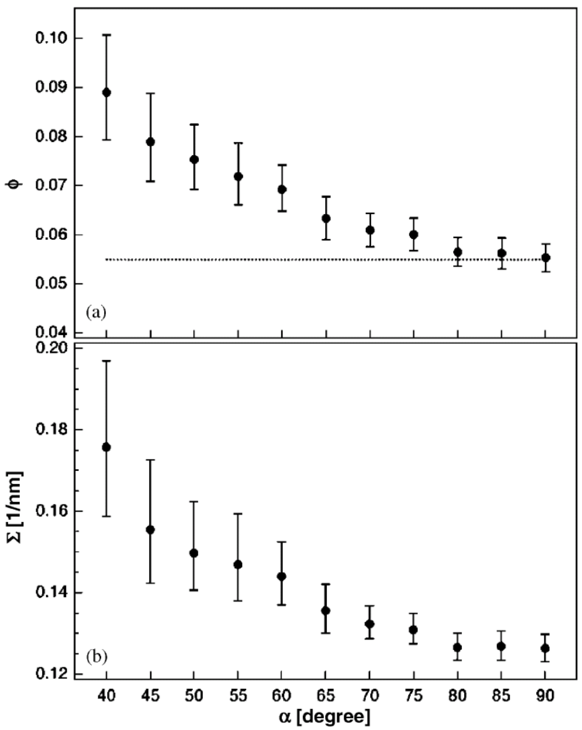

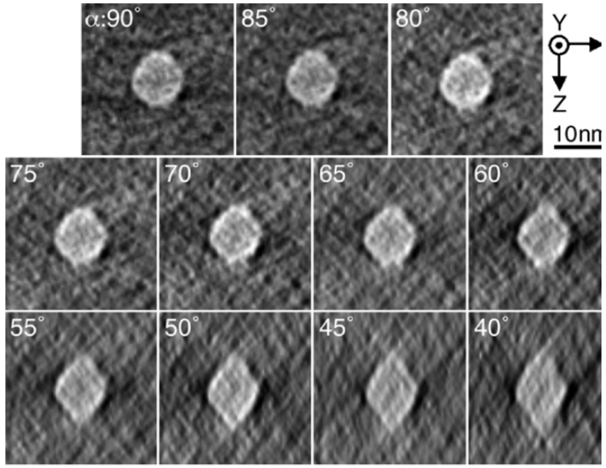

(a)

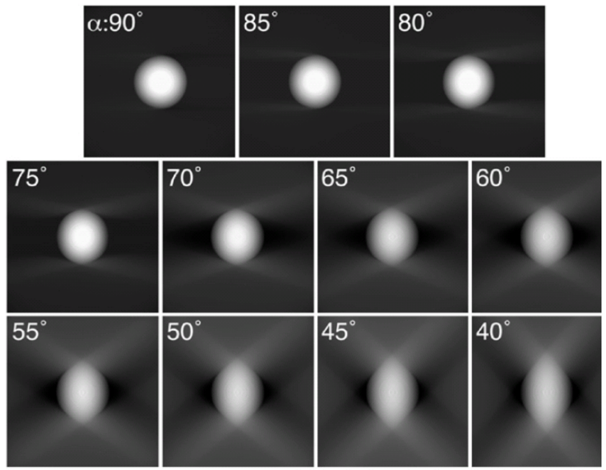

(b)

Fig. 8. (a) A series of reconstructed slices through a single spherical zirconia grain with a diameter of ca. 10 nm, reconstructed for various α values from 40° to 90°. (b) Simulated X–Z images reconstructed from a spherical model according to the same tilt angular range shown in (a).

Fig. 11. (a) Plot of volume fractions (zirconia/nanocomposite), ϕ, experimentally determined from the 3D reconstruction series from $\alpha = 40°$ to $\alpha = 90°$. Dashed line represents the known composition of the zirconia grain. (b) Plot of surface(zirconia)/volume ratio, Σ, experimentally determined from the 3D-reconstruction series.

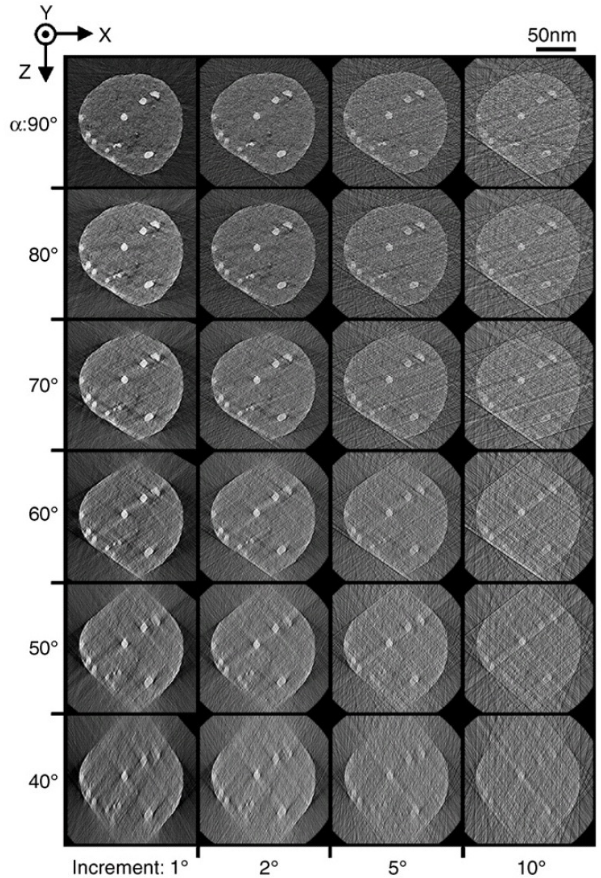

Fig. 12. A series of X–Z cross-sections of the same region in the rod-shaped specimen reconstructed with various tilt increments (1°, 2°, 5° and 10°) for typical α values from 40° to 90°.

Influence of electron absorption for a foil specimen

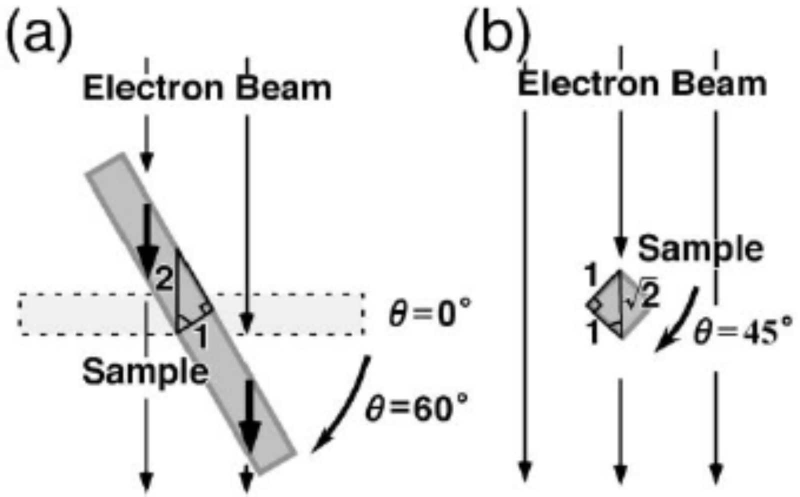

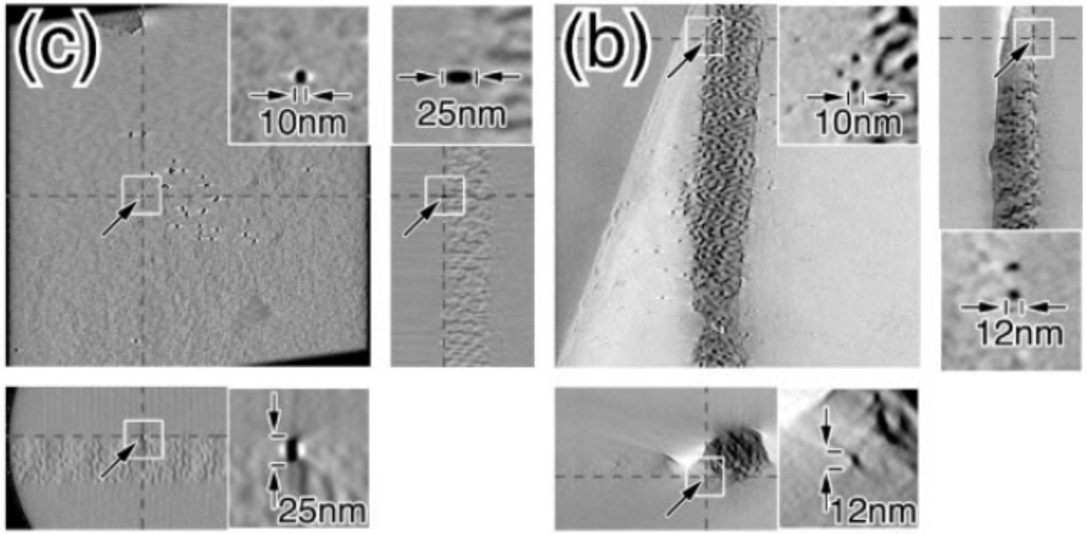

Different shapes of 3D reconstructed Au particle (10 nm) supported on polymer film (200 nm) or prism-shaped polymer section

→ Reduce transmittance of electron beam (< 10 %)

→ Less contribution of high tilt-angle series

→ Missing information along *z*

Kaneko *et al. J. Electron Microsc.* (2005)

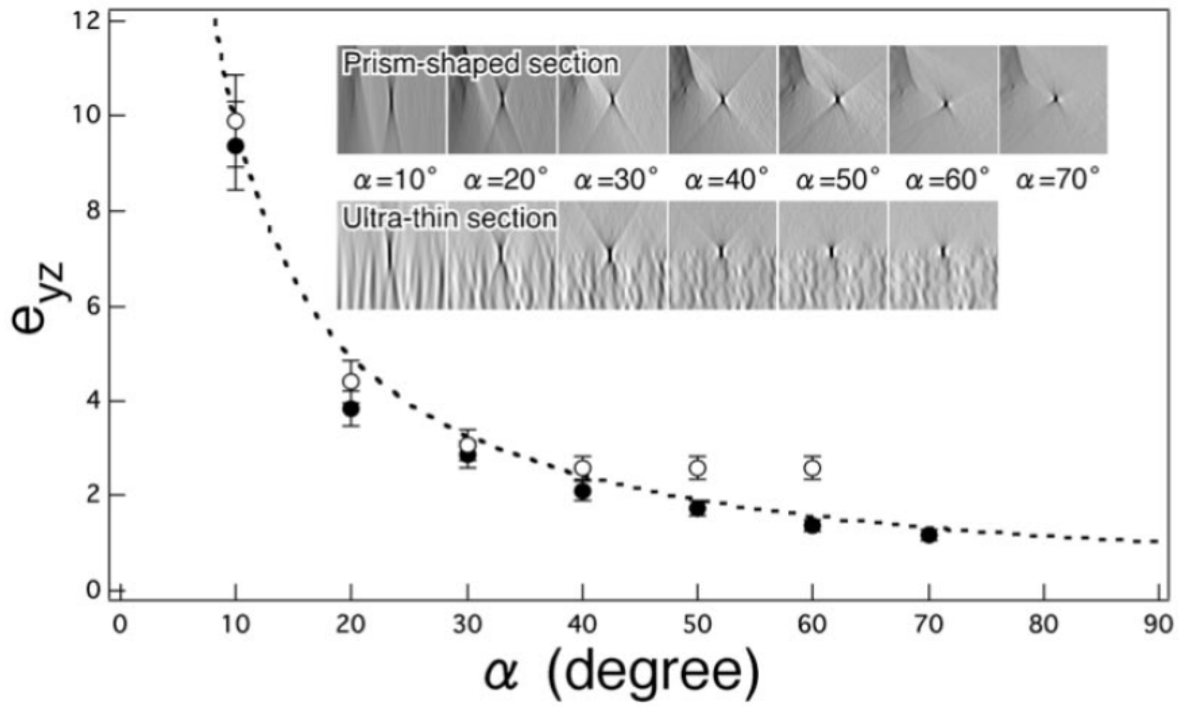

- Simulation
- Tilt series from -65° to +65° with 5°increment

New 3D reconstruction algorithm: compressive sensing (CS) algorithm capable of reducing number of tilt-series images

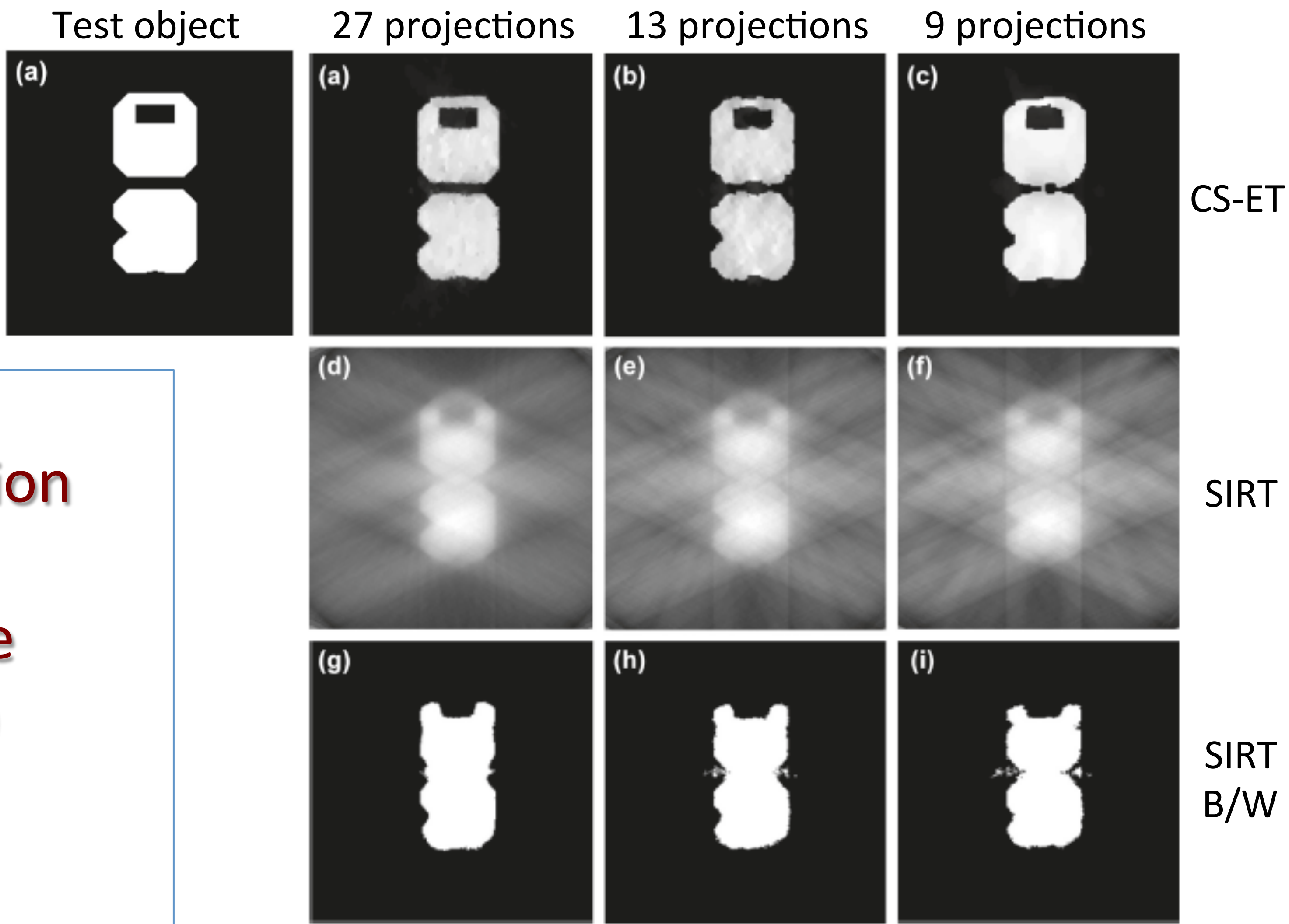

Figure 2. CS-ET (top row) and SIRT (middle row) reconstructions from 27 (a ,d), 13 (b, e), and 9 (c, f) projections. The bottom row shows the SIRT reconstructions thresholded using Otsu's method.

Saghi *et al.*: *NANO Lett.* (2011)
Goris *et al.*: *Ultramicroscopy* (2012)
Monsegue *et al.*: *Microsc. & Microanal.* (2012)

STEM ADF tilt series of precipitate & dislocation in 9Cr steel

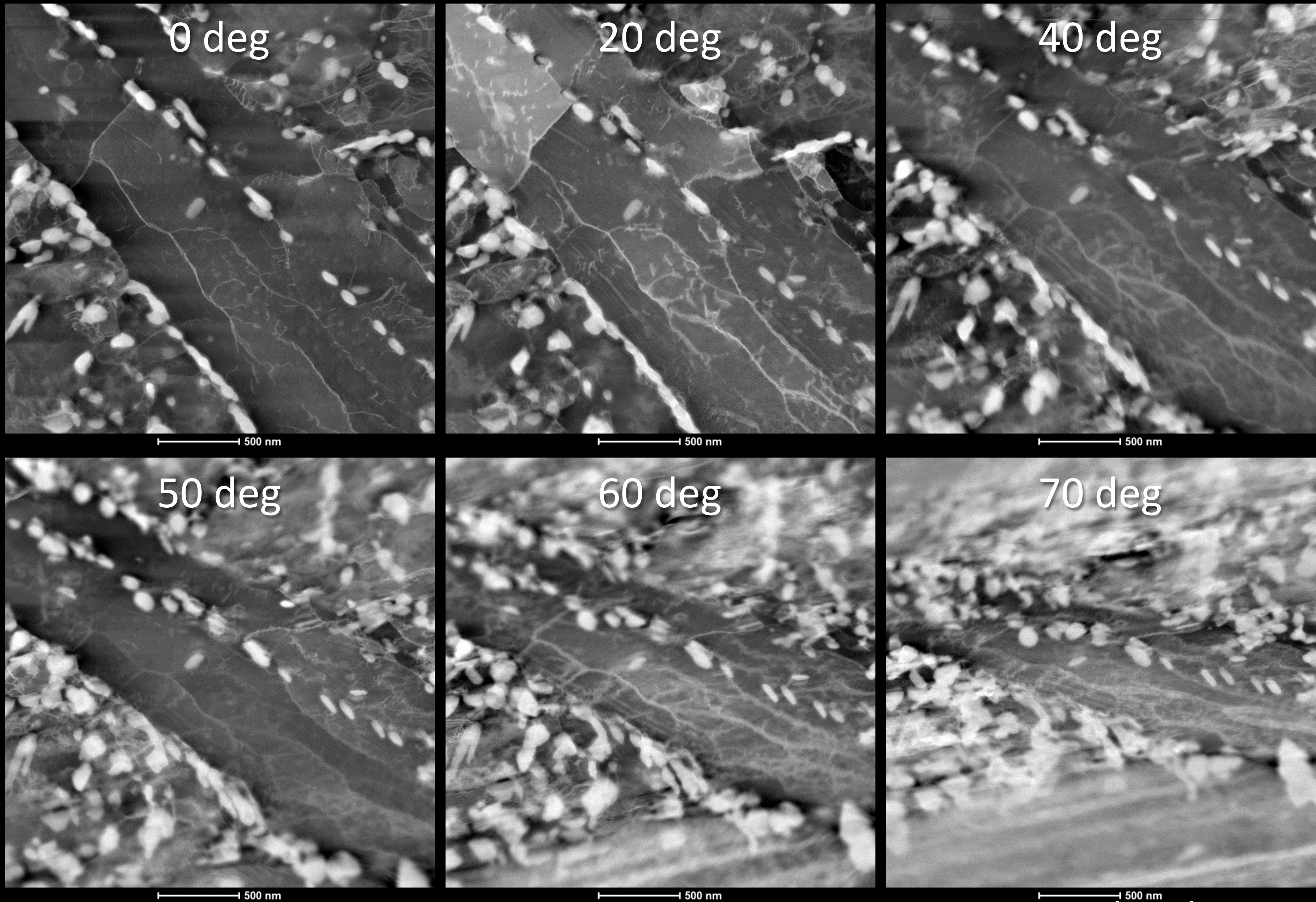

Hata *et al.* Under review

Energy-filtered HVEM

JEM-1300NEF

(Installation completed in 2010, Kyushu University, Japan)

Omega type energy filter, Tomography, STEM

Penetration power of electrons as a function of accelerating voltage (assuming unity for 200 kV)

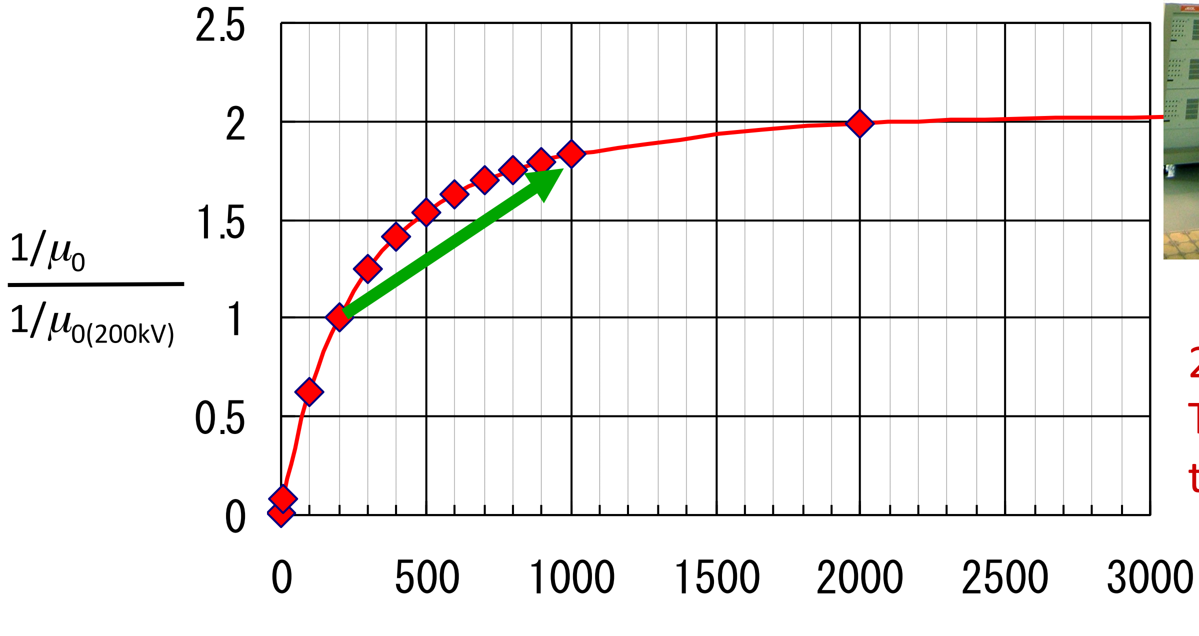

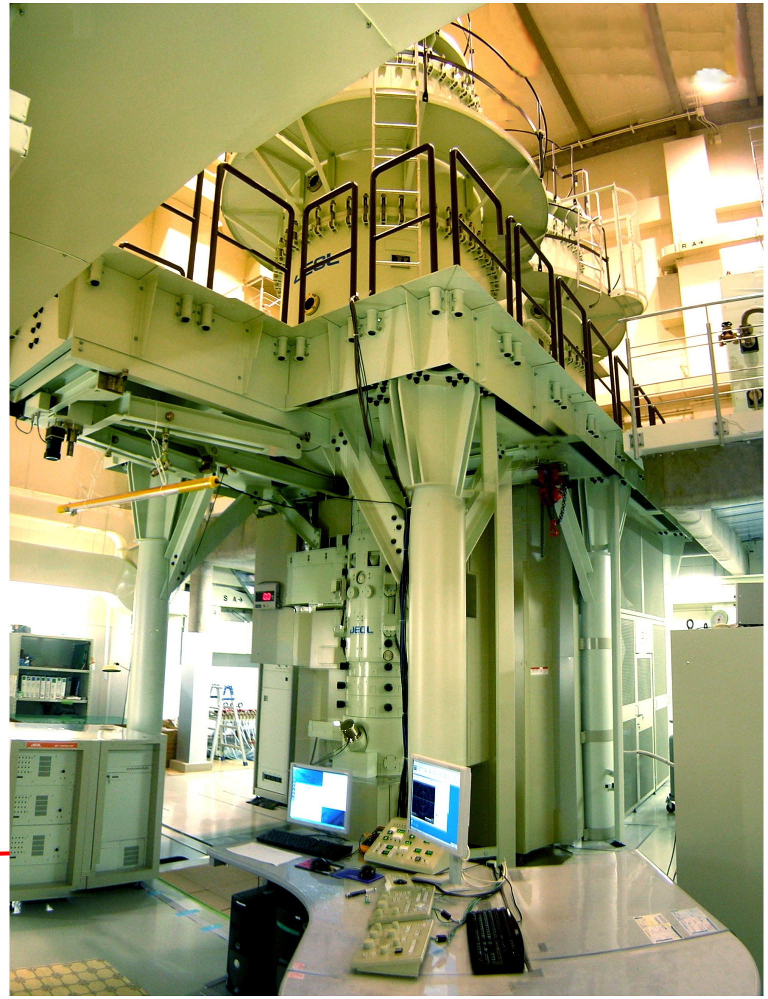

200 kV → 1000 kV
The penetration power becomes 1.8 times.

High-angle double-tilt & rotation holder for HVEM: application to thick (~3 μm) Si crystal

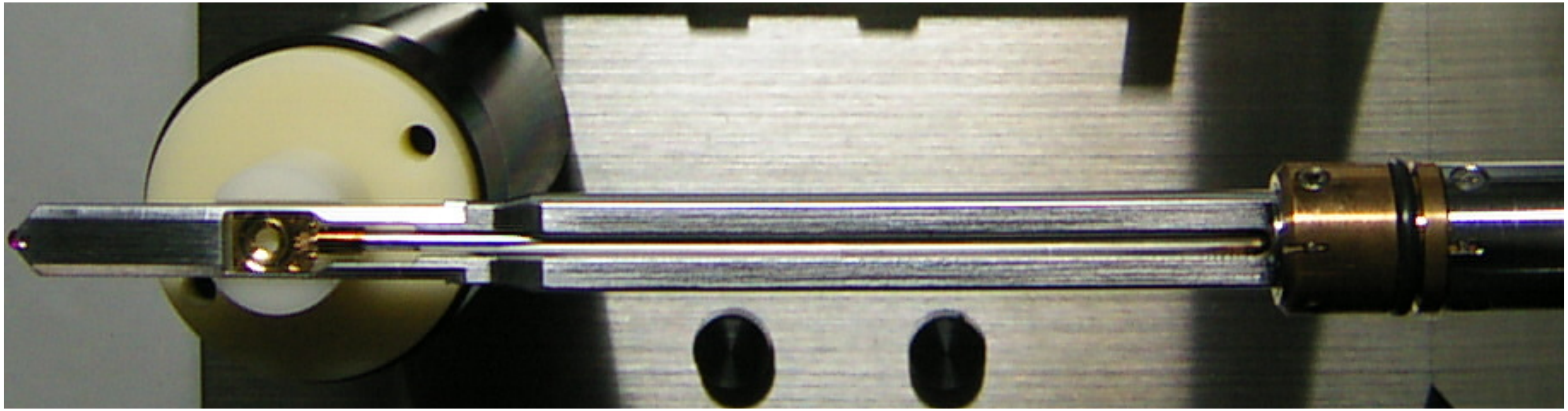

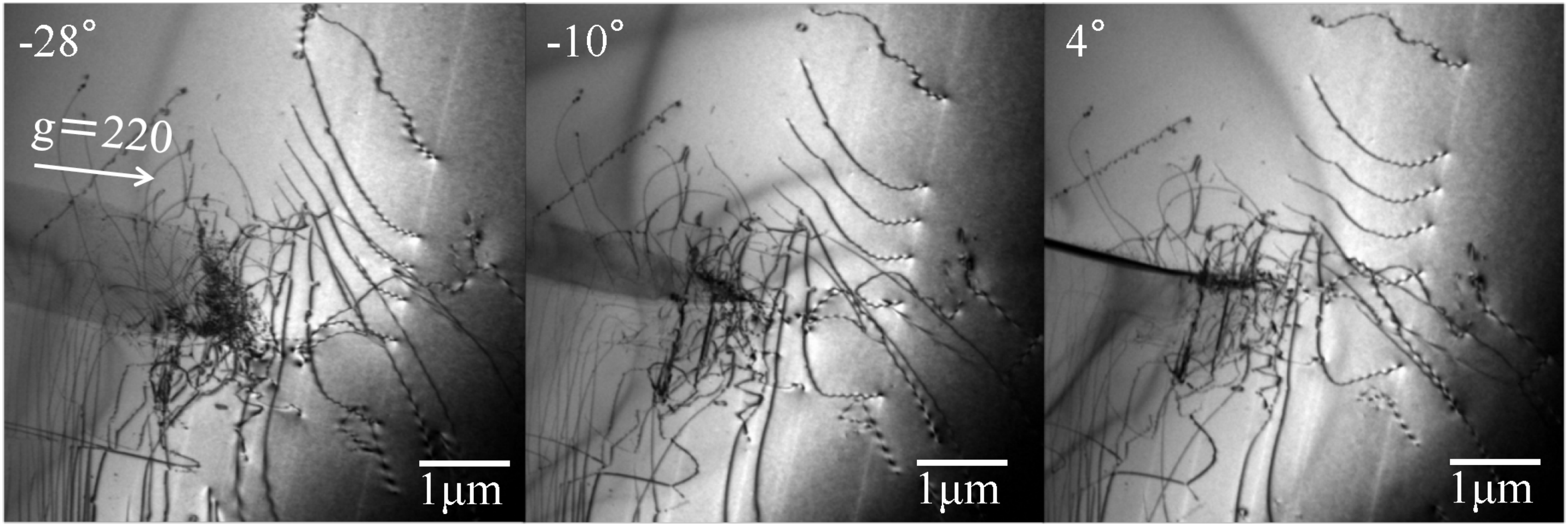

Tanaka and Higashida

Electron tomography at 2.4-ångström resolution

M. C. Scott[1]*, Chien-Chun Chen[1]*, Matthew Mecklenburg[1]*, Chun Zhu[1], Rui Xu[1], Peter Ercius[2], Ulrich Dahmen[2], B. C. Regan[1] & Jianwei Miao[1]

[1]Department of Physics and Astronomy and California NanoSystems Institute, University of California, Los Angeles, California 90095, USA. [2]National Center for Electron Microscopy, Lawrence Berkeley National Laboratory, Berkeley, California 94720, USA.

*These authors contributed equally to this work.

444 | NATURE | VOL 483 | 22 MARCH 2012

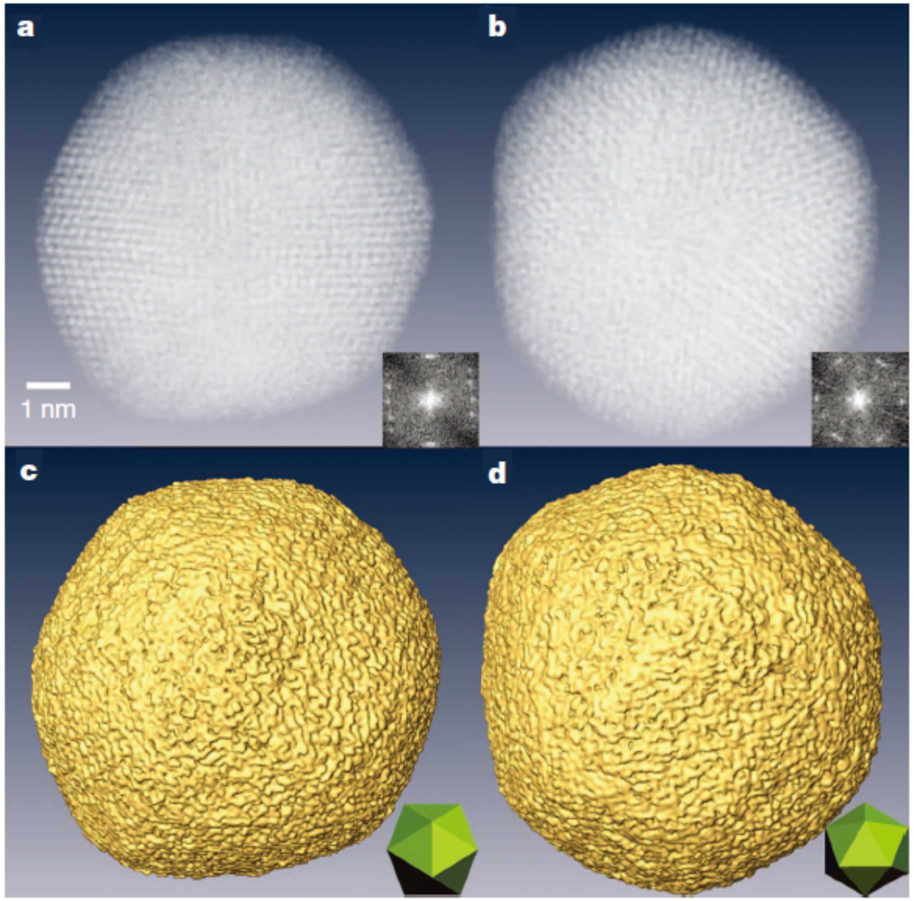

Figure 3 | 3D structure of the reconstructed gold nanoparticle. **a**, **b**, 3D volume renderings of the nanoparticle and their Fourier transforms (insets) at the two-fold (**a**) and three-fold (**b**) symmetry orientations. **c**, **d**, Iso-surface renderings of the nanoparticle at the two-fold (**c**) and three-fold (**d**) symmetry orientations. Insets show a model icosahedron at the same orientations.

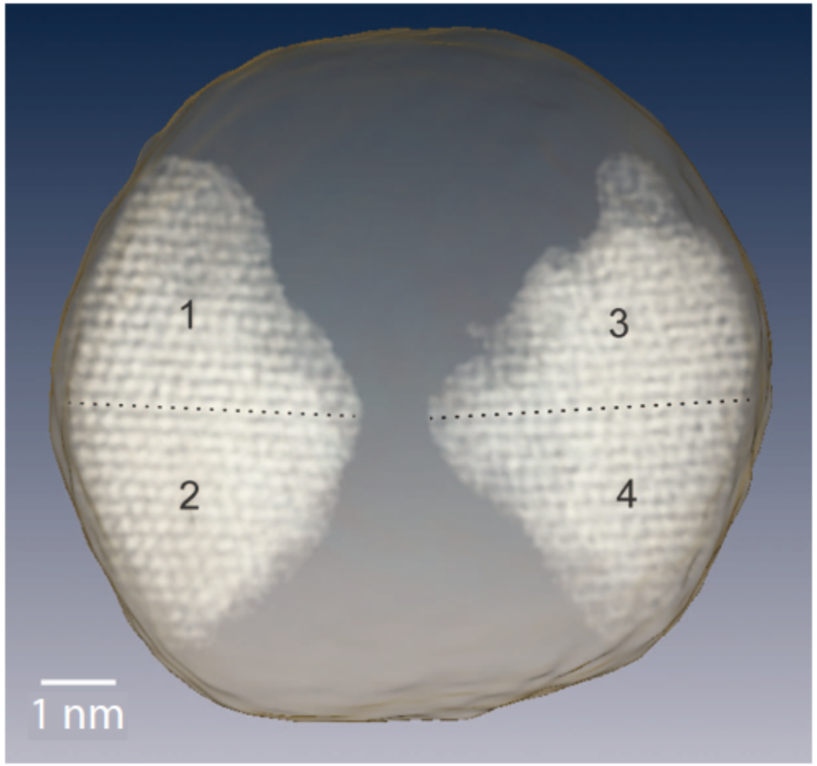

Figure 4 | Identification of four major grains inside the gold nanoparticle in three dimensions. Grains 1, 2 and grains 3, 4 are related by mirror-reflection across the horizontal interfaces marked by dotted lines. The angle enclosed by close-packed planes across these interfaces was measured to be 69.9° ± 0.8° between grains 1 and 2, and 71.3° ± 0.8° between grains 3 and 4, both of which are consistent with the angle for a face-centred cubic twin boundary (70.53°).

4D Electron Tomography

Oh-Hoon Kwon and Ahmed H. Zewail*

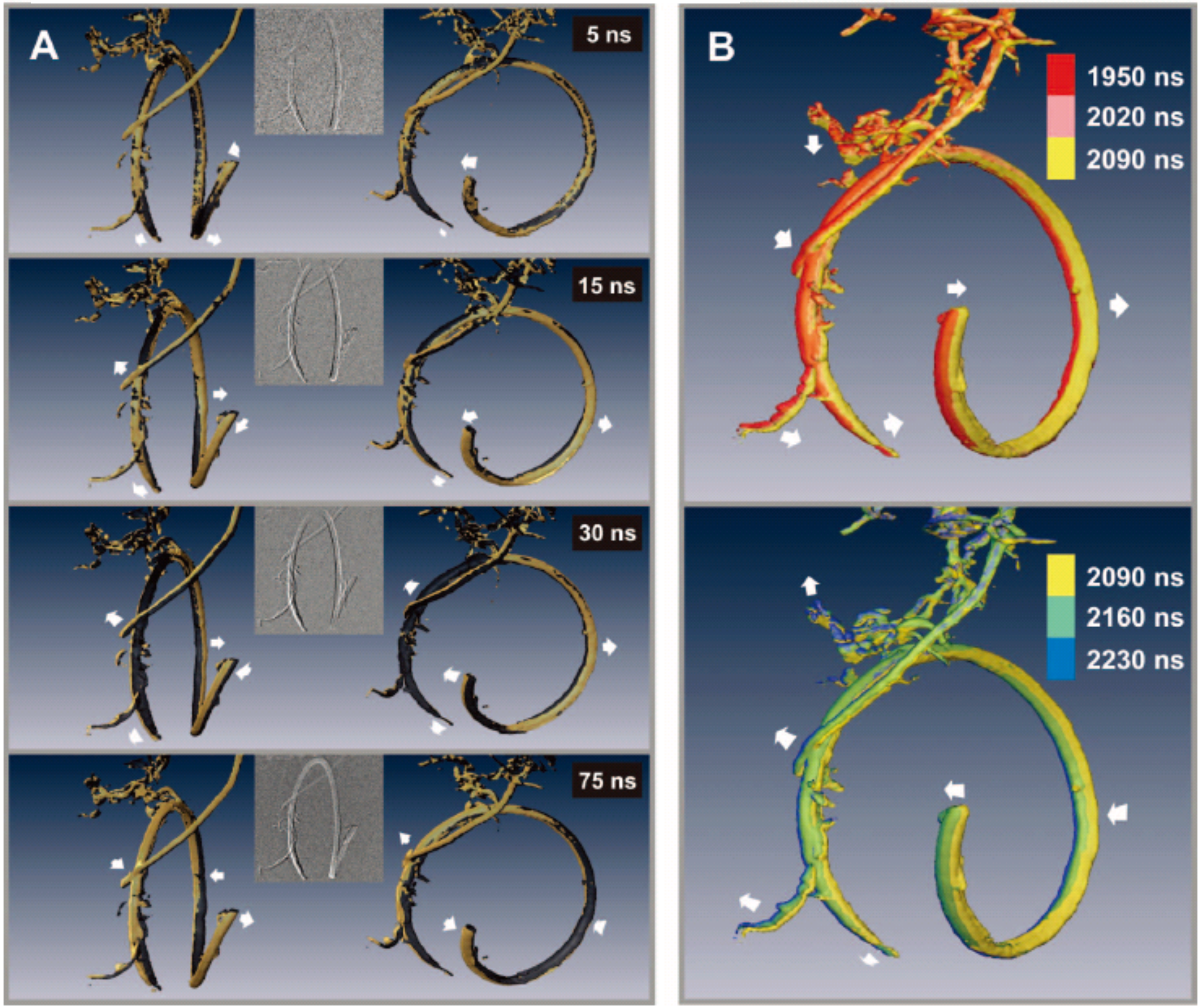

Fig. 4. 4D tomographic visualization of motion. (**A**) Representative 3D volume snapshots of the nanotubes at relatively early times. Each 3D rendered structure at different time delay (beige) is shown at two view angles. A reference volume model taken at t = 0 ns (black) is merged in each panel to highlight the resolved nanometer displacements. Arrows in each panel indicate the direction of motion. (**B**) The time-dependent structures visualized at later times and with various colors to indicate different temporal evolution. The wiggling motion of the whole bracelet is highlighted with arrows. From these tomograms, movies were constructed in the two different time domains (movies S2 and S3). Note that the time scale given here is chosen to display clearly the objects' motions, as opposed to the early ultrashort time domain (see text).

Elastic deformation of CNT

Combination of ET and in-situ with pulse-beam illumination

Acknowledgments

M. Mitsuhara, M. Shimizu, R. Akiyoshi, K. Ikeda, K. Kimura, K. Kaneko, M. Tanaka, K. Higashida, S. Matsumura, H. Nakashima (Kyushu Univ., Japan)

S. Miyazaki, H. Miyazaki (Mel-Build, Japan)

K. Inoke (FEI, Japan)

J. S. Barnard, P. A. Midgley (Univ. of Cambridge, UK)

J. H. Sharp (Univ. of Scheffield, UK)

H. Idrissi, D. Schryvers (Univ. of Antwerp, Belgium)

T. Kasama, A. Ramar, X. Huang, R. E. D. Borkowski, G. Winther, N. Hansen (Technical Univ. of Denmark, Denmark)

T. Pollock (UCSB, USA)

Kyushu University, Japan

MEXT, Japan

JSPS, Japan

EPSRC, UK

FWO, Belgium

DTU, Denmark

ICMR, USA